AD NUMBER
AD375937
CLASSIFICATION CHANGES
TO: **UNCLASSIFIED**
FROM: **CONFIDENTIAL**
LIMITATION CHANGES
TO: **Approved for public release; distribution is unlimited.**
FROM: **Distribution authorized to U.S. Gov't. agencies and their contractors; Critical Technology; 15 SEP 1966. Other requests shall be referred to Air Force Rocket Propulsion Lab., Attn: RPPR-STINFO, Edwards AFB, CA 93525. This document contains export-controlled technical data. NOFORN.**
AUTHORITY
30 Sep 1978, Group-4, DoDD 5200.10, per document marking AFRPL ltr dtd 12 Dec 1985

AD325932

AUTHORITY: AFAPL
ltr 12 DEC 85

SECURITY MARKING

The classified or limited status of this report applies to each page, unless otherwise marked.
Separate page printouts MUST be marked accordingly.

THIS DOCUMENT CONTAINS INFORMATION AFFECTING THE NATIONAL DEFENSE OF THE UNITED STATES WITHIN THE MEANING OF THE ESPIONAGE LAWS, TITLE 18, U.S.C., SECTIONS 793 AND 794. THE TRANSMISSION OR THE REVELATION OF ITS CONTENTS IN ANY MANNER TO AN UNAUTHORIZED PERSON IS PROHIBITED BY LAW.

NOTICE: When government or other drawings, specifications or other data are used for any purpose other than in connection with a definitely related government procurement operation, the U. S. Government thereby incurs no responsibility, nor any obligation whatsoever; and the fact that the Government may have formulated, furnished, or in any way supplied the said drawings, specifications, or other data is not to be regarded by implication or otherwise as in any manner licensing the holder or any other person or corporation, or conveying any rights or permission to manufacture, use or sell any patented invention that may in any way be related thereto.

CONFIDENTIAL

AFRPL-TR-66-231

AGC Quarterly Report 11205-Q-4

(u) A STUDY OF THE EFFECTS OF ENGINE PARAMETERS ON TWO-PHASE FLOW PERFORMANCE LOSSES USING N_2O_4/ALUMIZINE PROPELLANTS

By

J. O. Hartsell
M. J. Ditore

15 SEPTEMBER 1966

CONFIDENTIAL

SPECIAL HANDLING REQUIRED

NOT RELEASABLE TO FOREIGN NATIONALS

The information contained in this document will not be disclosed to foreign nationals or their representatives.

In addition to security requirements which must be met, this document is subject to special export controls and each transmittal to foreign governments or foreign nationals may be made only with prior approval of AFRPL (RPPR-STINFO), Edwards, California 93523

SPECIAL NOTICE

Standard MIL-STD-847 requires that each paragraph in a classified report be marked individually with the appropriate classification of the information contained in the paragraph.

None of the text in this report is classified. The only classified information in this report is contained in Tables and Figures which are marked with the appropriate classification.

Paragraph 3.24.4 of Standard MIL-STD-847 indicates that marking each paragraph individually need not be performed in instances where it would be impractical and misleading. Because none of the text in this report is classified, the paragraphs are not individually marked.

LEGAL NOTICE

AFRPL-TR-66-231 AGC Quarterly Report 11205-Q-4

(u) A STUDY OF THE EFFECTS OF ENGINE PARAMETERS ON TWO-PHASE FLOW PERFORMANCE LOSSES USING N_2O_4/ALUMIZINE PROPELLANTS

By

J. C. Hartsell

M. J. Ditore

15 September 1966

FOREWORD

This is the fourth quarterly report of work performed under Contract AF 04(611)-11205, Program Structure 7500, AFSC Project 3058. It covers the period 1 June 1966 through 31 August 1966.

This program is being conducted by the Liquid Advanced Technology Department of Research and Technology Operations, Aerojet-General Corporation, Sacramento, California. The program is being directed by Dr. C. M. Beighley, Program Manager. Mr. M. J. Ditore is project manager, and Mr. J. O. Hartsell is the project engineer. Lt. A. Tatkenhorst is the Air Force Project Engineer at the Rocket Propulsion Laboratory at Edwards Air Force Base, California.

The authors wish to acknowledge the services of personnel of the Aerojet-General physics laboratory, under the direction of Mr. R. Keith, during the engine testing phase. In addition, the data analysis provided by Messrs. R. M. Thomas, P. J. Petrozzi, and J. I. Ito is greatly appreciated.

This report contains no classified material extracted from other classified documents. Publication of this report does not constitute Air Force approval of the report's findings or conclusions. It is published only for the exchange and stimulation of ideas.

UNCLASSIFIED ABSTRACT

Studies were conducted to quantitatively evaluate the effects of liquid-engine design and operating parameters on two-phase flow performance losses using an N_2O_4/Alumizine-gel propellant combination. The theoretical-experimental efforts, conducted concurrently, consist of performance evaluations covering a range of variables sufficiently wide to provide an adequate basis for specific impulse prediction for large-scale engines. The theoretical analysis was made of two-phase flow performance losses resulting from the existence of aluminum oxide in the nozzle exhaust. Particle samples, collected during each 2K engine test, are being analyzed to determine the representative particle size and distribution data for the analysis. A one-dimensional gas-particle flow analysis is being used to determine the performance losses. Preliminary computations indicate that the use of the mass median for particle size classification yields performance losses comparable to those derived when the particle distribution is used in the analysis. Forty-two 2K engine tests were successfully conducted. Some of these tests were performed to resolve the feed system pressure-oscillation and hardware erosion problems encountered in early experimental testing. Observed specific impulse efficiency was nominally 87%. The range of efficiency variation, with one exception, was $\pm$1% depending upon operating conditions. A minimum specific impulse efficiency was observed for a chamber pressure of 500 psia, an L^* of 33, and a chamber contraction ratio of 3. Two-phase flow performance losses were calculated to be nominally 2% of the theoretical specific impulse and further, the influence of design and operating variables on two-phase flow performance were found to be in significant at the sea level expansion ratio. The single most significant loss was determined to be energy release loss; the absolute magnitude varying with engine design, but was found to be insensitive to mixture ratio or chamber pressure.

TABLE OF CONTENTS

TABLE OF CONTENTS (Cont'd)

LIST OF ILLUSTRATIONS

TABLE OF CONTENTS (Cont'd)

LIST OF ILLUSTRATIONS

TABLE OF CONTENTS (Cont'd)

LIST OF TABLES

SECTION I

INTRODUCTION

A. OBJECTIVES

The primary objective of the program is to demonstrate the altitude performance of the N_2O_4/Alumizine-43 propellant at three different mixture ratio combinations, three different nozzle expansion ratios, and at the 15,000-lb-thrust level.

The secondary objective is to quantatively evaluate the influence of engine design and operating variables upon two-phase flow performance losses and, also, overall performance. Two-phase flow investigations will be conducted at the 2,000-lb-thrust level. The experimental results, in which two-phase flow performance losses have been determined, will be compared with theoretical performance predictions. Results of these correlation studies will be used in predicting two-phase flow performance losses associated with optimized 30K and 100K engine designs using N_2O_4/Alumizine propellant. Existing analytical techniques are to be refined as appropriate to enhance performance prediction techniques.

B. TECHNICAL APPROACH

The overall objectives of the program will be accomplished by combined theoretical-experimental efforts directed towards evaluation of effects on performance resulting from hetrogeneous combustion products containing liquid-solid particles of aluminum oxide. The primary objective will be accomplished through experimental investigations using an existing 15,000-lb-thrust chamber and injector design developed under Contract AF 04(694)212. Actual testing will be conducted at

simulated altitude conditions. These tests will be conducted at an operating chamber pressure of 1500 psia and at mixture ratios of 0.4:1, 0.6:1 and 0.8:1. For each mixture ratio, two tests are scheduled using a nozzle expansion ratio of 50:1 and 100:1. Two additional tests, to serve as system calibration tests, will be conducted at a mixture ratio of 0.6:1 and a nozzle expansion ratio of 7:1. All tests of the 15,000-lb-thrust engine will be conducted in the altitude facilities at Arnold Engineering Development Center in Tullahoma, Tennessee. Testing of these engines at simulated altitude is scheduled during November and December, 1966.

The major tasks necessary to accomplish the secondary objective include:

1. Design, fabrication and assembly of the necessary test equipment. A major effort was expended in the acquisition of a portable, fuel feed system suitable for use with gelled propellants and capable of providing mass-flow requirements for both 2K and 15K engine tests. In addition, design, fabrication and assembly of 2K engine components along with manufacture of the alumizine gel propellant was accomplished as part of this task. The 15K chamber and injectors were available; however, chamber insulation and nozzle components were to be designed and procured in this effort.

This task is approximately ninety percent complete in that fabrication of the engine components required for the remaining altitude tests will be completed early in the next report period. The fuel feed system, engine

components and other test equipment have been described in previous quarterly reports References (1), (2) and (3), however, for convenience, a cursary description may be found in Section III.B.2. of this report.

2. A pre-experimental analysis to determine performance losses other than those attributed to two-phase flow. This task was to be accomplished so as to establish the performance level anticipated prior to actual experimental testing and to establish the magnitude of effects of chamber/injector interactions resulting from the specific component designs. In addition, evaluation of engine exhaust sampling techniques to determine both particle size and distribution was included in this task.

This task had been completed early in the program. The numerical procedures used in the analysis and results obtained were reported in Reference (2).

3. Conduct experimental investigations, using 2000-lb-thrust engines, to determine performance characteristics for various thrust chamber designs and operating conditions. In particular, these experiments are performed at sea level and simulated altitude conditions to experimentally demonstrate the influence of both design and operating conditions on two-phase flow performance losses. As such, exhaust samples are collected from each engine firing to determine the size and distribution of aluminum oxide existing in the exhaust. These data will then be used directly to compute two-phase flow losses and subsequently to establish performance trends.

4. Conduct extensive data analysis and correlation studies to evaluate

the influence of each design and operating parameter. This task includes utility of results of subscale experiments in conjunction with the interaction theory, described in Reference 4, to predict the altitude performance of the 15K engines tested. Also, the sea level specific impulse (or efficiency) of the 15K engine tested during the Titan Predevelopment program, Contract AF 04(694)212 will be predicted. Performance losses attributed to particles contained in the exhaust will be determined for both 2K and 15K engine designs. The results will be incorporated in the overall analysis to establish the effect of engine size and thus allow performance prediction of larger size engines.

Included in this task is a supplementary effort directed towards improvement or refinement of existing methods of analysis to determine individual or combined performance losses. In particular, the one-dimensional gas-particle flow computer program was modified to include the influence of particle distribution and the effect of particle solidification. A complete discussion of the numerical procedure including the specific computer program modifications were presented in Reference (3). Further, the method of determining performance losses due to friction and heat transfer in the chamber have been improved. The details of the present methods are presented in Section III.A of this report. Further refinement of existing methods of analysis is considered a continuing effort during the period of this program.

5. Evaluation of maintainability and durability of engine components used during the experimental phases will be documented for future reference and

for experimental evidence of material integrity when exposed to the thermal environment of N_2O_4/Alumizine propellant exhausts.

SECTION II

SUMMARY

To date, a total of forty-two test firings have been conducted, using a 2000-lb-thrust engine, to demonstrate the performance characteristics of N_2O_4/Alumizine-gel propellant combination. These sea level tests were performed at the physics laboratory of the Aerojet-General Corporation. Nozzle exhaust samples were obtained from each test and analyzed to determine the size and distribution of aluminum oxide particles contained in the exhaust. These data were then used to establish the two-phase flow performance losses.

Subsequent to initial data analysis, the method employed for analysis of particle samples was reviewed. Various methods of counting the number and size of particles observed from both the electron and optical microscope were compared to determine the optimum method of analysis. It was found that, in most cases, elimination of particles having a size of 0.5μ or less did not influence the calculated two-phase flow performance and therefore can be ignored in arriving at the mass median particle size. Further, it was determined that a minimum of 1000 particles are to be counted to insure survey of a representative sample. The differences in mass median particle diameter between viewing the collected samples using an optical and an electron microscope were significant. The observed anomaly is attributed to the restricted field of scope (70μ) when using the electron microscope. In observing the samples with an electron micro-

scope, care should be exercised in selecting a field which is considered to contain a representative distribution of all particle sizes. Since this approach would necessarily include a human bias, several locations of the sample should be photographed and subsequently pooled to assure reliable results.

Performance data observed from the sea level tests were selected so as to avoid those tests which experienced either pressure oscillations and/or hardware erosion. In all cases, engine designs including ATJ graphite chamber and nozzle inserts did not experience sufficient erosion to influence performance. Gain stabilization was effective in eliminating pressure oscillations for all engine designs and operating conditions without component modifications, with the exception of one condition. Stabilization of the 90 L^* engine design operating at a chamber pressure of 1500 psia would require major modification of the design of the injector. This modification would influence combustion characteristics and thus preclude reliable performance correlation studies. This test condition was therefore eliminated from the original test plan without loss of generality of program results.

The performance losses attributed to a hetrogeneous exhaust were determined. It was found, based on analysis of exhaust samples collected, that performance losses were nominally 2% of the theoretical value. Also, variations in two-phase flow performance losses were, in most cases, observed to be within experimental accuracy. Therefore, although trends in performance losses are indicated, the results will require further substantiation. In general, the influence of design and operating conditions on two-phase flow performance losses may be considered negligible. This conclusion will be verified during the

scheduled altitude tests which will be conducted at larger expansion ratios. In addition, the effect of particle agglomeration within the nozzle (if any) will be determined by comparison of particle size and distribution observed between sea level and altitude firings.

SECTION III

TECHNICAL DISCUSSION

A. ANALYSIS

1. General

The analytical techniques, used in conjunction with quantitative performance demonstrations, have the unique features of: (1) evaluation of individual losses associated with the particular injector/chamber configuration, (2) determination of the interactions between each parameter contributing to the inherent degradation of performance, and (3) establishing the variation in particle size and subsequent two-phase performance losses as a function of design and operating conditions.

The general methods adopted for numerical evaluation of individual performance losses were presented in References 2 and 3, whereas the interaction theory is discussed in detail in Reference 4. In general, the method of analytical performance prediction is not dependent upon the theoretically or empirically determined thrust coefficient and characteristic velocity. As such, it provides more accurate determination of individual system performance losses and, thus, overall performance.

The basic elements of theoverall technique involve estimating the magnitude of various performance losses and subtracting them from theoretical

shifting-equilibrium performance. The resulting value is then compared with experimentally determined specific impulse to establish the magnitude of loss attributed to incomplete mixing and combustion for a specific injector-chamber design. This loss, which can not be computed directly, is identified as energy release loss.

The correlations resulting from analysis of various engine configurations provide the basic information necessary to evaluate the interactive influence of any one or a multiple of parameters on system performance. Using these data, derived from studies of the interaction of design variables and operating conditions, the performance of full-scale engines can be accurately predicted.

An important aspect of performance evaluation of the N_2O_4/Aluminine-43 propellant combination is the loss in system kinetic energy caused by formation of aluminum oxide in the combustion process. In particular, the liquid-solid particles contained in the exhaust, while increasing the thermal energy of the system, will not remain in equilibrium with the gaseous species and will, therefore, degrade performance.

Reevaluation of individual performance losses, in compliance with new techniques, as well as determination of the loss in two-phase flow, has comprised a major portion of the analytical effort expended to date. Specifically, the methods of computing chamber heat transfer and friction have been revised and used in the data analysis of sea level tests. In addition, the methods of determining particle distribution and size have been refined to

facilitate accurate prediction of two-phase flow losses. The following subsections present detailed discussions of modifications made to the analyses and to the methods employed in particle size determination.

2. Methods of Loss Analyses

a. Chamber Friction Loss

Viscous shear drag on the chamber wall results in a loss in thrust for the total engine system. For most engines having practical utility, the chamber friction loss can justifiably be neglected due to the low subsonic gas velocities in the chamber and the low ratio of chamber surface area to engine weight flow rate. In the subscale hardware used in this program, however, this loss is not negligible. The large characteristic lengths (L^*) and small contraction ratio of the subscale hardware result in a large chamber length to diameter (L/D) ratio for which boundary layer effects become significant. The original estimate of this loss was calculated assuming one-dimensional pipe flow through the chamber. A more rigorous method of analyzing the chamber friction effects has been completed wherein determination of friction drag is related to boundary layer development which inturn is a function of chamber length. The numerical method is as follows:

The incompressible flow velocity distribution in a pipe for non-fully developed turbulent flow is:

$$\frac{u(r)}{U_o} = \left[\frac{R - r}{\delta_1}\right]^{\frac{1}{n}} \quad \text{when} \quad \begin{matrix} R - \delta < r < R \\ 0 < r < R - \delta \end{matrix} \qquad \text{(A-1)}$$

where

$u(r)$ = Axial gas velocity at radius, r

U_o = Free stream velocity

R = Chamber radius

δ_1 = Velocity boundary layer thickness

n^{-1} = Velocity profile exponent

The velocity profile exponent (1/n) is dependent upon Reynolds Number as shown in Table A-I.

TABLE A-I

Velocity Profile Exponent For High Reynolds Number Flows

R_e	2×10^4 to 3×10^5	3×10^5 to 8×10^5	8×10^5 to 2×10^6	2×10^6
n	7	8	9	10

The displacement boundary layer thickness, δ_1, in an axisymmetric pipe is defined by:

$$\delta_1 = \int_o^R \left[1 - \frac{u(r)}{u_o}\right] \frac{r}{R} dr \qquad (A\text{-}2)$$

Substitution of equation (A-1) into equation (A-2) yields:

$$\delta_1 = \frac{\delta}{n+1} - \frac{\delta^2}{2R(2n+1)} \qquad \text{(A-3)}$$

Similarly the momentum boundary layer thickness, θ, in axisymmetric pipe flow is defined by:

$$\theta = \int_0^R \frac{u(r)}{u_o}\left[1 - \frac{u(r)}{u_o}\right]\frac{r}{R}\,dr \qquad \text{(A-4)}$$

Solution of the integral using equation (A-1) yields:

$$\theta = \delta\left[\frac{n}{(n+1)(n+2)} - \frac{\delta}{2R}\frac{n}{(n+1)(2n+1)}\right] \qquad \text{(A-5)}$$

The cumulative chamber wall drag, D, is taken to be equal and opposite to the drag upon the fluid in the cylinder so that:

$$D = \int_0^R \left[U_o - u(r)\right]\rho\left[u(r)\right]2\pi r\,dr \qquad \text{(A-6)}$$

where ρ = fluid density.

Equation (A-6) can be rearranged to:

$$D = (2\pi r)(\rho U_o^2) \int_o^R \left(\frac{u(r)}{U_o}\right) \left[1 - \frac{u(r)}{U_o}\right] \frac{r}{R}\, dr \qquad (A-7)$$

But the integral in equation (A-7) is simply the momentum boundary layer thickness. Therefore, the following relationship was used to calculate chamber drag.

$$D = (2\pi R)(\rho U_o^2)\theta \qquad (A-8)$$

Equation (A-8) shows that the drag is only a function of the chamber wetted perimeter, dynamic pressure, and momentum thickness. Furthermore, it should be noted that the free stream velocity, U_o, varies in its relationship to the mean velocity, $\bar{u}$, with the velocity boundary layer thickness.

$$\frac{\bar{u}}{U_o} = \left[1 - \frac{\delta}{R}\left(\frac{2}{n+1}\right) + \left(\frac{\delta}{R}\right)^2 \frac{1}{(2n+1)}\right]$$

For the purpose of this preliminary analysis, one additional simplifying assumption was made that the velocity boundary layer grows at the same rate as for the velocity profile with the 1/7 power law (validity of this assumption requires further evaluation).

$$\delta(x) = .37 \times R_{e_x}^{-.2} \qquad (A-9)$$

where

$$R_{e_x} = \frac{\rho \bar{u} x}{\mu}$$

μ = viscosity

and

$$\rho \bar{u} = W_T / \pi R^2$$

Equation (A-9) was therefore rearranged in the form:

$$\frac{\delta(x)}{R} = .37 \left(\frac{\pi \mu}{W_T}\right)^{.2} R^{-.6} x^{.8} \qquad \text{(A-10)}$$

The velocity boundary layer thickness calculated by equation (A-10) was then substituted into equation (A-5) to determine the momentum thickness for equation (A-8).

Evaluation of chamber gas flow Reynolds Numbers indicated the use of the following values of n for given test conditions.

P_c	n
1500	9
1000	8.5
500	8

Frictional drag in the convergent portion of the nozzle was evaluated by dividing the convergent portion into four conic frustums. A mean diameter was selected for each frustum and treated as a cylindrical section.

Mean gas densities and gas velocities were selected corresponding to the mean contraction ratio of each section. Incremental drag due to each segment was then calculated in the above manner and added to determine cumulative drag. Although incompressible flow equations were used, the error is not expected to be significant since adjustments were made to the densities in each of the convergent segments. Cumulative cylindrical and convergent chamber drag force was then divided by total propellant flow rate to determine specific impulse loss due to chamber friction.

b. Chamber and Nozzle Heat Loss

A major performance loss inherent in the particular subscale hardware being used in this program is that due to heat absorption by the graphite chamber and nozzle components. The net effect of this absorption is a lowering of the stagnation enthalpy of the combustion products and, thus, a reduction in the potential energy available for the nozzle expansion process.

The calculation of this loss has, to date, been accomplished by considering the chamber and nozzle regions separately. Chamber heat loss was evaluated by incrementally determining the transient chamber wall temperature in one radial co-ordinate and multiplying the gas side heat transfer coefficient by the temperature differential between this wall temperature and the gas recovery temperature. Assumptions made in this analysis were:

- Axial heat transfer through the graphite chamber walls as insignificant in comparison to the radial component

since the radial temperature gradient greatly exceeds that in an axial direction.

- The graphite wall is initially at a uniform (ambient) temperature throughout.
- The heat flux determined by the heat transfer coefficient and the driving potential at the graphite surface is equal to the product of the graphite thermal conductivity and the radial temperature gradient at the inner wall.
- The outside wall of the graphite is insulated. (This last assumption is valid due to the thick walls of the graphite liners and the short duration firings.)

The total chamber heat loss was calculated by summing the local heat flux and incremental chamber surface area. Total performance loss was derived by expanding the reduced - enthalpy chamber products to the exit area ratio of the nozzle, and comparing these results with theoretical calculations assuming 100% combustion efficienty. The equations used in this procedure are as follows:

The gas side heat transfer coefficient was determined from Bartz's equation

$$h_g = \frac{.026}{1.6\mu\ d^{.2}} \left[\frac{\mu^{.2} C_p}{P_r^{.6}} \right]_{am} \left[\frac{\dot{W}_T}{A} \frac{T_{fs}}{T_{am}} \right]^{.8} \qquad \text{(B-1)}$$

where H_g = Gas side heat transfer coef., Btu/in.^{2}-sec-°R

d = Diameter, in.

μ = Viscosity, lb_m/ft-sec

C_p = Specific heat, Btu/lb_m-°R

P_r = Prandtl Number

$\dot{W}_T$ = Gas flow rate, lb_m/sec

A = Area, in.^{2}

T_{fs} = Free stream gas temp., °R

T_{am} = Arithmetic mean temp., °R $\left(\frac{Tr + Twg}{2}\right)$

T_r = Gas recovery temp., °R

T_{wg} = Gas side wall temp., °R

and where the transport properties are evaluated at the arithmetic mean temperature.

Having calculated the heat transfer coefficient by equation (B-1), it was used to determine the dimensionless Biot number:

$$Bi = (hg\ r_2/k) \qquad (B-2)$$

where r_2 = Outer radius of graphite wall, in.

k = Graphite thermal conductivity, Btu/in.-sec-°R

The time variable is also made dimensionless by introducing the Fourier Number:

$$F_o = \alpha t/r_2^2 \qquad (B-3)$$

where α = Graphite thermal diffusivity, $in.^2/sec$

t = Time, sec

One additional parameter, the inner wall radius to outer wall radius ratio, is required to graphically determine the inner wall temperature from Reference (4) using the Biot and Bourier Numbers.

If the wall temperature thus calculated does not agree with the assumed wall temperature used in equation (B-1), further iterations may be required until convergence is achieved. It should be noted that all transport properties are temperature dependent.

The heat flux in the nozzle convergence was calculated by dividing the zone into four segments and calculating the heat flux at each section and multiplying by its corresponding surface area.

The total chamber heat loss was then calculated by summing the local heat flux and incremental chamber surface area.

$$Q_c = \sum h_{gi}(T_r - T_{wg})_i A_i$$

To evaluate the effect of chamber heat loss upon engine specific impulse the reduced temperature option of the Chemical Composition Program (Ref. 4) was used to determine the effect of enthalpy decrease in the chamber (at Mach number zero) to reduced flame temperature ($\Delta H/\Delta T$).

$$\Delta T_{\text{cham. ht. loss}} = \frac{Q_c}{\dot{W}_T \, (\Delta H/\Delta T)} \qquad (B\text{-}4)$$

The reduced specific impulse at the applicable exit area ratio corresponding to the temperature reduction of equation (B-4) constitutes the chamber heat loss in terms of specific impulse. Since specific impulse loss increases in the nozzle with increasing exit area ratio for a given temperature reduction, chamber heat loss is one of the interaction losses.

c. Kinetic Losses

There is a performance loss associated with the condition that chemical equilibrium is not maintained throughout the expansion process. In rocket engines, the temperatures in the chambers are such that many of the species present dissociate. In the ideal case, these species are assumed to recombine as the temperature decreases in the expansion process. In practice, however, the temperature and pressure change in the expansion is frequently too rapid for recombination reaction to be completed; thus, the useable energy is not returned to the system and a performance loss results.

With the chamber pressures of interest in this study, it was originally assumed that recobination losses would, in all cases, be insignificant. The data of Reference 5, however, indicated that significant losses could occur in the cases of low chamber pressure (500 psia) and high area ratio (50:1 or 100:1). To verify or refute the original assumption, an analysis was conducted during this report period in which the recombination losses were calculated for the cases in question.

The method of analysis employed consisted of a modified form of the Bray Sudden Freezing Criteria discussed in detail in Reference 2. Essentially, this newer method calculates the nozzle freezing point through

a consideration of the reaction rates of each specie in the expanding gases. This technique, as opposed to the former method in which the reaction rate of a single "dominant" reaction is considered, was found to provide a nozzle freezing point nearly in agreement with the results of a more exact non-equilibrium flow program developed by United Aircraft under contract NAS 3-2572 (Reference 6).

Once the nozzle freezing point was known for the desired conditions of chamber pressure and mixture ratio, the differences in performance between the case with freezing and that without freezing were established at each of the higher area ratios. Figure 1 shows the respective curves of specific impulse versus area ratio for a chamber pressure of 500 psia and mixture ratio of 0.6. It may be seen that the total performance loss due to incomplete recombination in the expansion process is approximately 0.16% at area ratios of both 50:1 and 100:1.

Similar analyses were performed for engines operated at chamber pressures of 1000 psia and 1500 psia. In both cases, the performance loss due to incomplete species recombination was found to be less than that for the engine operating at 500 psia. It was thus concluded that the original assumption of insignificant kinetic losses was valid for the engines under consideration.

3. Particle Size Analysis

One of the primary objectives of this program is the determination of the effects of variable engine parameters on particle size and the resulting two-phase flow performance loss. As a consequence, considerable effort has been

RECOMBINATION LOSSES

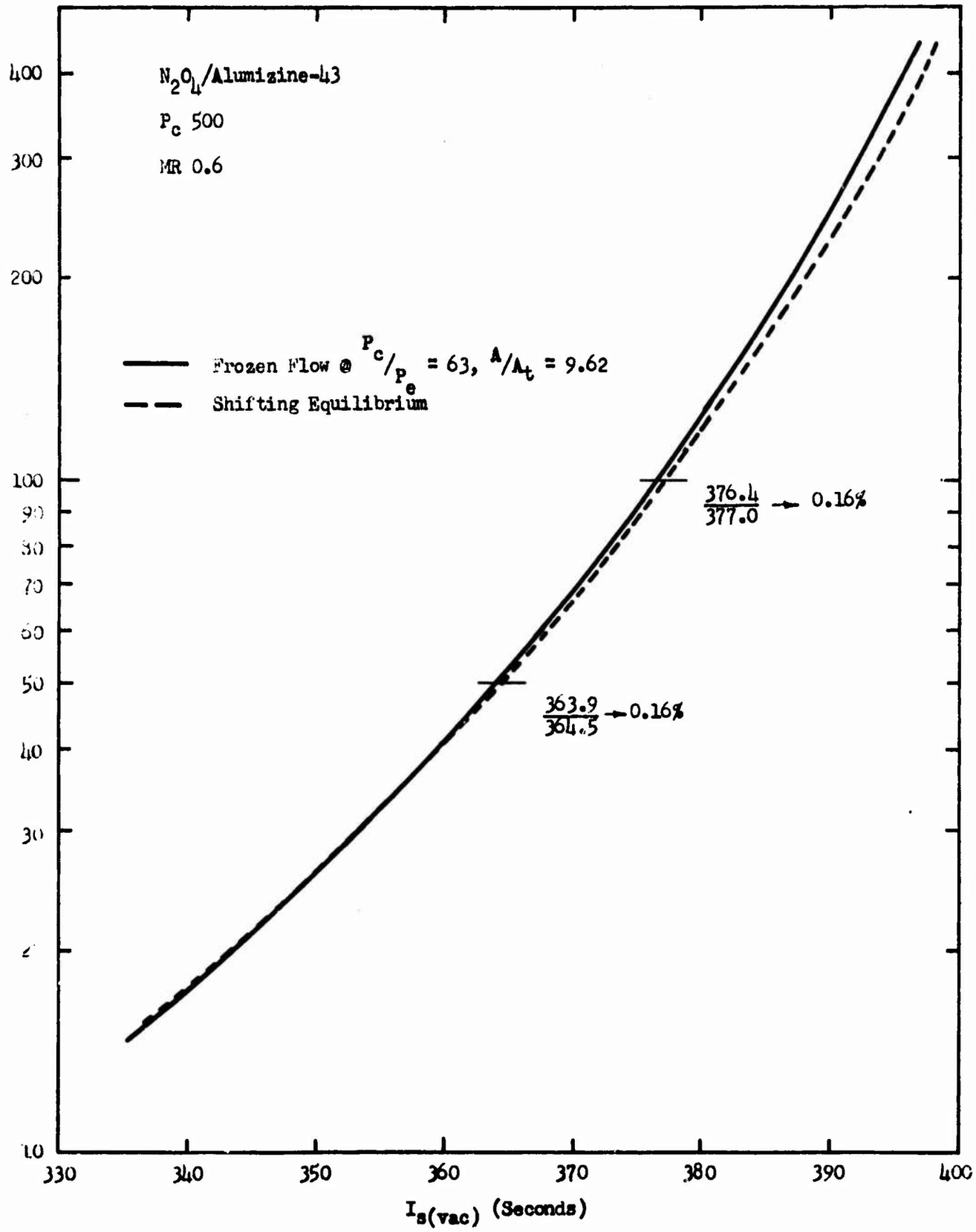

Figure 1

expended in particle collection and particle size analysis. The method adopted for exhaust plume sampling has been discussed in detail in past reports (References 2 and 3) and is reviewed briefly in Section III.B.2.d. The purpose of this section is to present recent findings in the area of particle size and distribution determination.

a. General Sizing Technique

In all subscale sea level tests, particles were collected on three Gelman GM-4 Metricel filter papers. After each test, the three filters were prepared for particle counting in the following manner. First, a narrow wedge, extending from the edge to somewhat past the center, was cut from each filter. This wedge was then placed in an evacuated chamber (Vacuum coater) where a thin film of carbon was deposited normal to the filter surface. (This carbon film was applied as a support for the particles and not for particle shadowing.) Next, a small square was cut from the carbonized wedge. Acetone was applied to this square to dissolve the filter paper, leaving only the carbon-particle film.

A 1/8 inch diameter circle of 200 mesh copper screen was then placed under this carbon substrate containing the oxide particles. This copper grid assembly was placed directly in the electron microscope.

The sample was enlarged 1600 times in the electron microscope. At this magnification, one mesh in the copper grid filled the viewing screen. Photographs were made of the first mesh encountered in the viewer which was completely covered and whose particle concentration was thin enough to allow resolution

of the individual particles. Sufficient pictures (four) were taken to completely cover the one mesh. The negatives obtained were printed on rectangular glass plates designed for use in a photograph enlarger. Adjustments were made so that a 1 micron particle measured 1 cm on the enlarger projection, thus giving an overall magnification of 10,000.

Particles were counted from the enlarged projection using a centimeter scale to measure particle diameters. Each diameter was recorded directly on a computer input sheet and the image of that particle marked on the projection to ensure against recounting the same particle. In order to further minimize any tendency toward biasing the sample through selection of the picture to be counted, all counts were made on the first picture in a plate, beginning at the left side and counting to the right until sufficient particles were recorded. In most cases, less than one-half of the first photo was used to complete the count.

Initially, 500 particles of all sizes down to and including 0.05 microns were counted from each filter sample. It was found, however, that the clarity of the picture affected the number of particles counted that were of a size large enough to affect the calculated mass median (0.2 microns and larger). In those cases where the smallest particles were clearly defined, the majority of the particles counted fell within the 0.2 to .05 micron range. This was due to the normal presence of a far greater number of smaller particles on the samples. When the small particles were agglomerated or less clearly defined, the count included a greater distribution of particles 0.2 microns and larger. This latter situation was statistically desirable, since the calculation

of the mass median could then be made from a sample containing a moderate amount of large size particles.

To ensure that the particle count of influential particles (those that are large enough to significantly affect the mass median) was consistent, a procedure was adopted whereby a minimum of 324 particles of 0.2 microns and larger were counted per filter sample. A background count of the smallest particles was then obtained by counting the smaller particles in a representative area and then extrapolating this data to the total area over which the larger particles were evaluated.

The particle sizes recorded on the computer input sheets were transferred to punched cards and processed on an IBM 1130 computer. The program used first sorts the particle diameters into groups with 0.2 micron increments and then calculates particle statistics from this classified data. The statistics calculated are the number ($\bar{d}_n$) and mass ($\bar{d}_m$) means as well as the calculative percent mass for each diameter classification. The mass median ($\bar{d}_{med}$) is determined graphically by plotting a cumulative mass versus particle diameter curve and reading the diameter corresponding to 50% of the mass.

The procedure described in the preceding paragraphs was that employed in deriving the particle size information presented in Section III.C. Following completion of the sea level tests, several aspects of particle

sample measurement were investigated for the final analysis phase of the program. The results of some of these studies have been instrumental in bringing about a re-evaluation of the techniques employed to date. The areas of analysis and the results obtained are presented in the following sections.

b. Effect of Small Particles on The Calculated Mass Median

The objective of this study was to determine the effect of the smaller particles on the particle mass median derived empirically from plots of sample distributions. To accomplish this objective, the original particle counts for tests 2K-1-117, 2K-1-126, and 2K-1-136 (Figures 2, 3, and 4 respectively) were modified by progressively deleting the smaller particle classifications. The modified distributions were then analyzed to determine the relative change in particle mass median.

Having obtained the mass median for each modified distribution, the one-dimensional two-phase flow computer program was employed to calculate the variance in specific impulse loss as a function of the size particles deleted. The results of this work are shown in Table 1. The maximum change in mass median due to the elimination of all particles 0.5 microns and smaller was found to be 0.31 microns, corresponding to a change in specific impulse loss of 0.44%. (As shall be seen in Section III.C. a variance in specific impulse of 0.50% represents the maximum deviation due to experimental data scatter. Elimination of particles less than 0.8 microns would in some cases

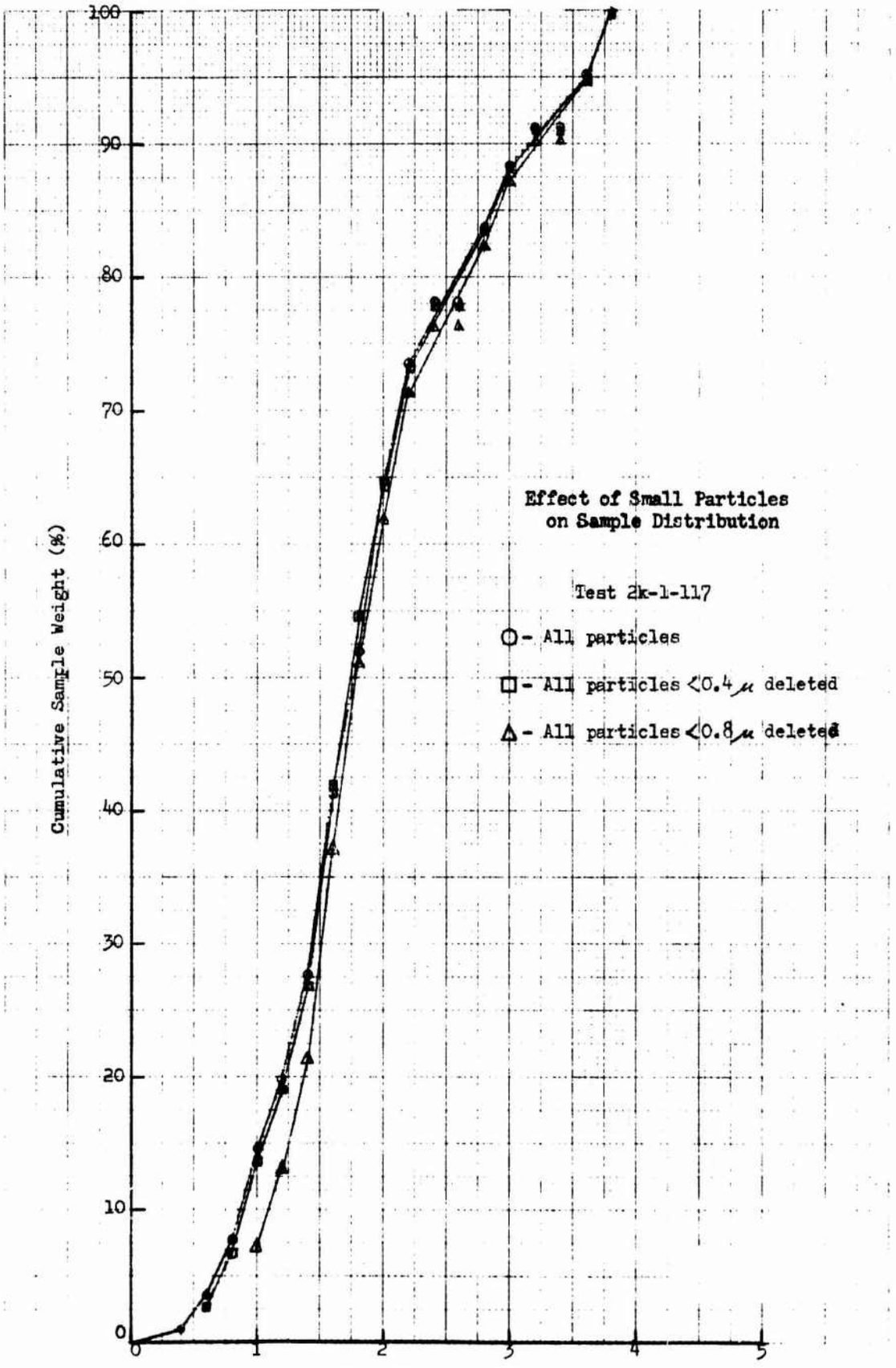
Cumulative Sample Weight (%)
100
90
80
70
60
50
40
30
20
10
0
0
1
2
3
4
5
Particle Diameter (Microns)
Effect of Small Particles on Sample Distribution
Test 2k-1-117
○ - All particles
□ - All particles <0.4 μ deleted
△ - All particles <0.8 μ deleted

Figure 2

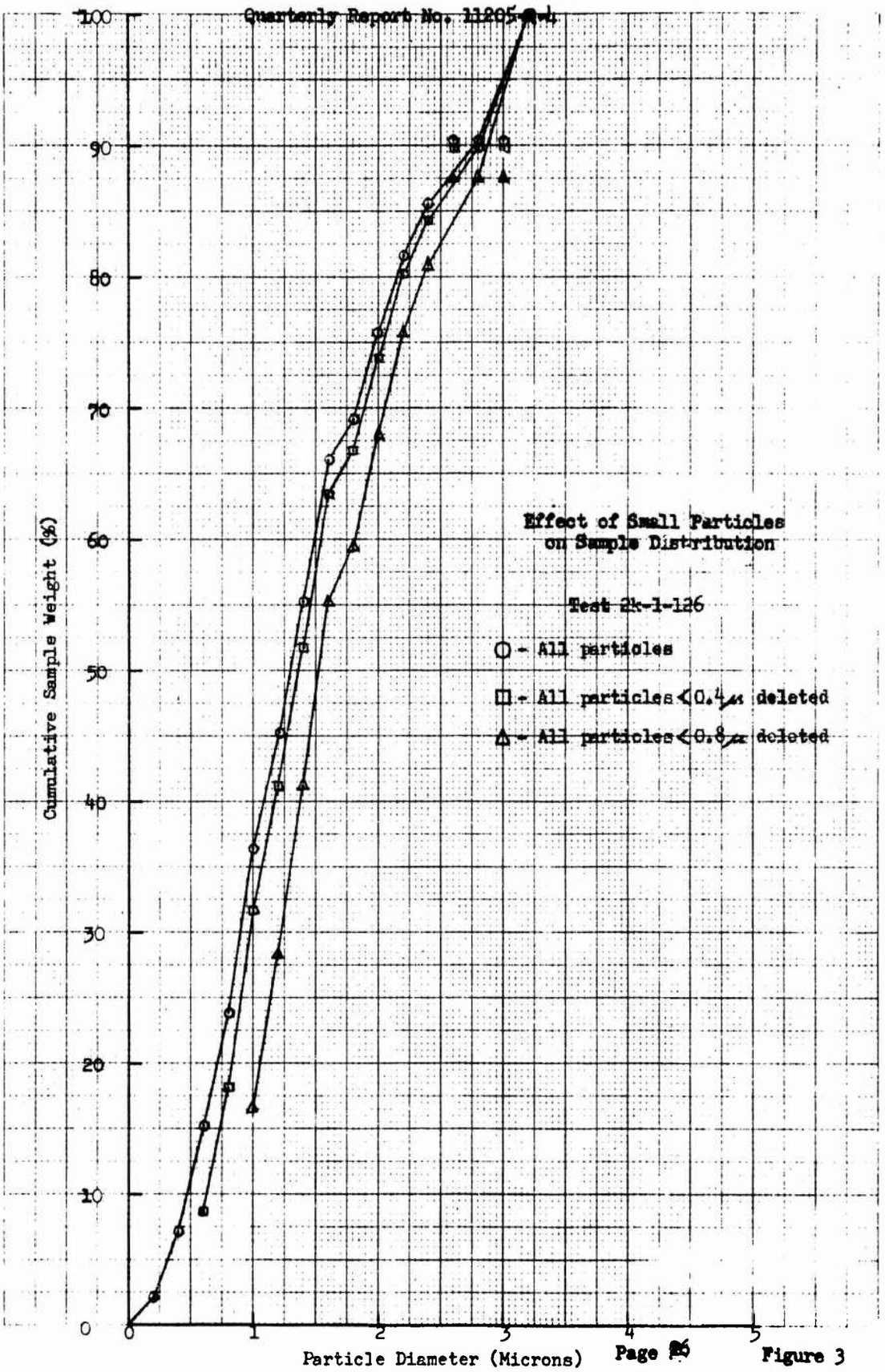
Effect of Small Particles on Sample Distribution
Test 2k-1-126
○ - All particles
□ - All particles < 0.4 μ deleted
△ - All particles < 0.8 μ deleted
Cumulative Sample Weight (%)
Particle Diameter (Microns)
0
10
20
30
40
50
60
70
80
90
100
1
2
3
4
5

Figure 3

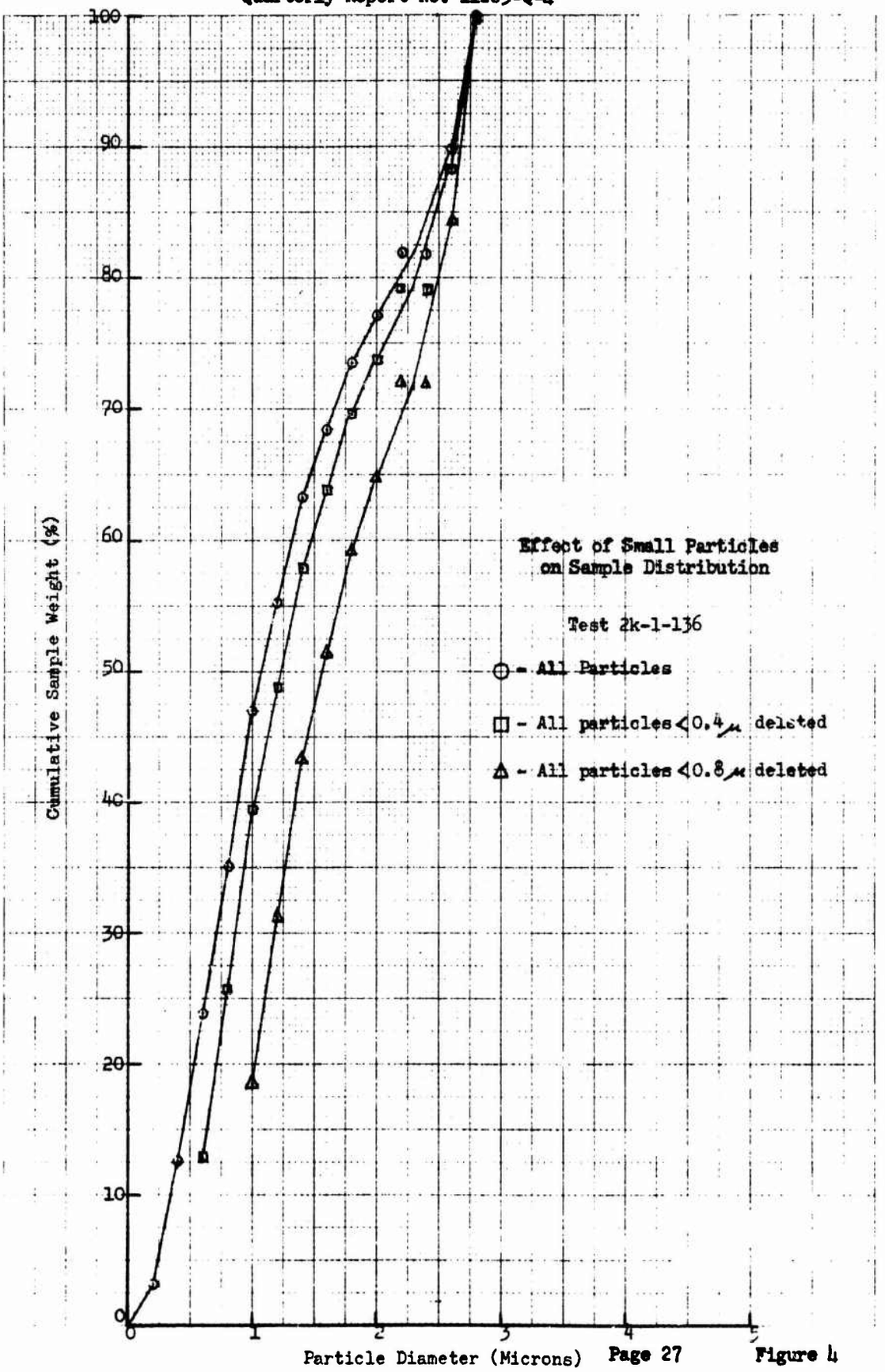
Cumulative Sample Weight (%)
100
90
80
70
60
50
40
30
20
10
0
0
1
2
3
4
5
Particle Diameter (Microns)
Effect of Small Particles on Sample Distribution
Test 2k-1-136
- All Particles
- All particles <0.4μ deleted
- All particles <0.8μ deleted

Figure 4

TABLE I

EFFECTS OF SAMLL PARTICLES
(All particles $< D_p$ deleted)

	D_p	$\bar{d}_{med}$	Mass Fraction of Particles Deleted	% I_s Loss (Nom.)
Test 2k-1-117	0	1.71	0	2.17
	.2	1.72	.0004	
	.4	1.73	.0100	2.20
	.6	1.75	.0360	
	.8	1.78	.0779	2.28
Test 2k-1-126	0	1.29	0	1.51
	.2	1.31	.0210	1.56
	.4	1.37	.0711	1.65
	.6	1.44	.1517	1.74
	.8	1.52	.2393	1.86
Test 2k-1-136	0	1.06	0	1.36
	.2	1.11	.0319	1.43
	.4	1.21	.1255	1.56
	.6	1.37	.2389	1.80
	.8	1.56	.3503	2.07

exceed this limit.) Based on these results, it was concluded that the small particles could be estimated, rather than actually counted. This was further substantiated by additional analysis. Table II shows the results of an analysis in which the estimated number of particles 0.5 microns and smaller was varied by ±50%. It may be seen that the maximum change in measured mass median was only 0.12 microns. Further, it was established from the modified curves of Figures 2 - 4 that an estimate of smaller particles need only be made for a distribution in which there are few large particles.

c. Effect of Counting Technique and the Number of Particles Counted

The objectives of this study were first to determine the effect of the method of counting a particle sample on the calculated mass median and, second, to determine the effect of the number of particles counted. To accomplish the first of these goals, two methods of counting were employed. The first consisted of a total count of 972 particles (0.2 microns and larger) from a randomly selected portion of the entire photographed sample. A comparative count using this technique was obtained by analyzing a different portion of the photographed sample.

The second method of counting consisted of a count of all particles 0.5 microns and larger present in all of the particle sample photographs. The distribution obtained in this fashion was then compared to those obtained using the former technique. This comparison is shown in Figure 5.

TABLE II

EFFECT OF BACKGROUND ESTIMATE ON MEASURED MASS MEDIAN

Test No.	Estimated No. of Particles < 0.5μ	Mass Median Diameter
2k-1-134	10302	1.55μ
"	10302 + 25%	1.49μ
"	10302 + 50%	1.43μ
"	10302 - 25%	1.59μ
"	10302 - 50%	1.66μ
"	none	1.77μ

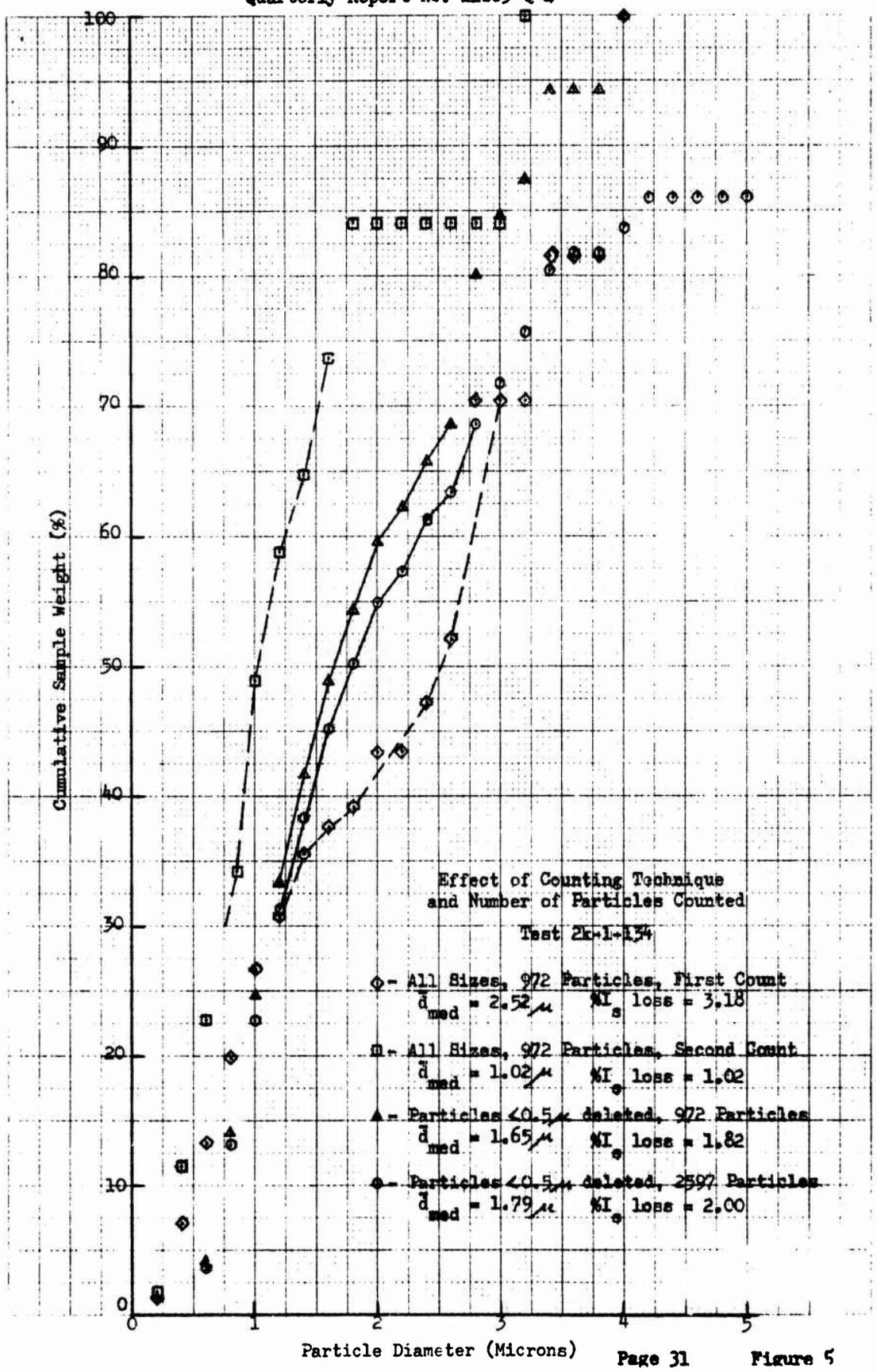
Cumulative Sample Weight (%)
Particle Diameter (Microns)
Effect of Counting Technique
and Number of Particles Counted
Test 2k-1-154
◇- All Sizes, 972 Particles, First Count
$\bar{d}_{med}$ = 2.52 μ %I_s loss = 3.18
□- All Sizes, 972 Particles, Second Count
$\bar{d}_{med}$ = 1.02 μ %I_s loss = 1.02
△- Particles <0.5 μ deleted, 972 Particles
$\bar{d}_{med}$ = 1.65 μ %I_s loss = 1.82
○- Particles <0.5 μ deleted, 2597 Particles
$\bar{d}_{med}$ = 1.79 μ %I_s loss = 2.00

Figure 5

The second objective was accomplished by comparing different numbers of particles from the count obtained using the latter of the methods discussed above. One distribution was derived using only the first 324 particles from each of three filters; the second was based upon all 2597 particles counted. The results of this comparison are also shown in Figure 5.

It may be seen from Figure 5 that significant deviations in the measured mass median are possible when the method of counting employed considers an actual count of particles 0.5 microns and smaller and only a small portion of the photographed sample. These deviations occur depending upon whether or not a full range of particle sizes is present in the portion of the sample counted. It is apparent from the Figure that the method of counting which allows, as a minimum, sizing of 1000 particles 0.5 microns and larger provides the most consistant calculation of mass median.

d. Comparison of Optical Versus Electron Microscopy Techniques

In all analyses conducted to date, the electron microscope has been used exclusively in the sizing of the particle samples. The decision to use only this microscope was made early in the program and was based upon the results of a comparative study conducted on the samples obtained during test 2K-1-107. This data, shown in Figure 6, was obtained using both the optical and electron microscopes. As may be seen from the Figure, the variance in mass median derived using the two techniques was not sufficient to warrant exclusive use of the more difficult optical method of analysis.

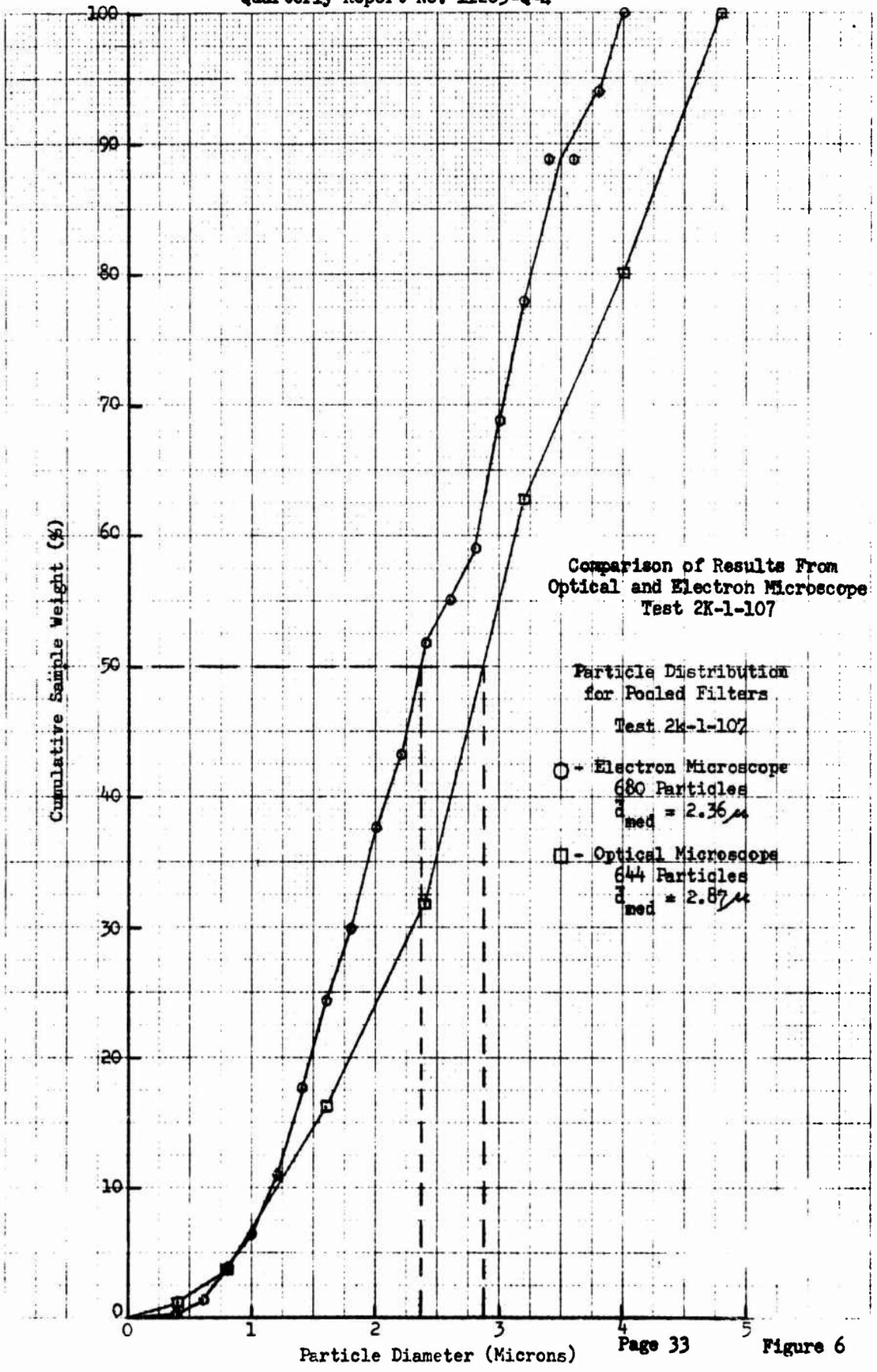
Cumulative Sample Weight (%)
100
90
80
70
60
50
40
30
20
10
0
0
1
2
3
4
5
Particle Diameter (Microns)
Comparison of Results From
Optical and Electron Microscope
Test 2K-1-107
Particle Distribution
for Pooled Filters
Test 2K-1-107
○ - Electron Microscope
680 Particles
d_{med} = 2.36 μ
□ - Optical Microscope
644 Particles
d_{med} = 2.87 μ

Figure 6

With the acquisition of more particle data, a comparative analysis of the two techniques was again conducted using the samples from test 2K-1-129. In addition to the optical and electron sizing by Aerojet, results obtained using an optical system were supplied by the Industrial Hygiene Department of the Lawrence Radiation Laboratories in Livermore, California. The cumulation of these studies are presented in Figure 7 and Table III. It may be seen that significant differences in mass median can exist, depending upon whether or not the electron or optical system is used in sizing. The reasons for the magnitude of the discrepancy are not exactly understood, since the optical system is capable of sizing particles down to approximately 0.6 microns, the point below which no particles were counted in the electron techniqus and, since the electron microscope is capable of photographing distinct particles as large as those measured under the optical microscope. The results have, however, indicated the possibility of error if only the electron microscope is employed.

e. Effect of Sample Location on Particle Size Distribution

In all particle analysis conducted to date, the assumption that the particles were distributed randomly over the collecting surface of the filters has been made, thus allowing analysis of an arbitrarily selected portion of the entire filter. Analysis of particle samples are being conducted to verify this assumption.

The objective of this work will be attained by first sizing samples from different meshs within the same grid, and second by sizing particles

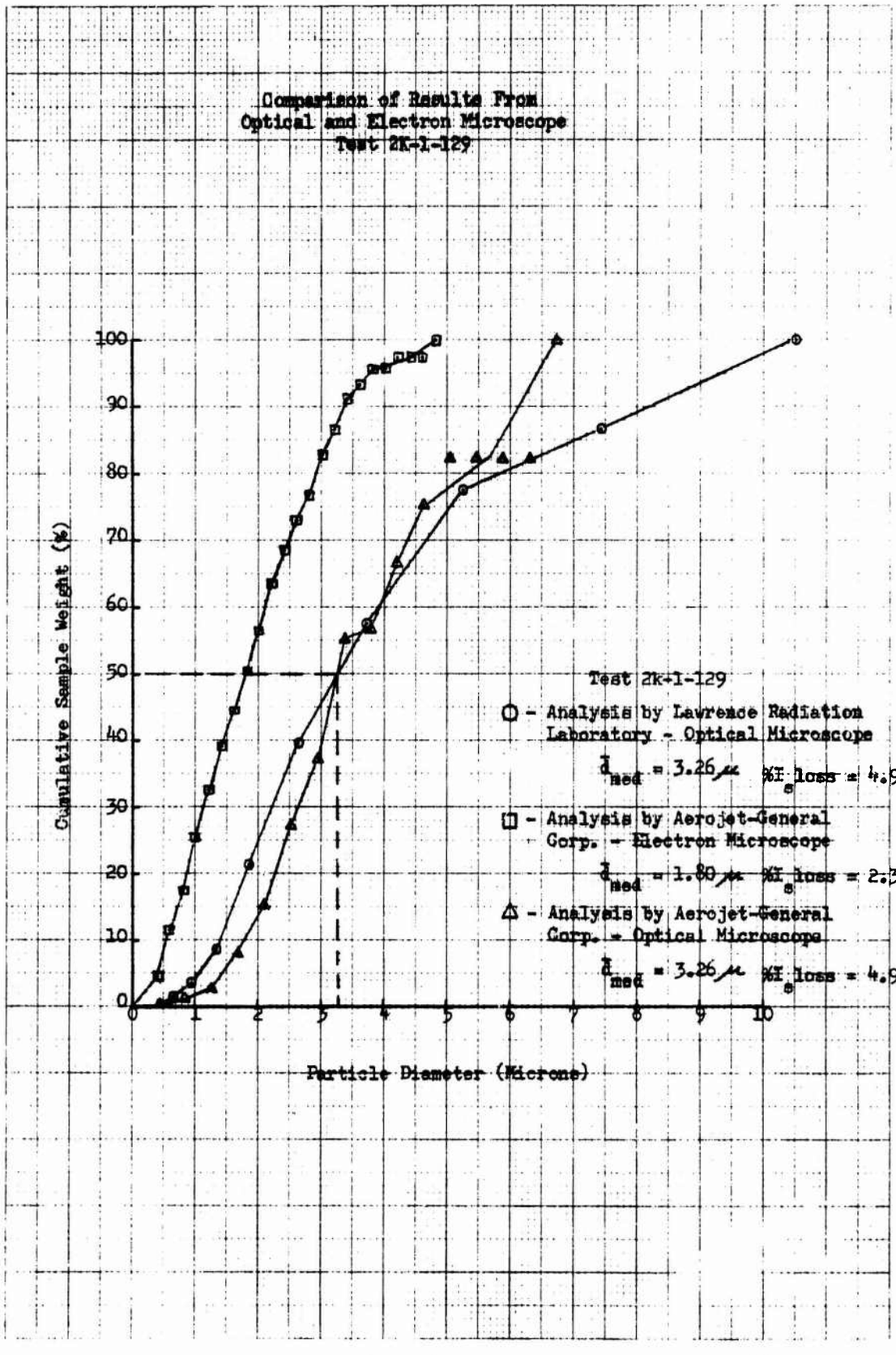

Figure 7

TABLE III

COMPARISON OF RESULTS FROM OPTICAL AND ELECTRON MICROSCOPES

Company	Microscope Used	Test No.	Measured Mass Median	%Is Loss
Aerojet-General Corp.	Optical	2k-1-107	2.87 μ	4.02
Aerojet-General Corp.	Electron	2k-1-107	2.36 μ	3.13
Aerojet-General Corp.	Electron	2k-1-129	1.80 μ	2.35
Aerojet-General Corp.	Optical	2k-1-129	3.26 μ	4.90
Lawrence Radiation Lab.	Optical	2k-1-129	3.26 μ	4.90

obtained at different locations on the filter sample. To date, only the first of these tasks has been completed. The results of this work are shown in Figure 8. From the results shown, it has been concluded that the assumption of a random distribution over the surface of a single grid is valid. Completion of the second task will occur during the next report period.

B. EXPERIMENTAL ENGINE TESTS

1. Test Plan

Performance demonstration tests using the 15,000-lb-thrust engine are to be conducted at simulated altitude conditions. The eight basic tests, shown in Figure 9, will provide quantitative performance evaluations as a function of mixture ratio and expansion ratio. A precise firing date for these tests is, however, uncertain at this time due to conditions of facility scheduling of the proposed Arnold Engineering Center (AEDC) test site.

Performance testing to evaluate the effects of engine design and operating parameters are being conducted using a 2000-lb-thrust engine. The basic test plan for these tests is presented in Figure 10. This test plan has been modified from that presented in the last report (Reference 3) as a result of analysis of sea level performance obtained to date. The scheduled sea level tests were conducted at Aerojet General and were completed on 14 June 1966. The altitude test phase for both 2K and 15K engines is presently scheduled to be completed at AEDC by December 1966.

The first series of thirteen sea level subscale tests shown in Figure 10 have been completed. In addition, the particle size variation and consequent two-phase flow performance loss has been determined through an analysis

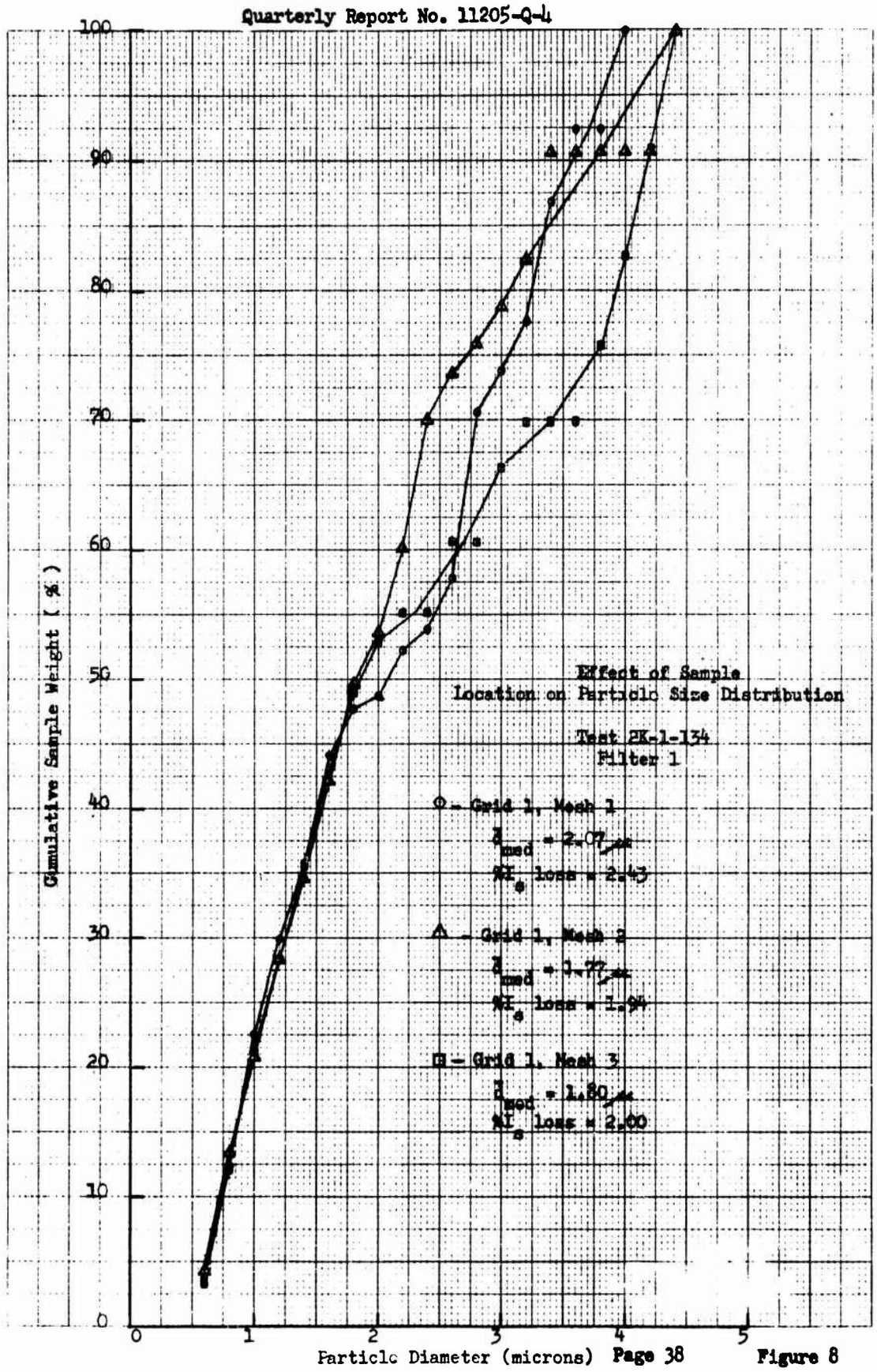

Figure 8

15K Performance Demonstration Plan

A_e/A_t / MR	7	50	100
0.4		T-3	T-6
0.6	T-1 T-2	T-4	T-7
0.8		T-5	T-8

CR = 5.5

L^* = 105 in.

P_c = 1500 psia

F = 15,000 lb

Figure 9

2K Engine Test Plan

	CR	3						6					
		9/7 (S)		50 (T)		100 (T)		9/7 (S)		50 (T)		100 (T)	
MR	P_c \ L*	60	90	60	90	60	90	60	90	60	90	60	90
0.4	500												
	1000												
	1500	25		5		6							
0.6	500	48	10	1		2							
	1000	45	8	3		4							
	1500	24		9		10		7					
0.8	500												
	1000												
	1500	28		7		8							

AL = 43% S - Test 11 @ CR = 3, = 7, L* = 33, MR = 0.6, P_c = 500
AL = 33% S - Tests 13, 14 @ CR = 3, = 9, L* = 63, MR = 0.6, P_c = 1000
AL = 50% S - Tests 15, 16

Spare Tests - 2

Figure 10

of particle samples collected during each test. Results of this work are reported in subsequent sections of this report.

2. Equipment and Hardware

Past reports (References 1, 2, and 3) have included detailed descriptions of the originally selected engine and feed system configurations as well as of the modifications that have been affected since the start of testing. For convenience, only brief descriptions of the major test items as they now appear shall be included in this report.

a. 2K Hardware

The injectors used successfully at the 2000-lb-thrust level are similar in design to those proved successful during the Improved Titan Predevelopment Program (Contract AF 04(694)-212). They consist of radially-drilled oxidizer channels feeding impinging oxidizer doublets and fuel showerhead orifices that are fed from a fuel plenum above the N_2O_4 circuit.

Individual injector size requirements (dictated by the three desired chamber pressures and two contraction ratios) have been met by drilling the injector pattern only in that portion of the face that matches the specific chamber cross-sectional area. A schematic of each injector size is shown in Figure 11. In all cases, the number and size of fuel and oxidizer orifices are the same. Only the relative spacing between orifices has been changed in expanding the pattern from one face area to the next.

The metal (4130 steel) chamber shells are designed to allow versatility over a range of engine geometries (Figure 12). All shells

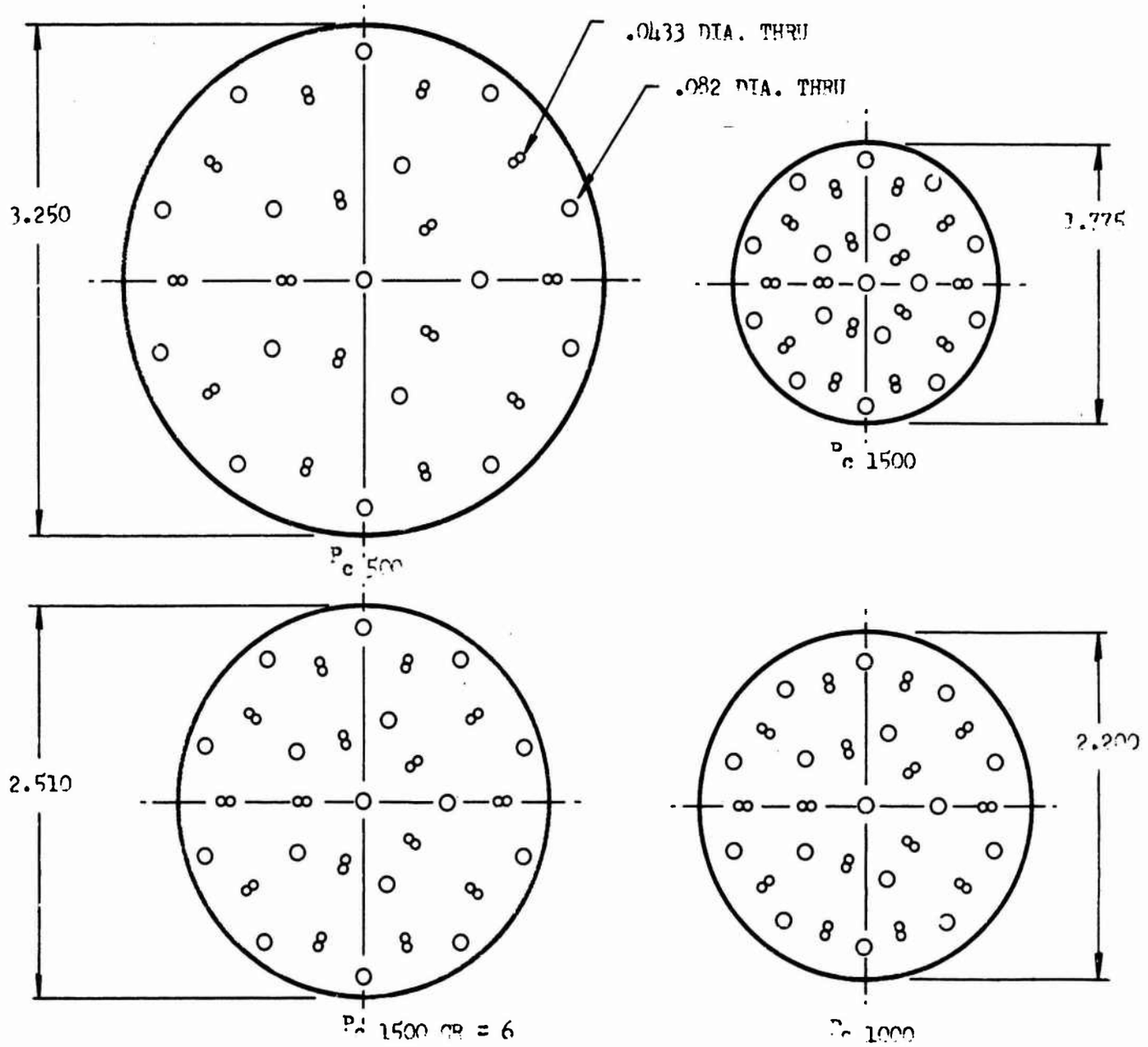

Figure 11 2K Injector Pattern

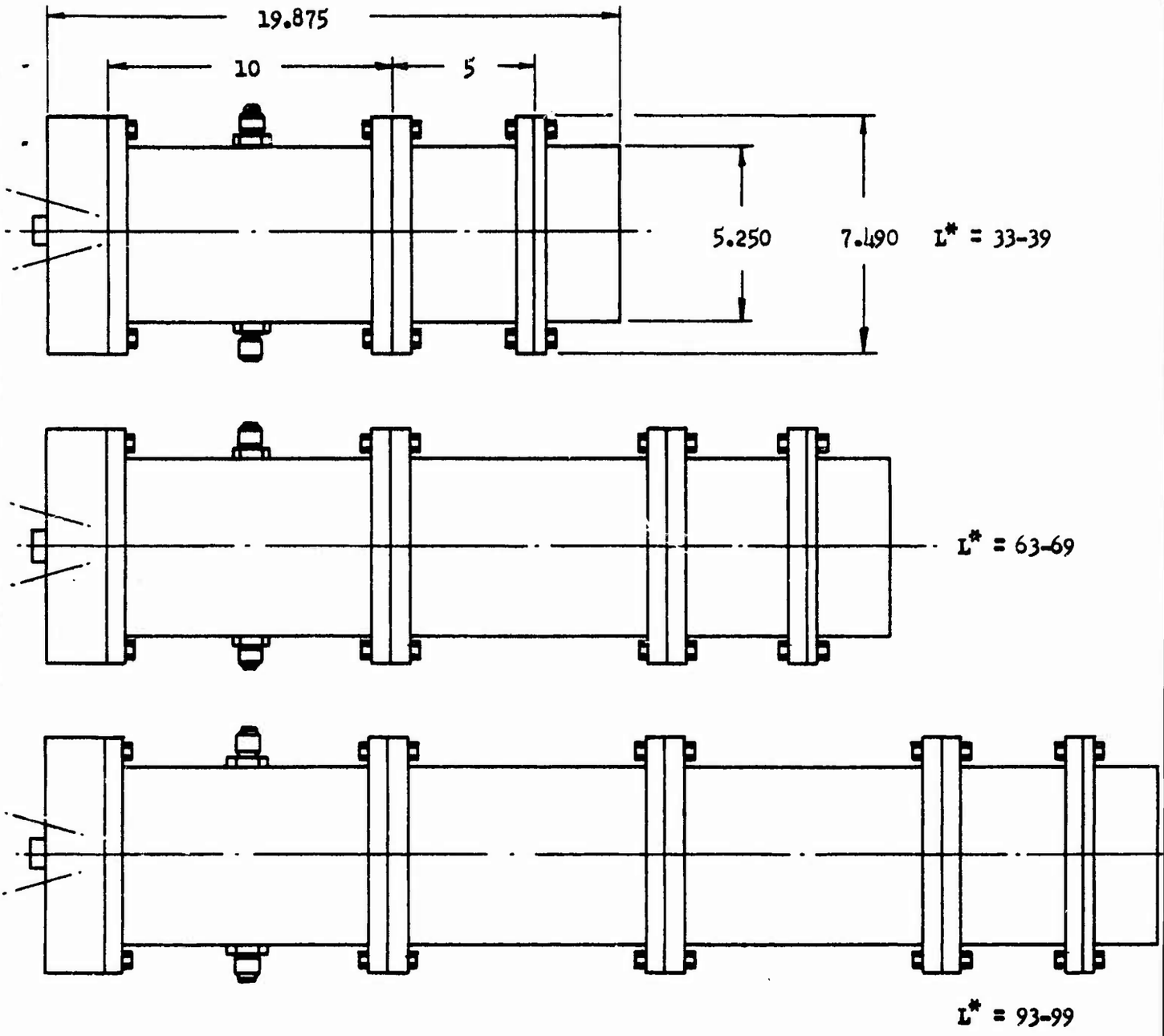

Typical Thrust Chamber Assembly

Figure 12

are one of two lengths and have a constant internal diameter. Because of this constant diameter, each shell can be used with any insulation insert, thus eliminating the need for a number of individually sized and matched casing-insert sets. The lengths, 10- and 5-in., were chosen on the basis of the desired range of characteristic length and contraction ratio. A 10-in. casing provides 30 L^* for the assemblies with 3:1 contraction ratio. The 5-in. casings provide a 30 L^* for the assemblies with a 6:1 contraction ratio and can be used interchangeably with all throat assemblies. Thus, any chamber configuration can be achieved by varying only the internal insulation and number of segments.

The chamber and nozzle inserts are, in all cases, ATJ commercial grade graphite. The chamber inserts are all of the same external dimension; only the internal bore diameter and mating end contours vary depending upon the pressure level and location in the assembly. RTV-60 silicone rubber is used to seal the liner in the metal can and to provide protection against hot gas leaks at all joints within the engine. Additional protection against thermal failure of the metal can is provided by phenolic seal rings at all joints and by O-rings at each chamber interface (Figure 13). Leak protection is provided at the chamber-injector interface by a layer of zinc chromate putty applied during engine installation and by an O-ring at the mating surface of the injector and chamber can.

The nozzle inserts employed are solid ATJ graphite. These inserts comprise the convergent region, the throat, and the divergent section to an area ratio of 5:1. In all cases, the convergent and divergent angles are 15°;

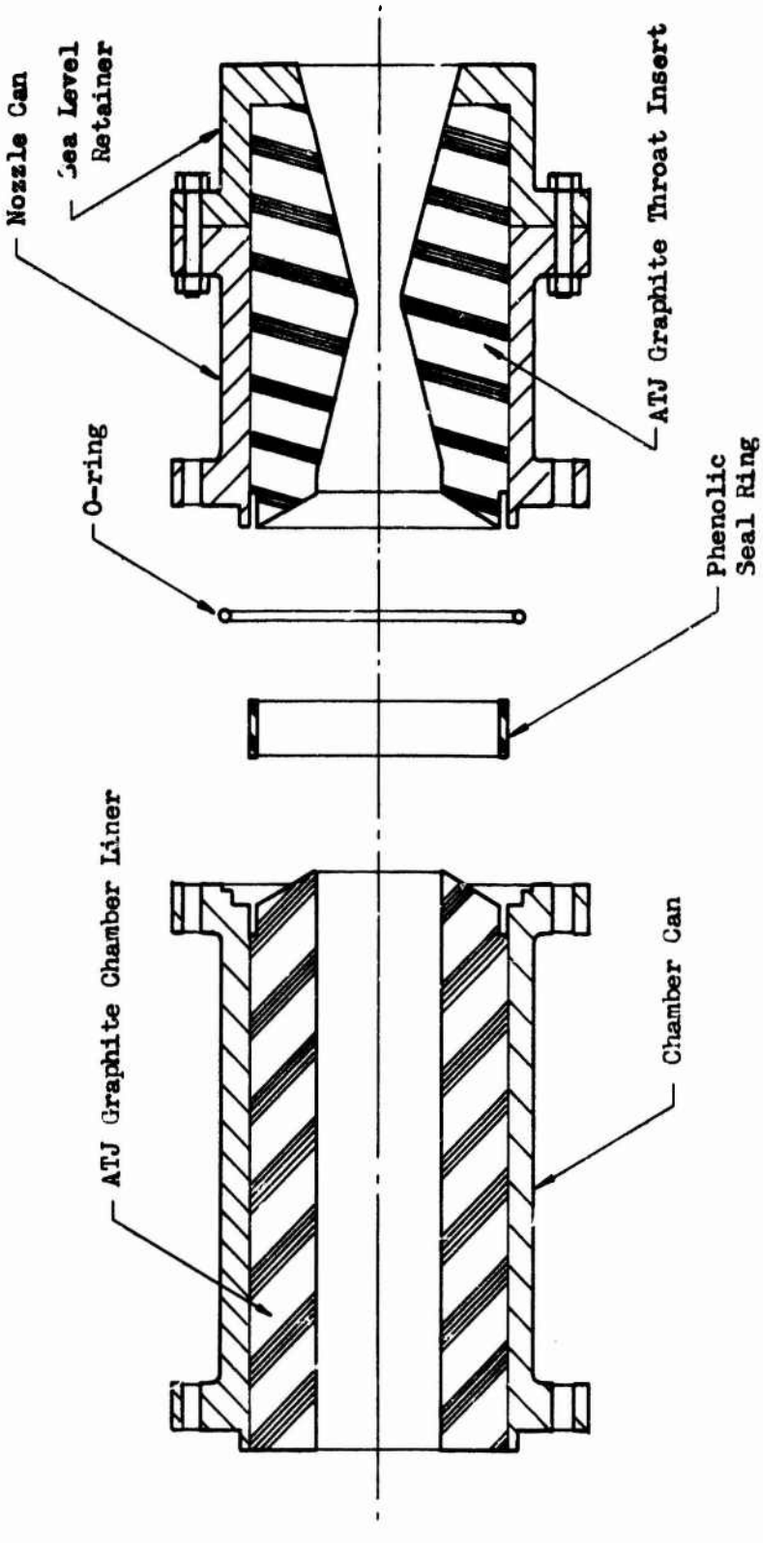

Typical Nozzle-Chamber Design

Figure 13

the radius of curvature both upstream and downstream of the throat plane is 6 times the throat radius. As with the chamber liners, RTV-60 rubber is used to seal the nozzles in the metal can.

The sea level retainers and altitude extensions, similar in design except for exit area ratio, mate to the graphite nozzle at an area ratio of 5:1. A hot gas seal is provided at the graphite-metal interface by a layer of zinc chromate putty.

b. 15K Hardware

Selection of the injector to be used with the 15,000-lb-thrust systems was based on the results of the injector development tests conducted during the Improved Titan Predevelopment Program (Reference 7). Similar to the injector to be used with the 2K hardware, this injector consists of alternating rings of fuel showerhead and impinging-oxidizer orifices. The fuel is fed through a reservoir at the back of the injector; oxidizer is fed to the orifices through an internal oxidizer torus and radially drilled channels.

The chamber assemblies for the 15K hardware are identical to those phenolic components originally intended for use in the 2K tests. The nozzles and nozzle extensions are similar to the hardware now used at the 2K level.

c. Test Stand Construction

(1) Fuel Feed System

The fuel feed system now used in this program is shown schematically in Figure 14. Basically, the flow path is as follows:

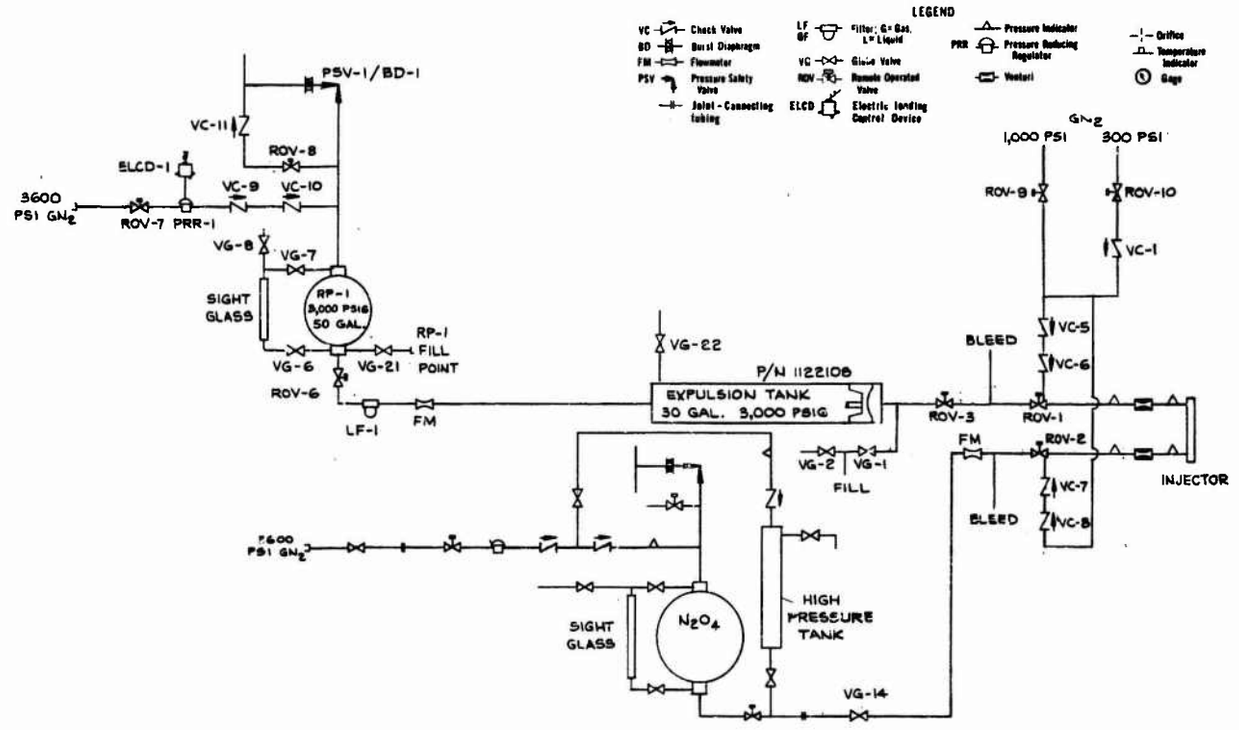

Figure 146 Two-Phase Flow Feed System Schematic

High pressure GN_2 (3600 psia) is fed, through a regulator, into the top of the 50-gallon RP-1 storage vessel. The pressurized RP-1 flows from the bottom of the tank through a safety valve (ROV-6), flow meter, and into the pressurant side of the 30-gallon gel expulsion tank. The Alumizine gel, forced out of the tank in volumetric proportion to the incoming flow rate of RP-1, flows through a safety valve (ROV-3), thrust chamber valve (ROV-1), flow-control venturi, pressure-control orifice, and into the injector. Supplementry components in the fuel feed system consist of an automatic 300 psia GN_2 purge connected to the thrust chamber valve, and a manual 1500 psia GN_2 purge, also plumbed into the TCV. A sight glass on the RP-1 tank allows visualization of the liquid and gel content of the system. All remote-operated valves are actuated by 28 volts DC. The fuel thrust chamber valve is operated pneumatically; a supplementry hydraulic system controls the rise rate of the pintle.

(2) Oxidizer Feed System

The oxidizer feed system, shown schematically in Figure 14, consists of a large N_2O_4 storage vessel with sight glass, a smaller high-pressure (3600 psia) N_2O_4 run tank, flow meter, thrust chamber valve, flow-control venturi, and pressure-control orifice. Associated plumbing supplies high pressure GN_2 to the tanks and purge circuits. As in the fuel system, all remote-operated valves are actuated by 28 volts DC; the oxidizer thrust chamber valve is pneumatically operated and hydraulically controlled.

(3) Engine Mount

The 2K engines used in this program are mounted as shown in Figure 15. The engine rests on a flexure mounted table, which in turn

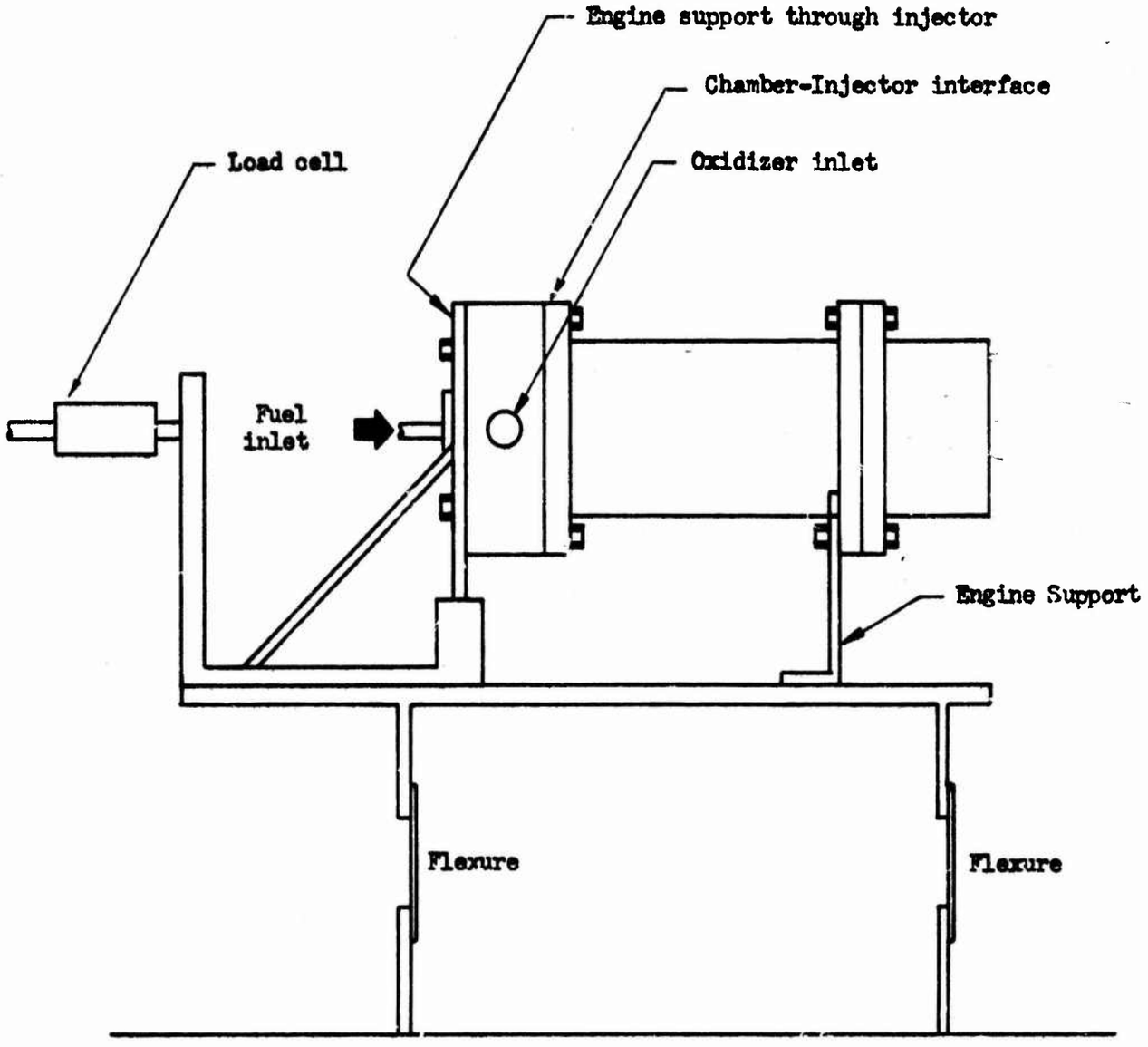

2K Engine Mount

Figure 15

is connected to the thrust take-out structure through an appropriate load cell. Engine support is provided at the injector and by a cradle at the second chamber flange. The injector mount is fixed and connects to the engine independantly of the chamber assembly. This arrangement allows removal of the chamber at the injector face, thus eliminating the need to disconnect propellant feed lines after each test.

(4) Particle Sampler

The exhaust sampling apparatus used during 2K sea level tests is shown in Figure 16. Essentially, this sampler consists of three Gelman filter samplers, each located at the exit of an electrostatic precipitator (Reference 1 - 3). A solenoid-operated shutter in front of each precipitator inlet precludes sampling of the stream during transient periods and allows preselection of the sampling period during steady state operation. The rigid support structure provides collector alignment at three discrete points in the exhaust plume.

3. Test Program Results

a. Test Summaries

As of this report period, 42 sea level 2K tests have been conducted. The first 29 of these tests were discussed in detail in Reference 3 and will not be repeated in this report. Rather, a brief summary of the first 29 tests, plus a detailed description of the 13 tests conducted during this report period are presented in the following paragraphs.

(1) Tests 2K-1-101 through 2K-1-104A

Each of the initial five tests evidenced chamber and injector manifold pressure oscillation, propellant weight flow oscillations, and

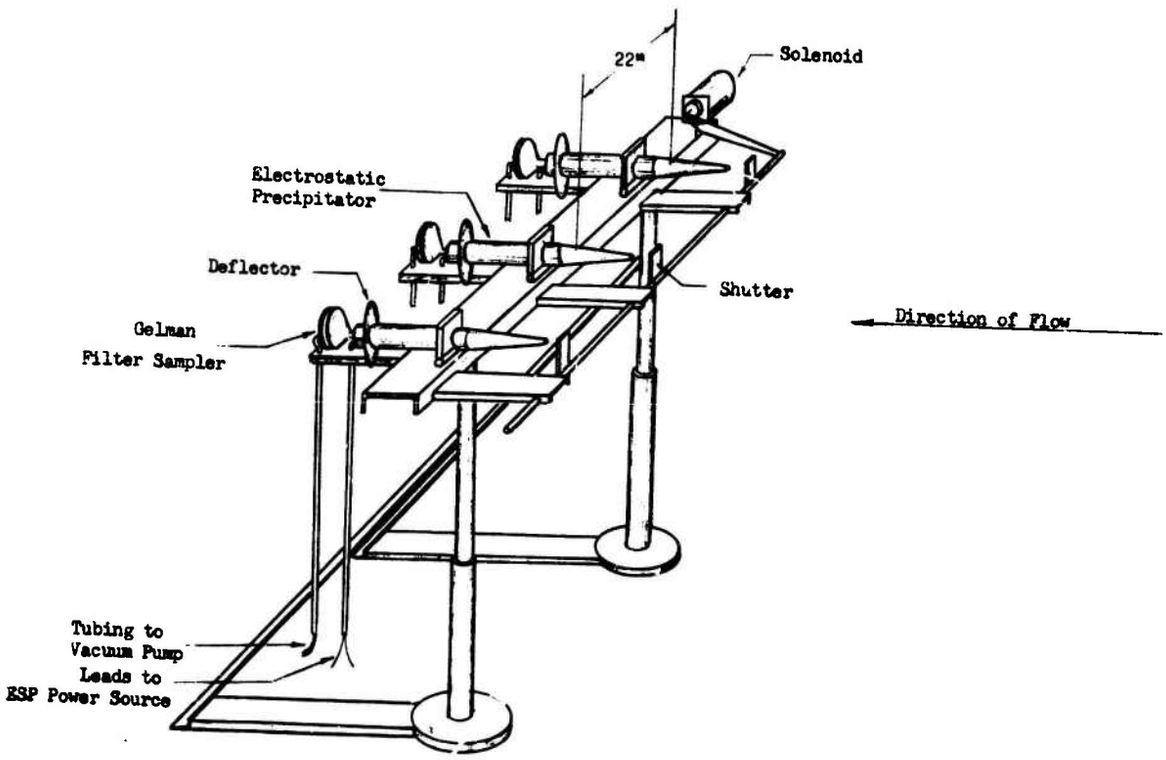

Figure 16 Exhaust Plume Sampling Apparatus

inordinately high pressure drops across the injector orifices. In an effort to solve these problems, the oxidizer venturi manifold was removed from the feed system and, as a check, the injectors were returned to the hydraulics laboratory for redetermination of injector resistances. Both efforts proved unnecessary, since the injector resistances were found to be identical to the prefire values, and further, the same type of oscillations were noted during test 2K-1-104A, which was conducted without the venturi header.

Following test -104A, a series of cold flow tests (using water) was conducted on the oxidizer feed circuit. Conclusions drawn from these tests were as follows:

(a) The source of oscillations in the oxidizer feed circuit was the cavitating venturi.

(b) The controlling factor in predicting the magnitude of the oscillations produced is the pressure drop across the venturi. (When operating at a low pressure drop/high recovery factor, the venturi produced an oscillation of lowest amplitude.)

(c) Restriction of the flow both upstream and downstream of the venturi would harden the system to facilitate a reduction in the amplitude of the oscillations and to prevent initiation of oscillation by disturbances from other sources.

(d) An orifice downstream of the venturi through which most of the system ΔP can be obtained is necessary to allow the venturi to operate at a high recovery factor.

The factors noted from the results of these cold flow tests were incorporated prior to test 2K-1-105. The oxidizer propellant lines were reduced from 1-in. tubing to 1/2-in. tubing. Also, orifices were placed in both propellant lines at the injector inlet to allow operation of the cavitating venturis at a high recovery factor. These orifices were sized when possible, considering tank pressure limitations, to provide a total orifice-injector pressure drop equal to or greater than one-half the desired chamber pressure and thus satisfy the gain stability criterion.

(2) Tests 2K-1-105 through 2K-1-108

Of the following four tests, two, one at a chamber pressure of 500 psia and one at 1000 psia, were conducted successfully. The remaining tests, both at a pressure level of 1500 psia, were unstable. In an effort to solve the stability problem, the venturi was removed from the N_2O_4 side during test -108 and replaced with an orifice. The resulting lack of oxidizer flow control during the start transient resulted in a pressure spike which fractured the throat assembly and expelled the chamber liner from the engine.

Subsequent investigation of this latter test established the fact that a method of positively controlling the transient propellant flow rise rate into the chamber was necessary. The necessity for modification of the thrust chamber valves was apparent. The addition of the hydraulic pintle control system previously discussed in Reference 3 was made before further testing was conducted.

(3) Tests 2K-1-109 through 2K-1-113

The five tests following valve modification were successful with the exception of test 2K-1-112, which was run at a pressure of 1500 psia. A review of all tests through -113, however, led to the conclusion that, while the oscillation problem appeared to be solved, the erosion rates of the phenolic engine components was too excessive to warrant further use. Therefore, ATJ graphite components were procurred before further testing was done.

(4) Tests 2K-1-113A through 2K-1-125

Despite the successful operation of a previous high pressure test (2K-1-113), further testing showed that an oscillation problem was persisting at chamber pressures above 1100 psia. Limited success was achieved with the relocation of the flow control venturis from their original location to a new position immediately downstream of the thrust chamber valves. Despite repeated successes at all other conditions, it was noted that the tests of a 93 L^*, 3:1 contraction ratio engine, operated at a chamber pressure of 1500 psia, continued to be unstable. This particular test was, therefore, delayed. Through test -125, valid data points had been attained for three tests at 500 psia chamber pressure, two tests at a pressure level of 1000 psia, and two tests at a pressure of 1500 psia and characteristic length (L^*) of 63 inches.

(5) Test 2K-1-126

This test, the first to be run at a contraction ratio of 6:1, was successful in that there were no pressure oscillations and the erosion

of the graphite hardware was not significant. As in past tests, both orifices and venturis were used in each propellant feed line. The total pressure drop across the oxidizer orifice-injector combination was 736 psia; the drop across the fuel circuit was 196 psia. The chamber pressure attained was 1492 psia.

As stated above, the erosion of the graphite was minor. This represented a significant improvement over the original phenolic hardware, since the engine length at this L^* and contraction ratio was only 10 inches. The throat eroded approximately .060 inches in diameter during the three second firing duration. The convergent and throat regions were entirely circular in cross-section. No gouging of the divergent section was evident.

(6) Test 2K-1-127

This test, conducted at an L^* of 93 inches, contraction ratio of three, and chamber pressure of 1470 psia, was unsuccessful in that pressure oscillations of 650 cps were noted. The pressure drop across the oxidizer orifice-injector circuit was 738 psia; that across the fuel circuit was 200 psia.

Since hardware erosion was minimal, both in terms of graphite erosion and injector face damage, the engine was scheduled to be fired at a later date.

(7) Test 2K-1-128

This test was run to complete the mixture ratio survey required during the sea level tests. The engine employed had an L^* of 63 inches, contraction ratio of 3, and was operated at 1465 psia chamber pressure. The mixture ratio achieved was 0.768. This test was successful in that there were no evident oscillations in any pressure trace. Pressure drops across the propellant injector circuits were 900 psia and 200 psia for the oxidizer and fuel sides respectively.

Hardware erosion was evident in the throat (10% increase in diameter) and on the injector face. The face pitting of the injector was localized to those areas between orifices and thus presented no problems that would preclude refire.

(8) Tests 2K-1-129 and 2K-1-130

The next two tests in the sea level series were conducted in an effort to achieve stable operation at the conditions of 93 L^*, contraction ratio of 3:1, and chamber pressure of 1500 psia. In both tests, the pressure drop across the oxidizer orifice-injector circuit was maximized to attain the gain stabilization criterion $\frac{2\Delta P}{P_c} \geq 1$ discussed in past reports (References 2 and 3). This tactic was ineffectual in both tests; oscillations of 700 cps were observed in all pressure traces.

(9) Tests 2K-1-131 and 2K-1-132

Based upon the results of the previous two tests, the decision was made to rerun the large L^*, high pressure engine with no venturis and

achieve stable engine operation when testing at the conditions of 1500 P_c, 93 L^*, and 3:1 contraction ratio. The second problem not mentioned previously was the observed inconsistencies in the operation of the electrostatic precipitators used as particle samplers. These problems, and their solutions will be discussed separately in the following paragraphs.

As discussed previously, results observed during test 2K-1-132 verified the existance of an injector-chamber dynamic coupling which, under certain conditions, resulted in unstable engine operation. Following this test, a complete analysis of the injector dynamics was conducted. Using the analytical techniques of Reference 8, it was found that, for the 2K injectors operated at 1500 P_c, the inertance of the oxidizer circuit, combined with the capacitive effects of the oxidizer manifold volume, resulted in a resonance frequency of 650 cps. Because this resonance occurred downstream of the orifice, the pressure drop across the orifice was ineffective in stabilizing the system. The fact that the oscillations were noted only when using the 93 L^* chamber was due to the coincidental similarity between the injector oscillatory frequency and the natural longitudinal mode associated with the long engine. This similarity resulted in an inherent system gain capable of amplifying the manifold oscillations and nullifying the injector orifice resistance. This condition, peculiar to the particular injector-chamber design and operating pressure, cannot be interpreted to imply high pressure combustion instability. In fact, at the shorter lengths, the gain of the chambers was low. The injector orifice resistance, then, was capable of isolating the manifold resonance and thus provide stable operation.

PAGES 57_58_MISSING

To solve the problem, extensive modifications to the injectors would be required. It may be seen from Figure 17, a plot of stability zones as a funtion of manifold volume and injector orifice pressure drop, that either the oxidizer manifold volume would have to be reduced by a factor of 20 or the injector drop would have to be increased to 750 psi. Because either course would significantly change the injector characteristics, direct comparison between sea level data and subsequent altitude tests would be impossible. Therefore, further testing at the high-pressure, large L^* condition was eliminated from the test plan.

The second problem encountered was inconsistent operation of the electrostatic precipitators. These samplers, chosen as the primary method of particle collection based on their performance during the pre-experimental analysis phase, were employed during all sea level 2K tests in conjunction with a backup series of evacuated Gelman filter samplers. Analysis of the samples collected during initial tests showed heavy deposits in all regions of the precipitator body. As testing progressed, it was noted that the deposits on the filter-paper patches within the precipitator became thinner, even though no differences in deposition of the aluminum sampling paddle could be determined. This phenomenon persisted, even though the precipitator electrodes and power packs were replaced. Subsequent monitoring of the voltage across the precipitator showed the occurance of repeated sparking, or discharge, within the sampler during a firing. Reference (9) states that this sparking, in some cases, significantly redistributed the particles

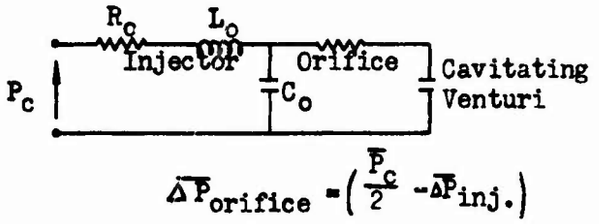

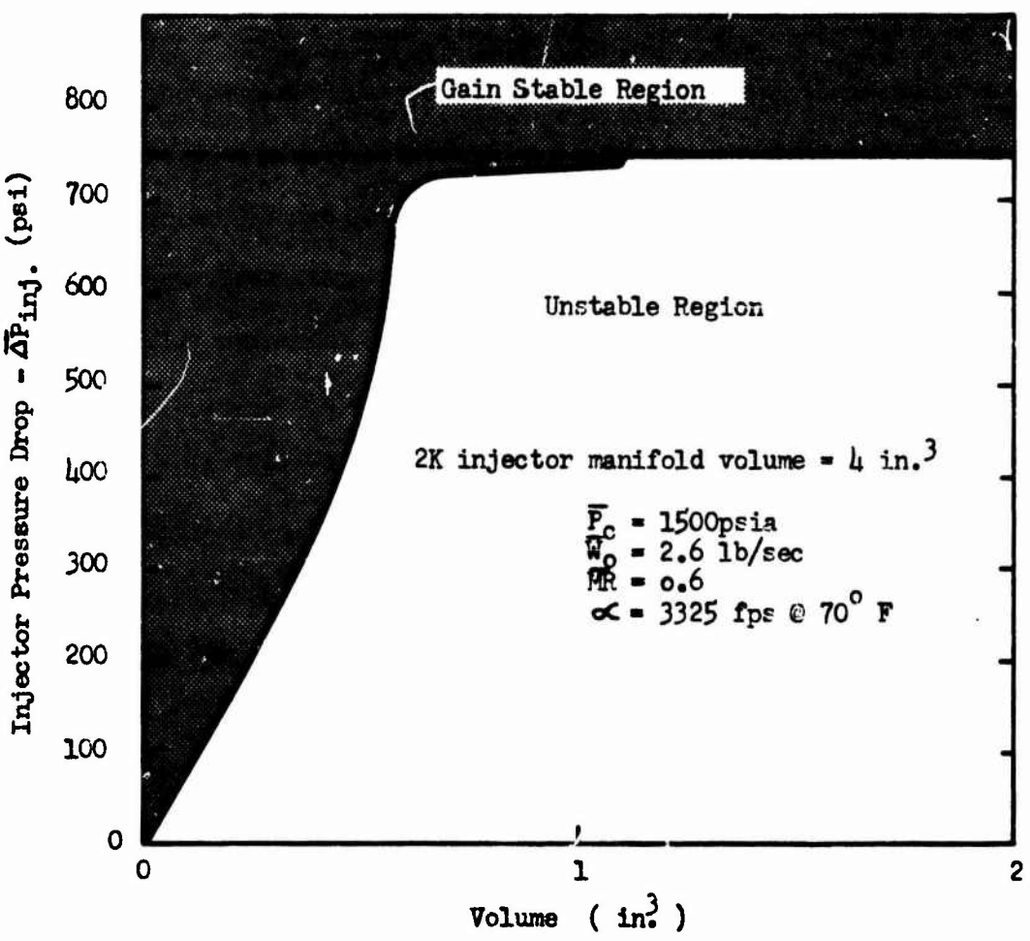

(volume downstream of orifice including injector)

Figure 17

collected on the sampling strip and, thus, precluded the measurement of a valid particle sample.

Checks of the samples obtained on the Gelman filters showed no deviation that could be attributed to a breakdown in the operation of the precipitator units. Since previous analysis of collected particle samples showed the Gelman filters to provide the same particle size and distribution as the precipitator, the decision was made to discontinue analysis of the precipitator samples and to evaluate only those samples collected from the Gelman filters. The power units were subsequently removed from the outboard sampling locations; for consistency between all tests, however, use of the precipitator was continued at the middle location. This mode of operation had no effect on the validity of the samples collected, since no consistent variation in the results obtained from each of the three filters could be detected.

C. TEST PROGRAM RESULTS

1. General

As of this reporting period, 42 sea level 2K engine tests have been conducted. The basic engine operating conditions, performance levels, and remarks as to the validity of each of these tests are presented in Table IV. It may be seen from this table that a large number of the tests are assumed to be invalid because of chamber pressure oscillations and for severe hardware erosion. No final performance data or particle size information has been presented for these anomalous tests.

Tables V and VI present the results of those thirteen tests designated in Table IV as being valid. Table V presents the actual steady state engine operating conditions as well as the attained levels of performance; Table VI includes the values calculated for each of the pertinent engine losses associated with each valid test configuration.

The majority of the losses presented in Table VI are normally evaluated in the performance determination of any rocket engine system. As expected, nozzle/chamber heat transfer and friction will be influenced by the engine component design. The losses due to mixture ratio distribution, energy release efficiency, and two-phase flow are, on the other hand, influenced primarily by the injector type and thrust chamber configuration.

TABLE IV

SUMMARY OF SEA LEVEL TESTS (U)

Test Sequence No.	Test No.	Test Date	P_c, psia	CR	L^*, in.	A_e/A_t	$\dot{w}_t$, lb/sec	MR	I_s(vac), sec	% Theo. I_s	Remarks
2K-1-101	S-1	2/22/66	1300	3	33	8.6	6.72	0.607	281.8	87.2	First calibration test: Assumed invalid due to oscillations in P_c, weight flow.
-102	S-1	2/24/66	1305	3	33	8.7	7.57	0.577	265.9	80.8	Second calibration test: Assumed invalid due to oscillations in P_c, weight flow.
-103	S-10	2/25/66	450	3	95	3.9	7.85	0.618	267.2	90.7	Assumed invalid due to chamber pressure oscillations.
-104	S-11	2/28/66	340	3	35	3.4	7.95	0.600	224.7	78.1	Assumed invalid due to chamber pressure oscillations.
-104A	S-11	3/2/66	298	3	35	2.8	7.87	0.588	234.3	82.9	Assumed invalid due to chamber pressure oscillations and excessive hardware erosion.
-105	S-11	3/14/66	434	3	35	6.6	7.86	0.596	253.0	80.8	Assumed invalid due to excessive chamber erosion. No oscillation.

TABLE IV (Cont'd)

Test Sequence No.	Test No.	Test Date	P_c, psia	CR	L^*, in.	A_e/A_t	$\dot{w}_t$, lb/sec	MR	I_s(vac), sec	% Theo. I_s	Remarks
-106	S-5	3/15/66	1522	3	93	9.3	7.24	0.585	290.2	89.2	Assumed invalid due to chamber pressure oscillations.
-107	S-8	3/16/66	986	3	93	8.7	7.28	0.587	297.6	92.1	No oscillations. Assumed invalid due to hardware erosion.
-108	S-1	3/21/66	----	3	33	---	----	----	----	----	No data - Engine malfunction.
-109	S-10	4/5/66	522	3	95	3.6	7.91	0.606	282.8	96.4	Assumed invalid due to hardware erosion, fuel flow anomalies. No oscillations.
-110	S-11	4/6/66	378	3	35	3.5*	7.94	0.610	246.8	84.8	Assumed invalid due to excessive hardware erosion. No oscillations.
-111	S-9	4/7/66	875	3	33	8.2	7.27	0.604	280.2	87.5	Assumed invalid due to excessive hardware erosion. No oscillations.
-112	S-5	4/7/66	1474	3	93	8.3	7.33	0.643	296.3	92.1	Assumed invalid due to chamber pressure oscillations.
-113	S-6	4/11/66	1241	3	33	6.59	7.68	0.745	281.5	89.9	Invalid due to excessive chamber erosion and nozzle fracture.
-113A	S-24	5/4/66	1435	3	63	7.44	7.24	0.563	301.5	94.7	Invalid due to chamber pressure oscillations.

TABLE IV (Cont'd)

Test Sequence No.	Test No.	Test Date	P_c, psia	CR	L^*, in.	A_e/A_t	$\dot{w}_t$, lb/sec	MR	$I_{s(vac)}$, sec	% Theo. I_s	Remarks
-114	S-5	5/4/66	1405	3	93	8.32	7.36	0.592	281.1	87.3	Invalid due to chamber pressure oscillations.
-114A	S-5	5/5/66	1315	3	93	7.80	7.62	0.638	286.6	89.6	Invalid due to chamber pressure oscillations.
-115	S-5	5/9/66	1168	3	93	7.40	6.72	0.653	279.6	87.1	Invalid due to low chamber pressure attained. No oscillations.
-115A	S-23	5/9/66	1068	3	93	6.50	7.24	0.778	285.4	91.6	Invalid due to low chamber pressure. No oscillations.
-116	S-24	5/11/66	1442	3	63	8.66	7.40	0.579	275.3	85.2	Invalid due to chamber pressure oscillations.
-117	S-24	5/12/66	1358	3	63	7.71	7.51	0.602	279.0	87.2	Valid test. No chamber pressure oscillations or significant hardware erosion.
-118	S-25	5/13/66	1433	3	63	8.42	7.26	0.413	268.5	86.3	Valid test. No oscillations or significant hardware erosion.
-119	S-28	5/16/66	1455	3	63	8.40	7.34	0.797	282.2	89.2	Assumed invalid due to a period in which chamber pressure oscillated.
-120	S-8	5/18/66	991	3	95	8.88	7.36	0.603	283.4	87.8	Valid test. No oscillations or hardware erosion.
-121	S-45	5/18/66	994	3	65	9.13	7.35	0.607	282.0	87.2	Valid test. No oscillations or hardware erosion.

TABLE IV (Cont'd)

Test Sequence No.	Test No.	Test Date	P_c, psia	CR	L^*, in.	A_e/A_t	$\dot{w}_t$, lb/sec	MR	I_s(vac), sec	% Theo. I_s	Remarks
-122	S-10	5/19/66	----	3	65	----	----	----	-----	----	No data - Millisedic data acquistion system malfunctioned.
-123	S-48	5/20/66	493	3	65	7.26	7.83	0.611	271.9	86.0	Valid test. No oscillations or hardware erosion.
-124	S-10	5/20/66	504	3	95	7.39	7.93	0.601	273.2	86.3	Valid test. No oscillations or hardware erosion.
-125	S-11	5/20/66	465	3	35	7.26	7.90	0.605	255.3	80.8	Valid test. No oscillations or hardware erosion.
-126	S-7	5/26/66	1492	6	63	9.00	7.57	0.598	274.9	85.1	Valid test. No oscillations or hardware erosion.
-127	S-5	5/26/66	1470	3	93	9.00	7.54	0.598	275.9	85.2	Invalid due to 650 cps chamber pressure oscillation.
-128	S-4	5/27/66	1465	3	63	9.00	7.40	0.768	281.3	88.5	Valid test. No oscillations or hardware erosion.
-129	S-5	5/27/66	1384	3	93	9.00	7.44	0.595	277.8	86.5	Invalid due to 700 cps chamber pressure oscillation.
-130	S-5	5/31/66	1460	3	93	9.00	7.58	0.560	278.5	86.6	Invalid due to 700 cps chamber pressure oscillation.
-131	S-5	6/2/66	1539	3	93	9.00	8.31	0.624	274.0	84.6	Invalid due to 650 cps pressure oscillation; max orifice drop.

TABLE IV (Cont'd)

Test Sequence No.	Test No.	Test Date	P_c, psia	CR	L^*, in.	A_e/A_t	$\dot{w}_t$, lb/sec	MR	$I_{s(vac)}$, sec	% Theo. I_s	Remarks
-132	S-5	6/2/66	----	3	93	9.00	----	-----	-----	----	Invalid due to 650 cps chamber pressure oscillations; data acquisition malfunction.
-133	S-12	6/6/66	1440	3	63	9.00	6.78	0.681	280.0	87.2	Invalid due to gel leak in fuel feed line.
-134	S-13	6/7/66	1415	3	63	9.00	6.98	0.665	291.4	89.3	Valid test; no oscillations or hardware erosion.
-135	S-14	6/7/66	1422	3	63	9.00	7.21	0.603	289.5	88.99	Valid test; no oscillations or hardware erosion.
-136	S-15	6/9/66	1341	3	63	9.00	7.27	0.598	269.6	85.91	Valid test; no oscillations or hardware erosion.
-137	S-16	6/10/66	1177	3	63	9.00	7.27	0.597	266.4	85.03	Valid test; no oscillations, low chamber pressure.
-138	S-5	6/14/66	----	3	93	9.00	----	-----	-----	----	Invalid due to malfunction of fuel thrust chamber valve.

TABLE V

TWO-PHASE FLOW PERFORMANCE SUMMARY (U)

Experimental Conditions

Seq. No.	Test Date	Test No.	PC	CR	L* Nom.		$\dot{w}_o$	$\dot{w}_f$	MR	$\dot{w}_t$	F(vac)	I_s(vac)	% Theo.	Theo. Perf. Exp. Cond.
-117	5/12/66	S-24	1370	2.63	61.9	7.71	2.84	4.67	0.607	7.51	2096	279.0	87.21	319.9
-118	5/13/66	S-25	1433	2.91	68.4	8.42	2.14	5.12	0.417	7.26	1949	268.5	86.31	311.1
-120	5/18/66	S-8	991	2.97	98.6	8.88	2.77	4.59	0.603	7.36	2086	283.4	87.77	322.9
-121	5/18/66	S-45	994	2.99	7.0	9.13	2.78	4.57	0.607	7.35	2072	282.0	87.25	323.2
-123	5/20/66	S-48	493	3.02	73.4	7.26	2.97	4.86	0.611	7.83	2128	271.9	86.02	316.1
-124	5/20/66	S-10	504	3.08	105.5	7.39	2.98	4.95	0.601	7.93	2165	273.2	86.29	316.6
-125	5/20/66	S-11	465	3.04	43.3	7.26	2.98	4.92	0.605	7.90	2017	255.3	80.77	316.1
-126	5/26/66	S-7	1492	5.77	76.0	8.51	2.83	4.74	0.598	7.57	2075	274.9	85.13	322.9
-128	5/27/66	S-4	1465	2.88	67.8	8.49	3.21	4.19	0.766	7.40	2079	281.3	88.54	317.7
-134	6/7/66	S-13	1415	2.98	70.0	8.80	2.79	4.19	0.665	6.98	2022	291.4	89.30	326.3
-135	6/7/66	S-14	1422	2.82	66.3	8.36	2.71	4.50	0.603	7.21	2075	289.5	88.99	325.3
-136	6/9/66	S-15	1341	2.89	68.0	8.54	2.71	4.56	0.594	7.27	1941	269.6	85.91	313.8
-137	6/10/66	S-16	1177	2.67	62.7	7.91	2.72	4.55	0.597	7.27	1898	266.4	85.03	313.3

TABLE VI - SUMMARY OF PERFORMANCE LOSSES

Test Seq. No.	I_s (Mixture Ratio Dist.) sec.	I_s (Nozzle Geom.) sec.	I_s (Nozzle Friction) sec.	I_s (Chamber Heat Transfer) sec.	I_s (Chamber Friction) sec.	I_s (Two-Phase Flow) sec.	I_s (Energy Release Loss) sec.	Particle Mass Median Diam. microns
2K-1-117	1.1	4.0	2.8	7.1	2.3	6.8	16.8	1.73
-118	+0.3	3.9	2.7	12.0	2.2	10.1	12.0	2.10
-120	1.3	4.1	3.0	9.8	2.6	11.0	7.7	2.51
-121	1.2	4.1	3.0	6.9	2.1	8.5	15.4	2.05
-123	1.0	3.9	2.8	7.4	1.7	6.4	21.0	1.87
-124	1.2	3.9	2.9	10.1	2.1	5.1	18.1	1.54
-125	1.1	3.6	2.8	4.9	1.3	5.1	42.0	1.55
-126	1.3	4.0	2.8	4.1	1.4	4.9	29.5	1.30
-128	0.2	4.2	2.9	8.2	3.0	4.4	13.5	1.32
-134	0.4	4.3	3.0	8.6	2.4	9.5	6.7	2.12
-135	0.4	4.3	3.0	8.4	2.4	5.5	11.8	1.36
-136	0.3	3.9	2.8	7.9	2.3	5.6	21.4	1.08
-137	0.3	3.9	2.8	8.0	2.3	9.1	20.5	1.80

The objectives of this program require first determination of the variability in applicable performance losses as a function of engine parameter, and second, to use the results to optimized engines of higher thrust levels. The sea level tests discussed in this section represent the completion of the first phase of these tasks. The following sections present the observed trends in mixture ratio distribution, particle size and two-phase flow loss, energy release loss, and overall engine efficiency as a function of variations in the major engine configuration and operating parameters. Analyses and experimentation to be conducted during the next report period will utilize these results in verifying the scaleability of the data and in predicting the performance levels of optimized 30K and 100K systems.

2. Mixture Ratio Distribution Versus Variable Engine Parameters

As seen in Table VI, the loss due to mixture ratio variation across the injector face is not significantly affected by variation in the parameters investigated. The greatest deviance from a nominal value occurs as the overall engine mixture ratio ($\dot{w}_o/\dot{w}_f$) is varied from 0.4 to 0.8. This is to be expected, since this parameter is the only one in which variation would alter the respective flow characteristics through the fuel and oxidizer orifices. In all cases, this loss was calculated as representing less than 1% of theoretical engine performance.

3. Particle Size Versus Variable Engine Parameters

The last row of Table VI shows the mass median particle diameter that was measured from the particle samples collected during each test. It is suspected at this time, based upon the results of subsequent particle analysis, that significant error may be present in these reported particle sizes. It is anticipated, however, that the reported trends of particle size with engine parameters are valid. The exhibited levels, may shift as corrected particle sizes are obtained. However, significant changes are not expected.

Figure 18 shows a plot of engine length (L) versus particle diameters presented in Table VI. It may be seen that the particle size tends to increase with an increase in the length of the combustion chamber. Such a relationship is repeated in Figures 19 and 20, which show particle size as a function of characteristic length (with constant contraction ratio) and contraction ratio (with constant L^*) respectively. This trend is consistent with the results of recent work performed by United Technology Center (Ref. 10) and with the results of past investigations performed at Aerojet-General Corporation (Ref. 11). In all cases, the trend of increasing particle size with an increase in engine length was observed.

Figure 21 shows the observed relationship between measured particle size and chamber pressure. It may be seen that no variation in particle size was detected as chamber pressure was varied from 500 to 1400 psia. This relationship is verified by the results of Dobbin's work

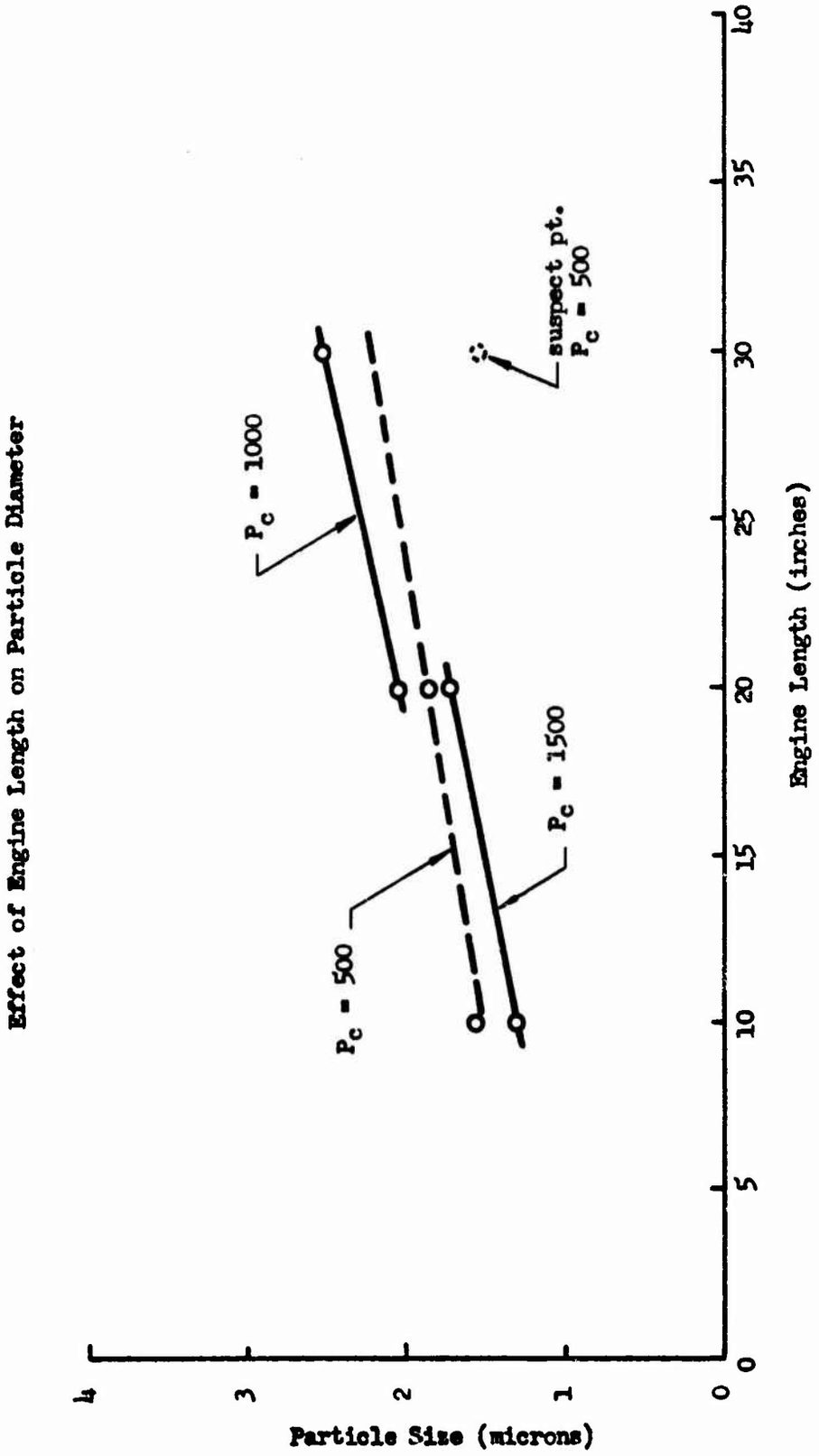
Effect of Engine Length on Particle Diameter
P_c = 1000
P_c = 500
P_c = 1500
P_c = 500
suspect pt.
Particle Size (microns)
Engine Length (inches)
0
1
2
3
4
0
5
10
15
20
25
30
35
40

Figure 18

EFFECT OF CHARACTERISTIC LENGTH ON PARTICLE DIAMETER

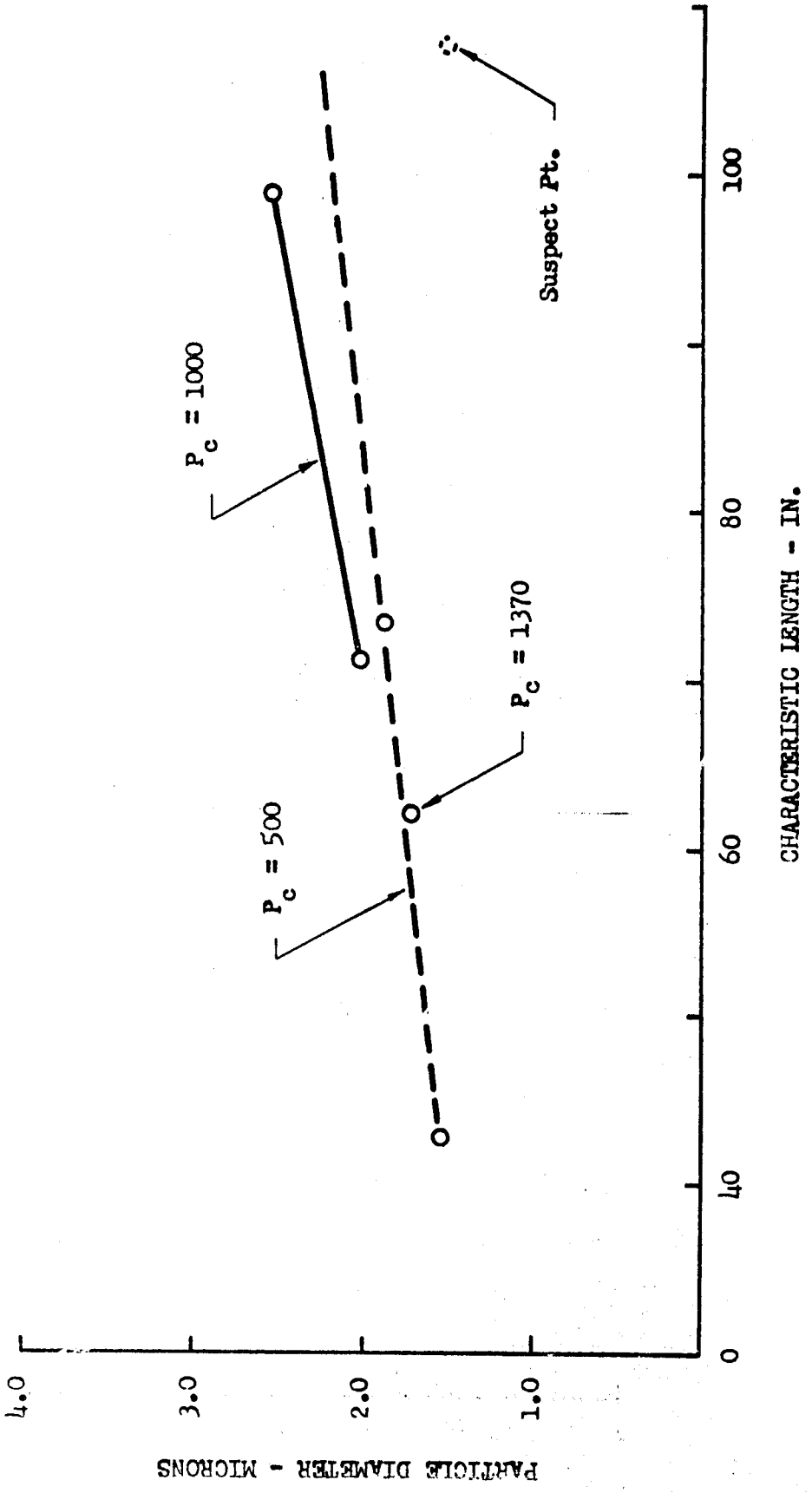

Figure 19

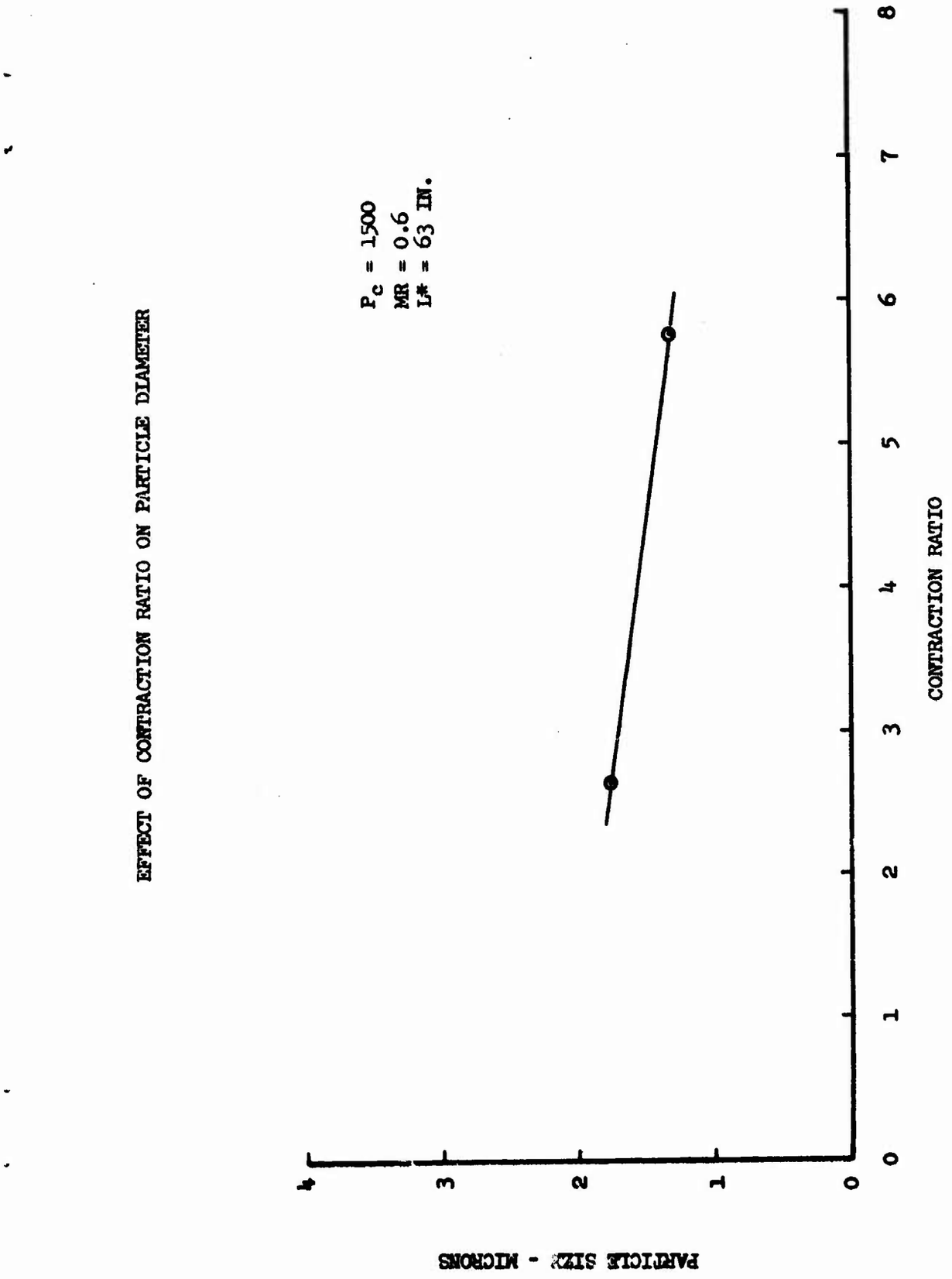
EFFECT OF CONTRACTION RATIO ON PARTICLE DIAMETER
P_c = 1500
MR = 0.6
L* = 63 IN.
PARTICLE SIZE - MICRONS
CONTRACTION RATIO
0
1
2
3
4
5
6
7
8

Figure 20

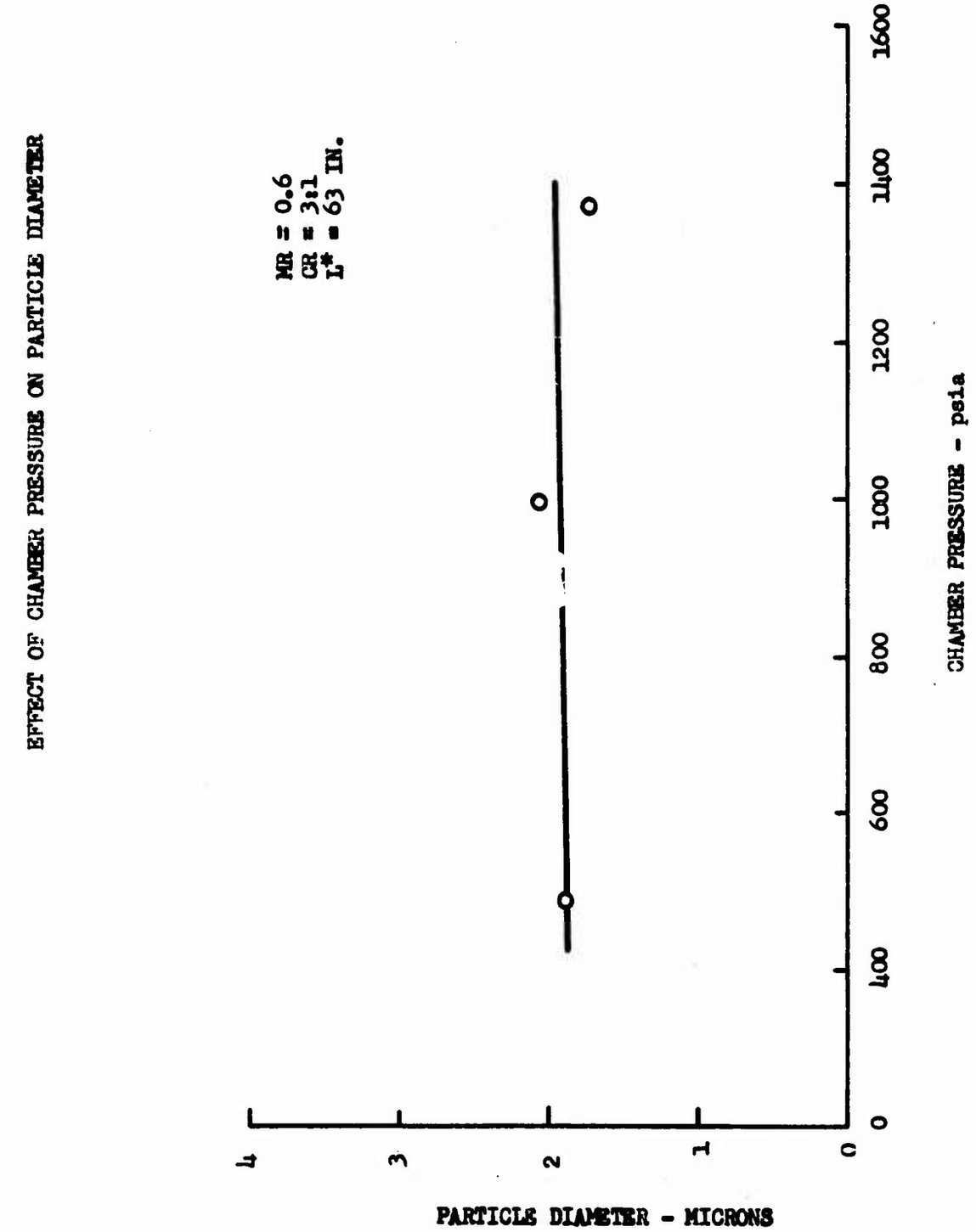
EFFECT OF CHAMBER PRESSURE ON PARTICLE DIAMETER
MR = 0.6
CR = 3:1
L* = 63 IN.
0
400
600
800
1000
1200
1400
1600
CHAMBER PRESSURE - psia
0
1
2
3
4
PARTICLE DIAMETER - MICRONS

Figure 21

(Ref. 10) and refuted by the results obtained by Sehgal (Ref. 10); each using a different technique in particle exhaust analysis. The method of exhaust sampling is expected to influence the results relative to two phase flow losses. As a consequence of obvious discrepancies between methods used in exhaust sampling and because of the lack of a suitable standard, it is difficult to ascertain the validity of reported data. Work is continuing in an effort to resolve this anomaly.

The observed relationship between particle diameter and mixture ratio is presented in Figure 22. The mechanism of particle combustion and growth that would explain this relationsip is not fully understood. Several particle combustion characteristics can be conjectured. Under conditions of relatively low chamber temperature (4000-5000°R), an aluminum-oxide coating can be formed around the injected particles which inhibits the burning rate of the metal and allows coated particles to pass unburned through the nozzle. At higher temperatures, the aluminum vaporizes and burns before the oxide can form; thus, particles must reform through nucleation and condensation at some point in the thrust chamber. These condensed-phase particles tend to be smaller than the originally injected particle. Since the 2K combustion temperature ranges from 5800°R to 7400°R at mixture ratios of 0.4 and 0.8 respectively, it is possible that the two regimes of burning characteristics have been included.

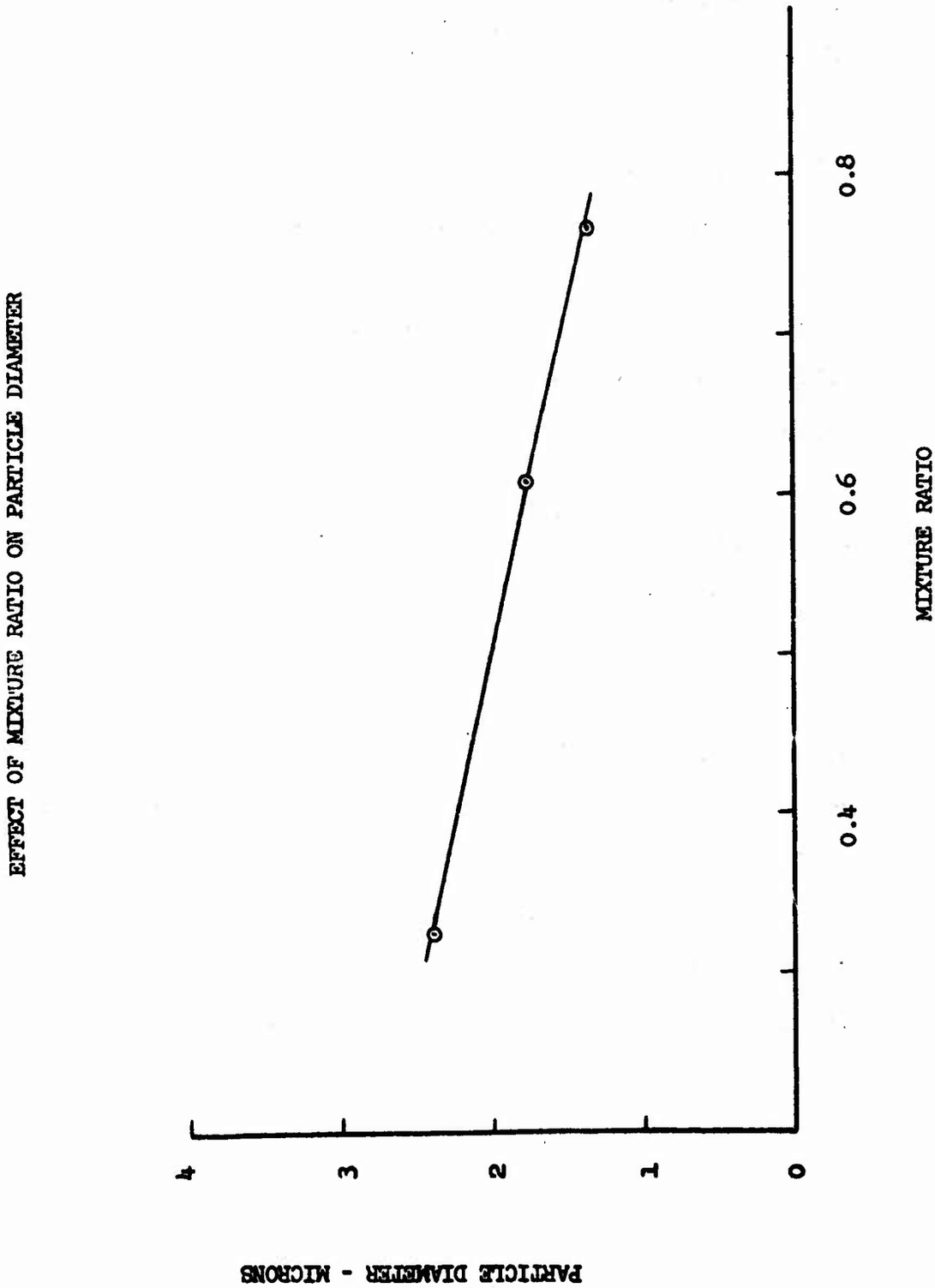
EFFECT OF MIXTURE RATIO ON PARTICLE DIAMETER
0.4
0.6
0.8
MIXTURE RATIO
0
1
2
3
4
PARTICLE DIAMETER - MICRONS

Figure 22

Another mechanism of particle growth that must be considered in explaining the observed trend deals with the concentration of particles present in the chamber and throat regions. This theory, presented by UTC in Reference 12, states that the particles grow in the convergent and throat regions due to agglomeration and coalescence, which in turn are functions of the density of the particles in these regions. Limited data shows that the greater the metal content of the propellant, the greater the degree of agglomeration in the finite nozzle entrance. Thus, at a mixture ratio of 0.4, the measured particle size should be larger due to the greater amount of aluminum injected into the chamber.

Figure 23 shows the effect of aluminum content in the fuel on measured particle size. The indicated decrease in particle diameter with increased metal content is contradictory to the theory presented in the previous paragraphs. Further analysis of the particles from these tests must be made before a firm relationship can be stated.

4. Two-Phase Flow Loss Versus Variable Engine Parameters

The relationships between the performance loss due to particles in the exhaust and the parameters L*, contraction ratio, chamber pressure, and mixture ratio are presented in Figures 24 through 27. It may be seen from these figures that, as would be expected, the losses due to particles exhibit the same trends as shown by the absolute particle size versus a given parameters. As stated previously, these curves are suspect until verification of the particle sizes can be obtained.

EFFECT OF PROPELLANT ON PARTICLE DIAMETER

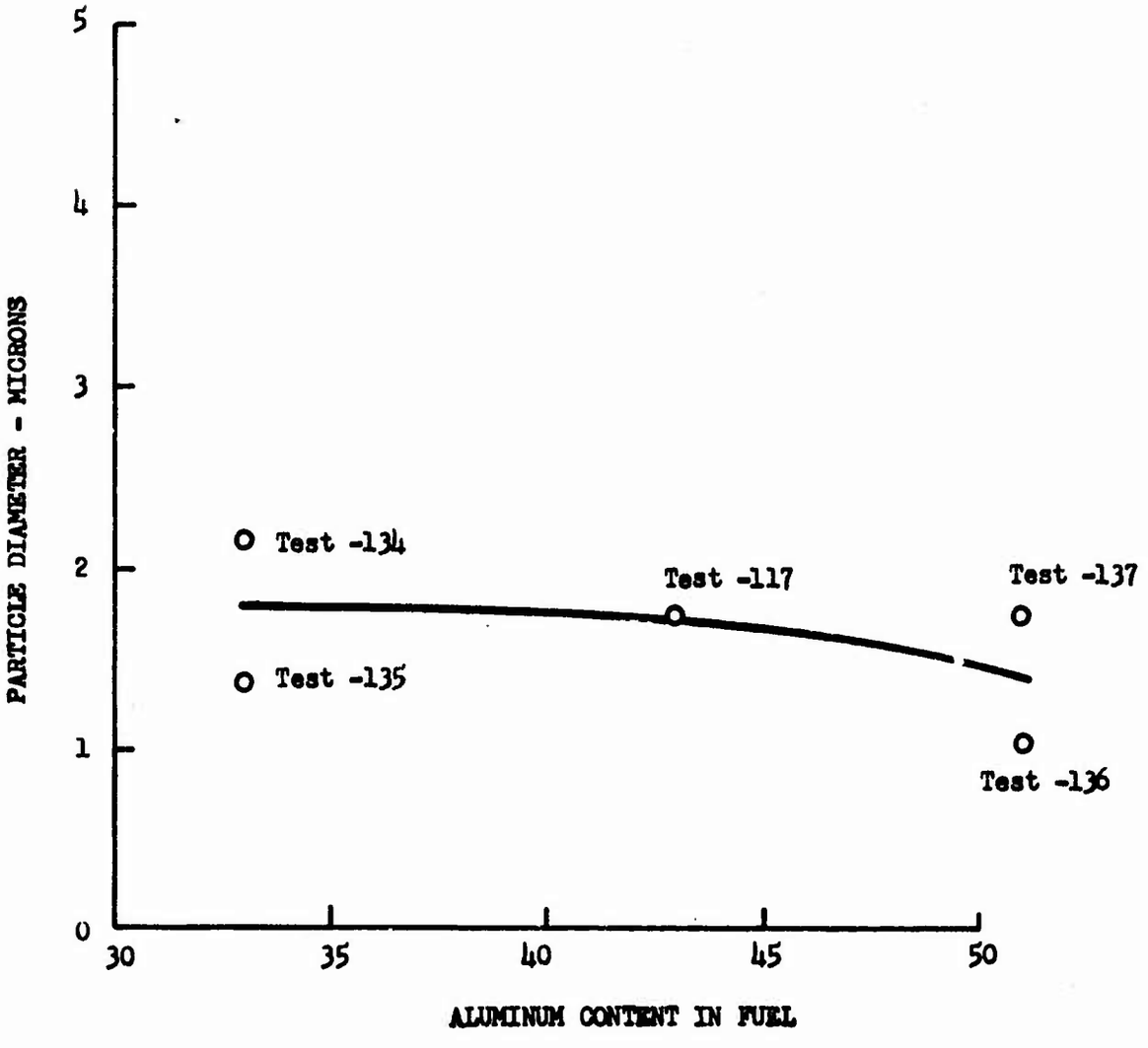

Figure 23

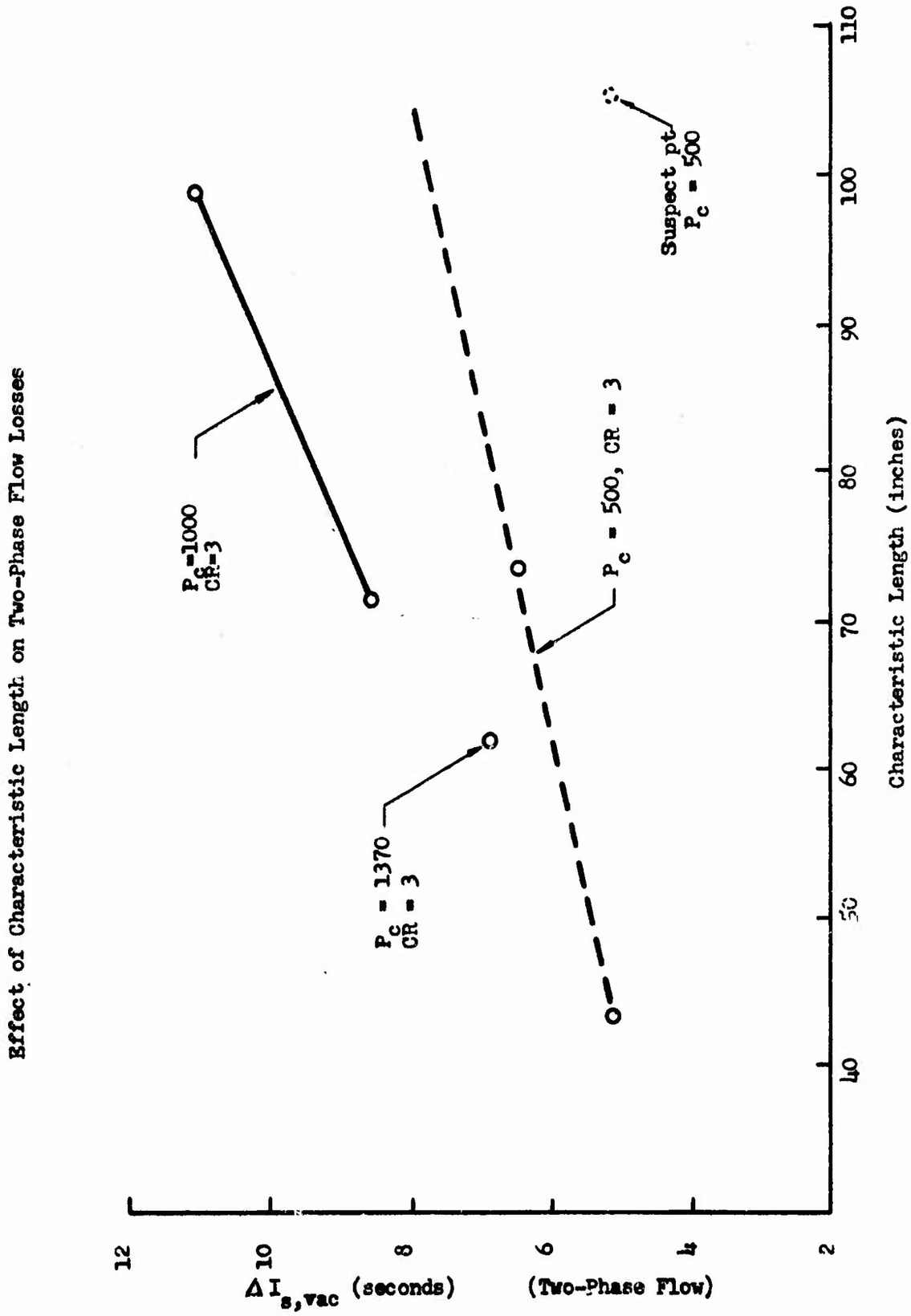
Effect of Characteristic Length on Two-Phase Flow Losses
P_c=1000
CR=3
P_c = 1370
CR = 3
P_c = 500, CR = 3
Suspect pt.
P_c = 500
12
10
8
6
4
2
$\Delta I_{s,vac}$ (seconds)
(Two-Phase Flow)
40
50
60
70
80
90
100
110
Characteristic Length (inches)

Figure 24

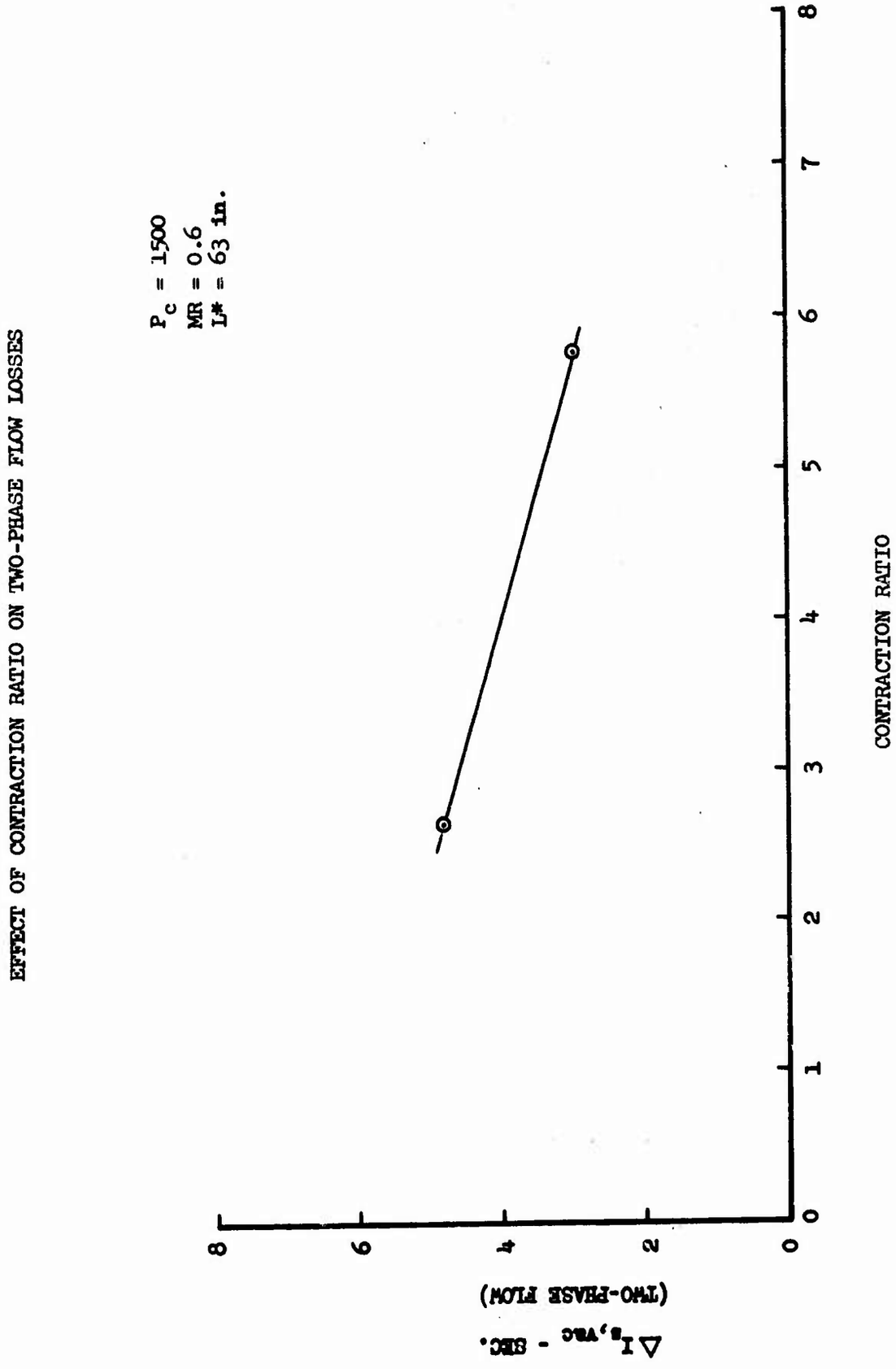

Figure 25
Page 82

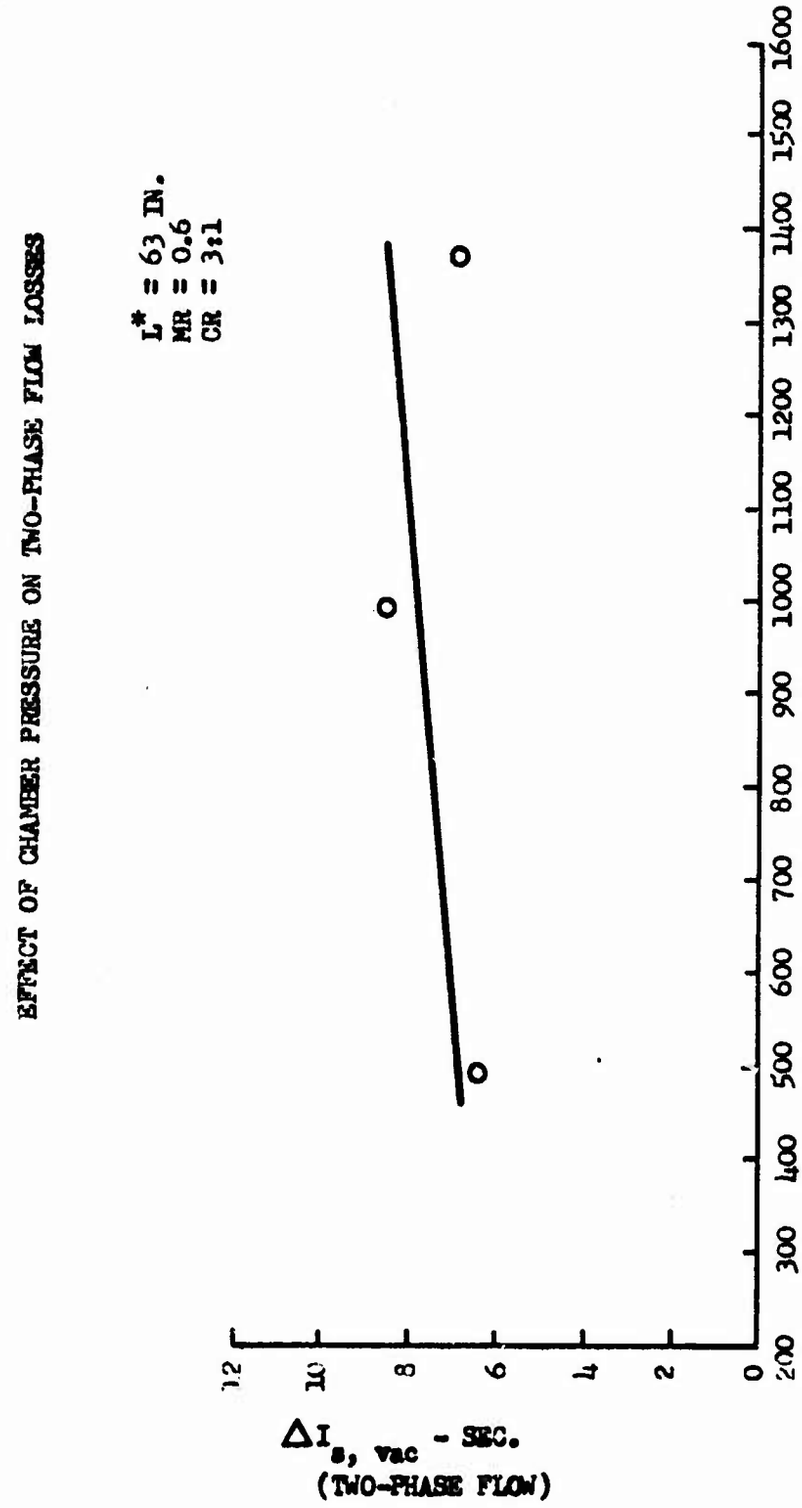
EFFECT OF CHAMBER PRESSURE ON TWO-PHASE FLOW LOSSES
L* = 63 IN.
MR = 0.6
CR = 3:1
ΔI s, vac - SEC.
(TWO-PHASE FLOW)
CHAMBER PRESSURE - psia
0
2
4
6
8
10
12
200
300
400
500
600
700
800
900
1000
1100
1200
1300
1400
1500
1600

Figure 26

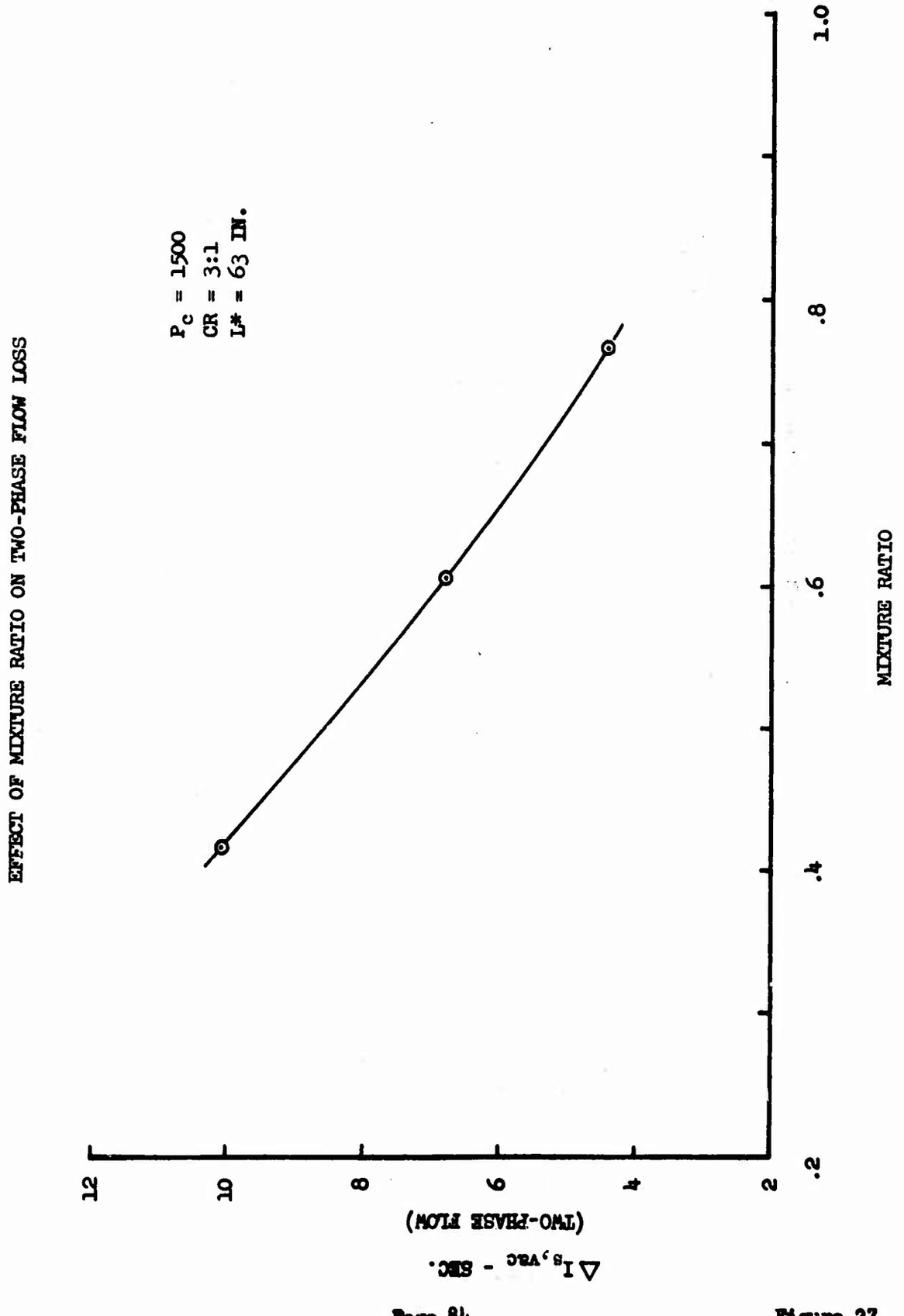
EFFECT OF MIXTURE RATIO ON TWO-PHASE FLOW LOSS
P_c = 1500
CR = 3:1
L* = 63 IN.
$\Delta I_{s,vac}$ - SHC.
(TWO-PHASE FLOW)
12
10
8
6
4
2
.2
.4
.6
.8
1.0
MIXTURE RATIO

Figure 27

5. Energy Release Efficiency Versus Variable Engine Parameters

The energy release efficiency is a measure of the ability of the injector elements to combine the propellants in a fixed flow path length. From this definition, it would be expected that variations in parameters affecting the chamber length would most affect the energy release efficiency. Figures 28 through 31 substantiate this premise. It may be seen from Figure 28 that the energy release loss increases sharply as the characteristic length is reduced below 60 in. (chamber length less than 20 inches). Similarly, Figure 29 shows a significant increase in energy release loss as the contraction ratio is increased from 3 to 6 while holding L^* constant. (This corresponds to a reduction in chamber length of from 20 in. to 10 in.) this trend was anticipated early in the program when it was observed that, at the shorter engine lengths, complete combustion was occurring in the convergent section of the nozzle, resulting in excessive hardware erosion (References 2 and 3). Optimization of this system would, therefore, consider the trade-off in L^* and contraction ratio in establishing an engine of sufficient length to allow complete combustion within the chamber.

Figures 30 and 31, ERE as a function of chamber pressure and mixture ratio respectively, show no variation that would exceed normal experimental data scatter. It may be stated, therefore, that these two parameters have no significant effect on energy release efficiency.

EFFECT OF CHARACTERISTIC LENGTH ON ENERGY RELEASE EFFICIENCY

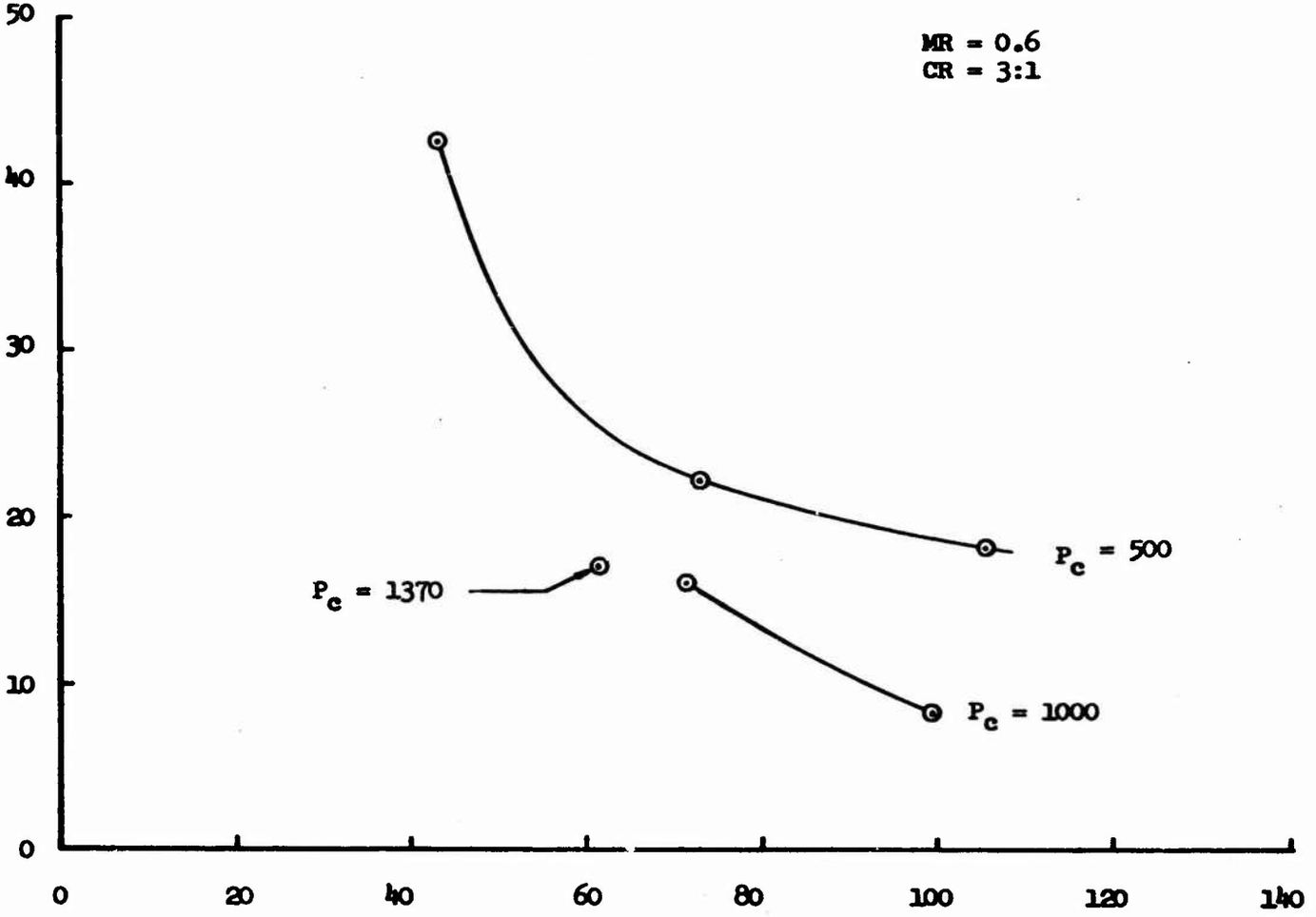

Figure 28

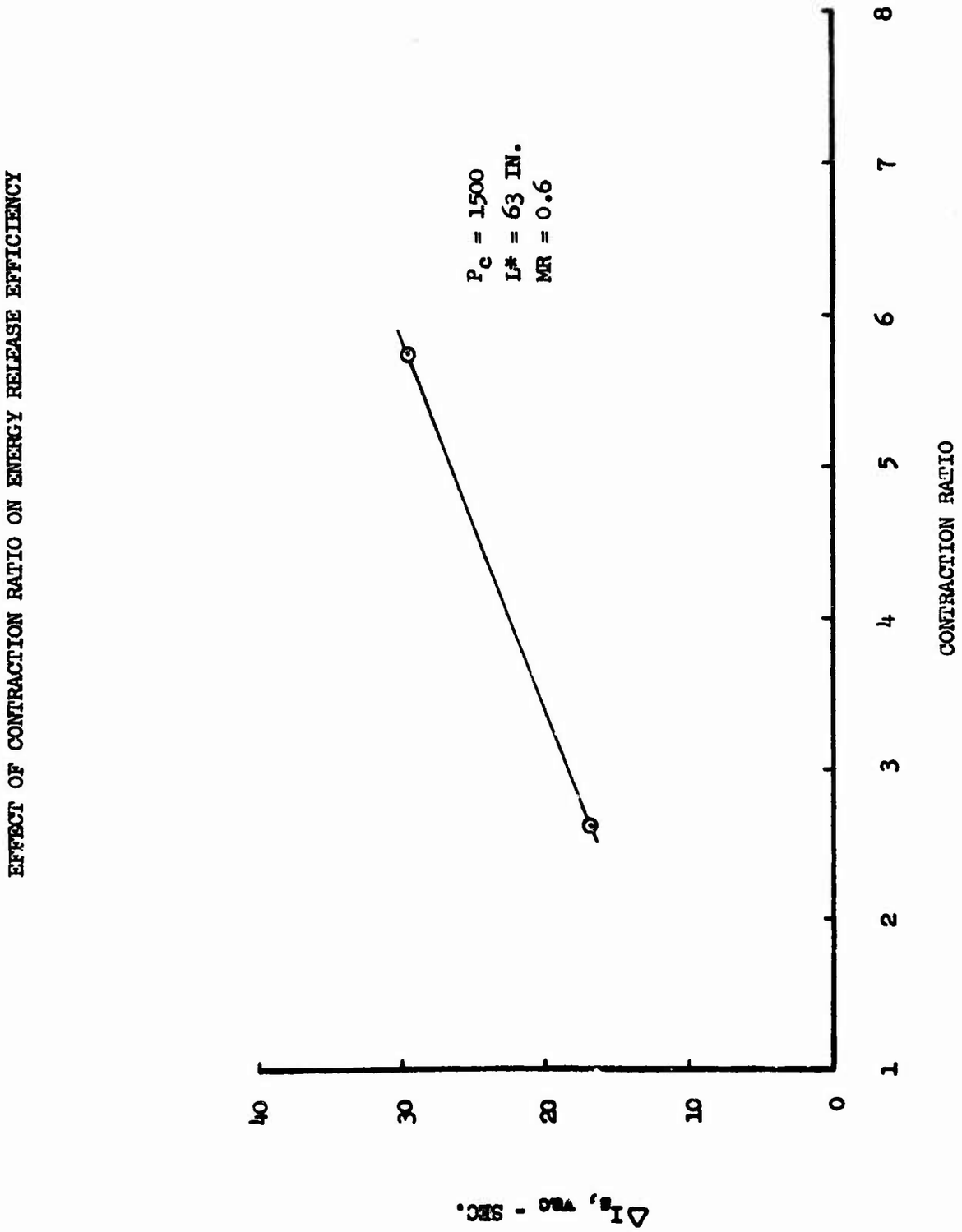
EFFECT OF CONTRACTION RATIO ON ENERGY RELEASE EFFICIENCY
P_c = 1500
L* = 63 IN.
MR = 0.6
ΔI_s, vac - SEC.
40
30
20
10
0
1
2
3
4
5
6
7
8
CONTRACTION RATIO

Figure 29

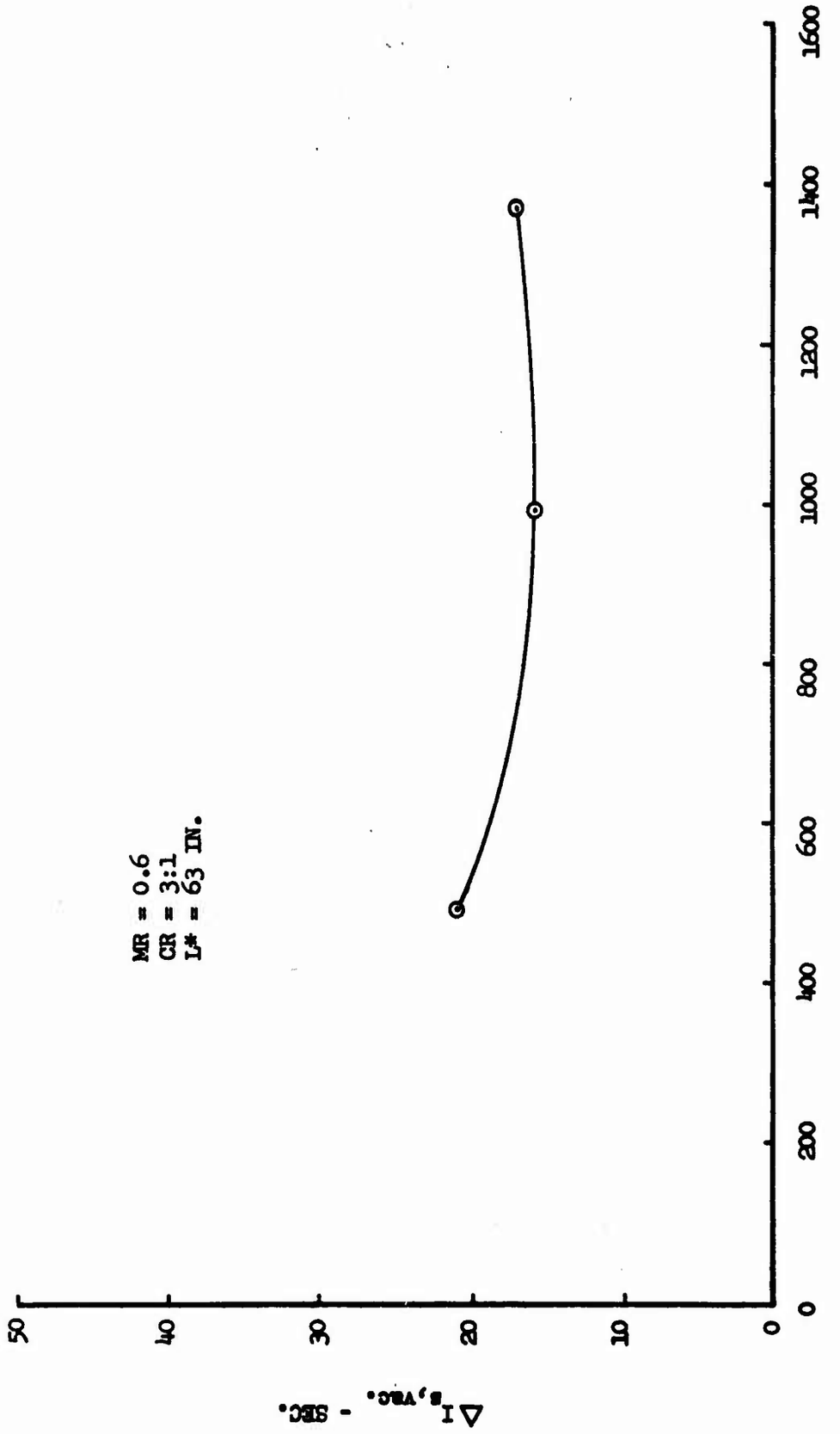
EFFECT OF CHAMBER PRESSURE ON ENERGY RELEASE EFFICIENCY
MR = 0.6
CR = 3:1
L* = 63 IN.
$\Delta I_{s,vac.}$ - SEC.
50
40
30
20
10
0
0
200
400
600
800
1000
1200
1400
1600
CHAMBER PRESSURE - psia

Figure 30

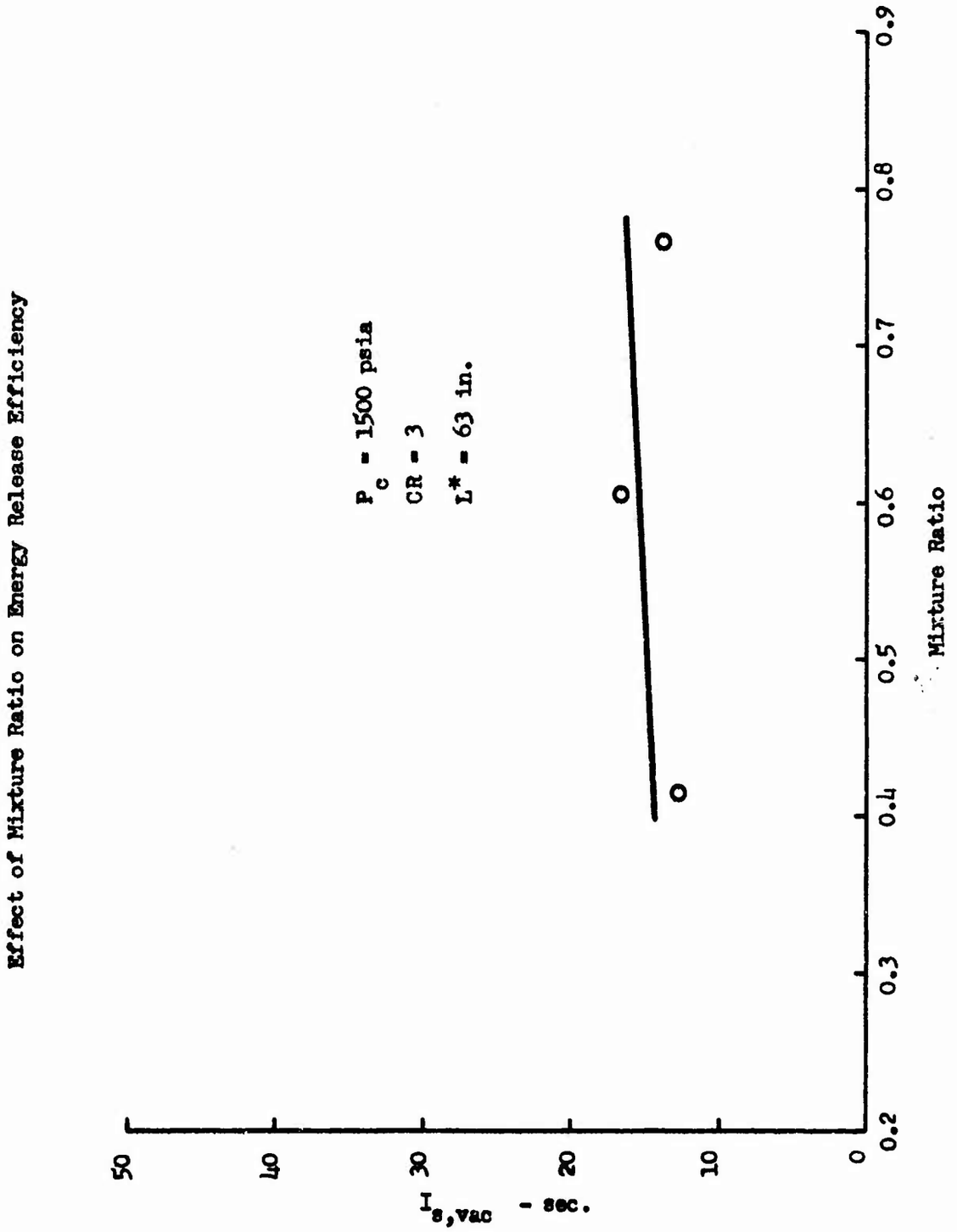
Effect of Mixture Ratio on Energy Release Efficiency
P_c = 1500 psia
CR = 3
L* = 63 in.
$I_{s,vac}$ - sec.
50
40
30
20
10
0
0.2
0.3
0.4
0.5
0.6
0.7
0.8
0.9
Mixture Ratio

Figure 31

6. Total Engine Performance Versus Variable Engine Parameters

The variation in total engine performance as a function of engine length, L*, contraction ratio, chamber pressure, mixture ratio, and metal content in the fuel is shown in Figures 32 through 37. The trends exhibited in the first three figures correlate with previous data plotted as a function of engine length and those parameters affecting length. While the upper limit on length has not been established, it may be concluded from these results, that complete combustion with this injector is not possible in an engine length less than 20 inches.

Figure 35, a plot of chamber pressure versus engine performance, shows the relative insensitivity of the system to changes (within the limits considered) in operating pressure. Further data is required to ascertain the gains that would be achieved with higher pressures and high-L* chambers.

The trend in performance as a function of mixture ratio, shown in Figure 36, is as expected. The greater thermal energy associated with the higher mixture ratios results in a rapidly increasing engine efficiency. It should be noted, however, that maximum performance is achieved at a mixture ratio lower than that corresponding to greatest efficiency. This is due to the combustion characteristics as shown by the theoretical specific impulse versus mixture ratio (Figures 16, 17, and 18 of Reference 1). It may be seen that maximum performance is attainable at a mixture ratio of 0.6.

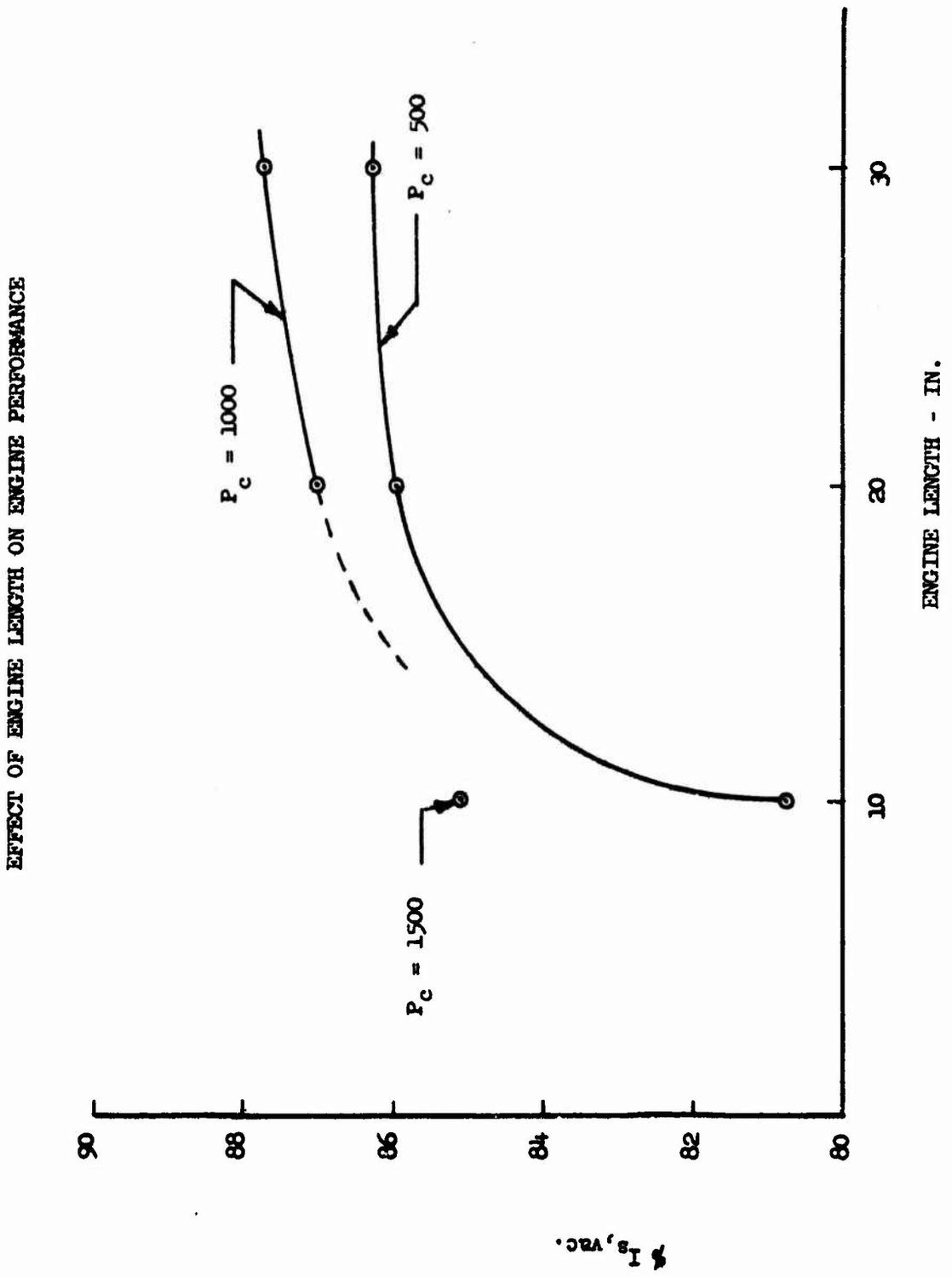
EFFECT OF ENGINE LENGTH ON ENGINE PERFORMANCE
P_c = 1000
P_c = 500
P_c = 1500
90
88
86
84
82
80
10
20
30
ENGINE LENGTH - IN.
% $I_{s,vac.}$

Figure 32

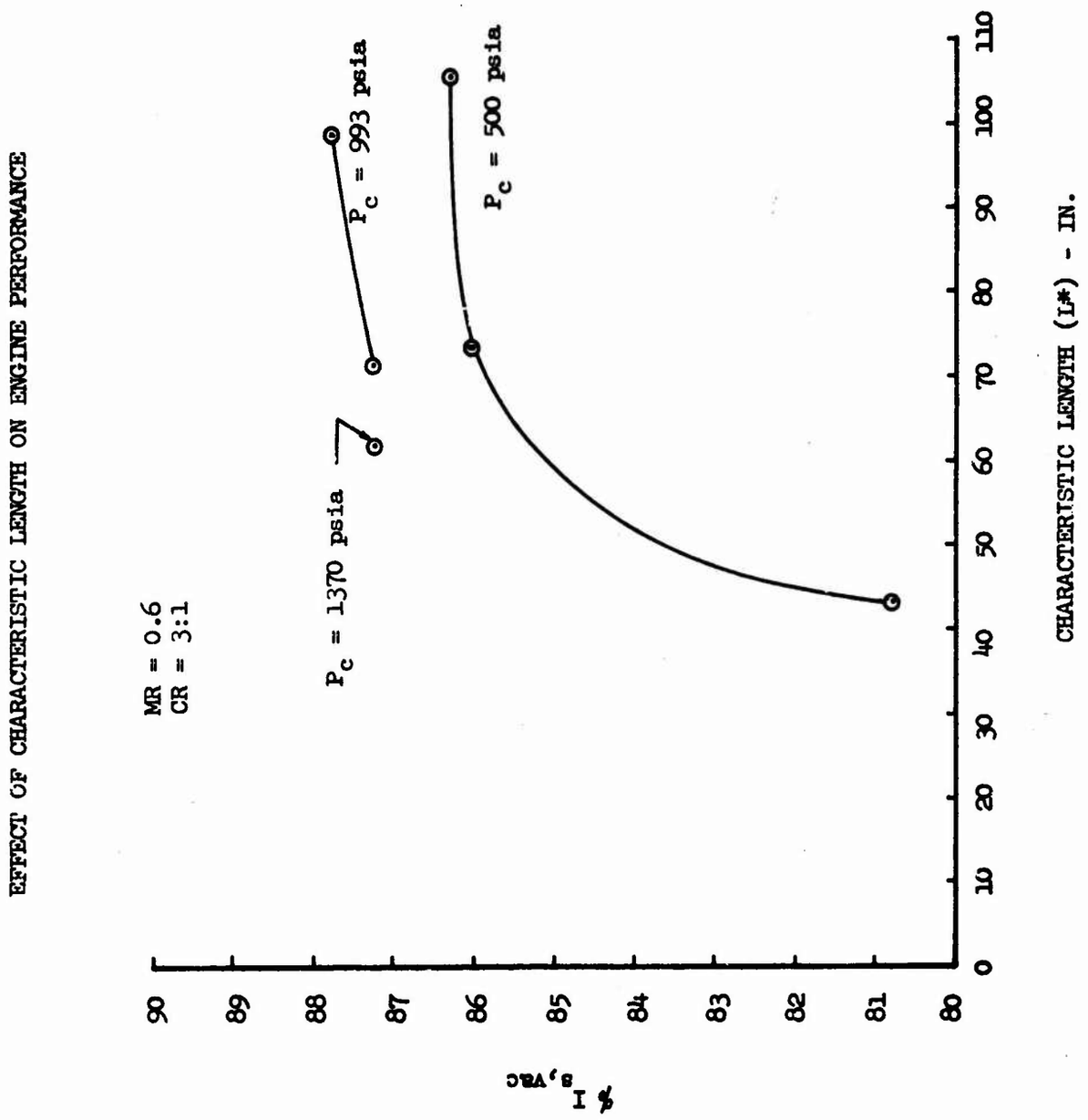
EFFECT OF CHARACTERISTIC LENGTH ON ENGINE PERFORMANCE
MR = 0.6
CR = 3:1
P_c = 1370 psia
P_c = 993 psia
P_c = 500 psia
% $I_{s,vac}$
90
89
88
87
86
85
84
83
82
81
80
0
10
20
30
40
50
60
70
80
90
100
110
CHARACTERISTIC LENGTH (L*) - IN.

Figure 33

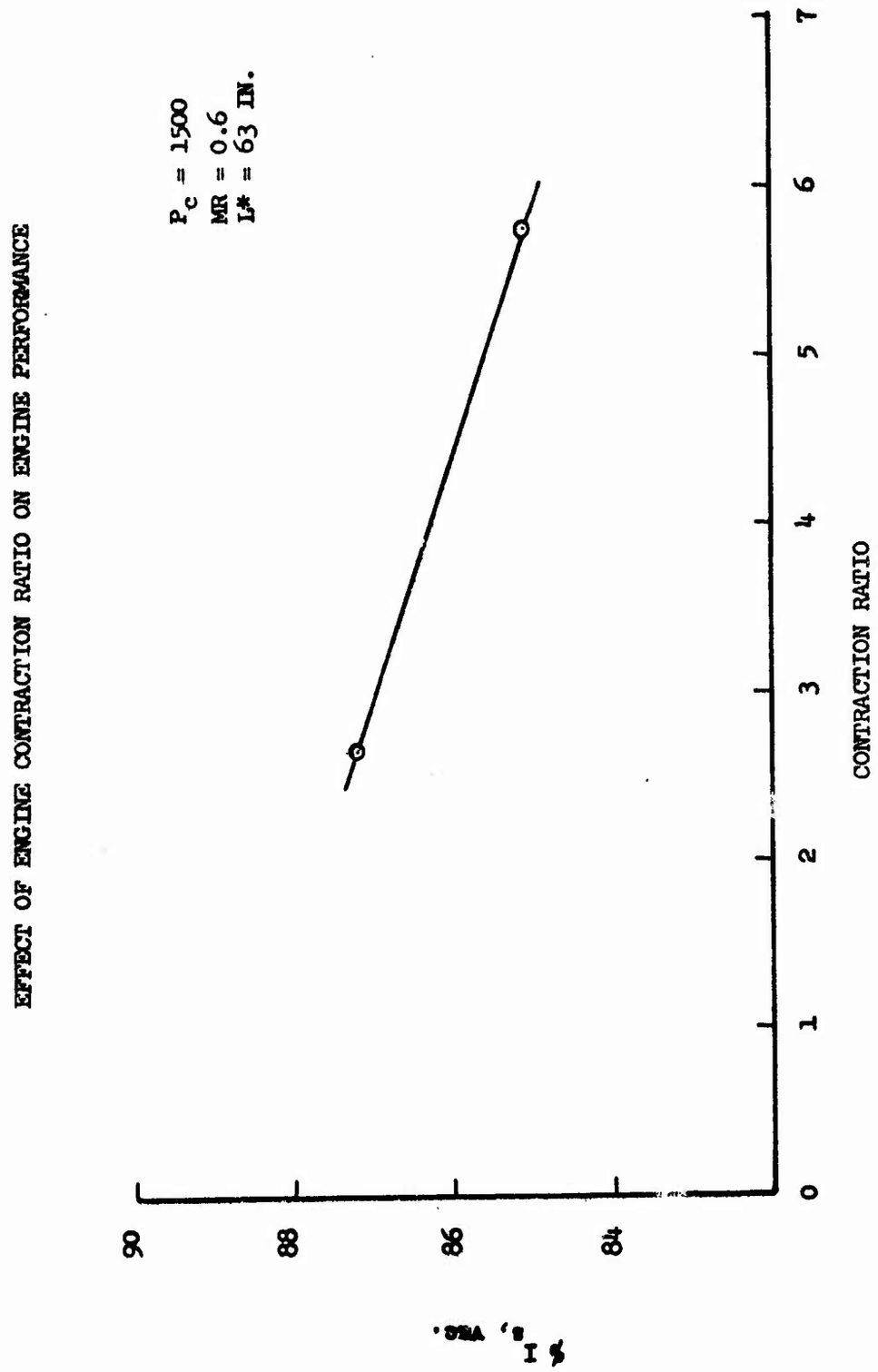
EFFECT OF ENGINE CONTRACTION RATIO ON ENGINE PERFORMANCE
P_c = 1500
MR = 0.6
L* = 63 IN.
I_s, VAC. %
90
88
86
84
0
1
2
3
4
5
6
7
CONTRACTION RATIO

Figure 34

EFFECT OF CHAMBER PRESSURE ON ENGINE PERFORMANCE

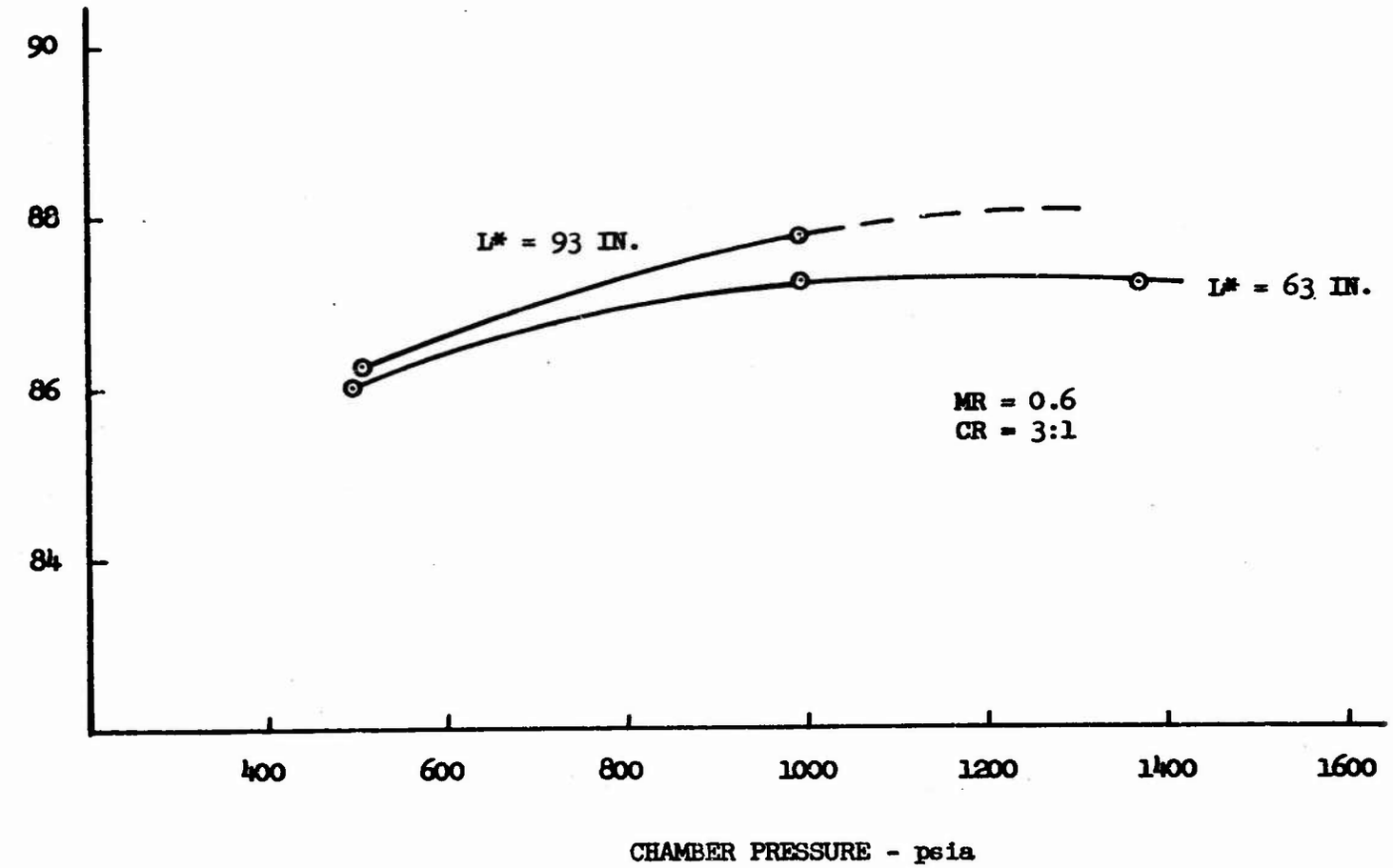

Figure 35
Page 94

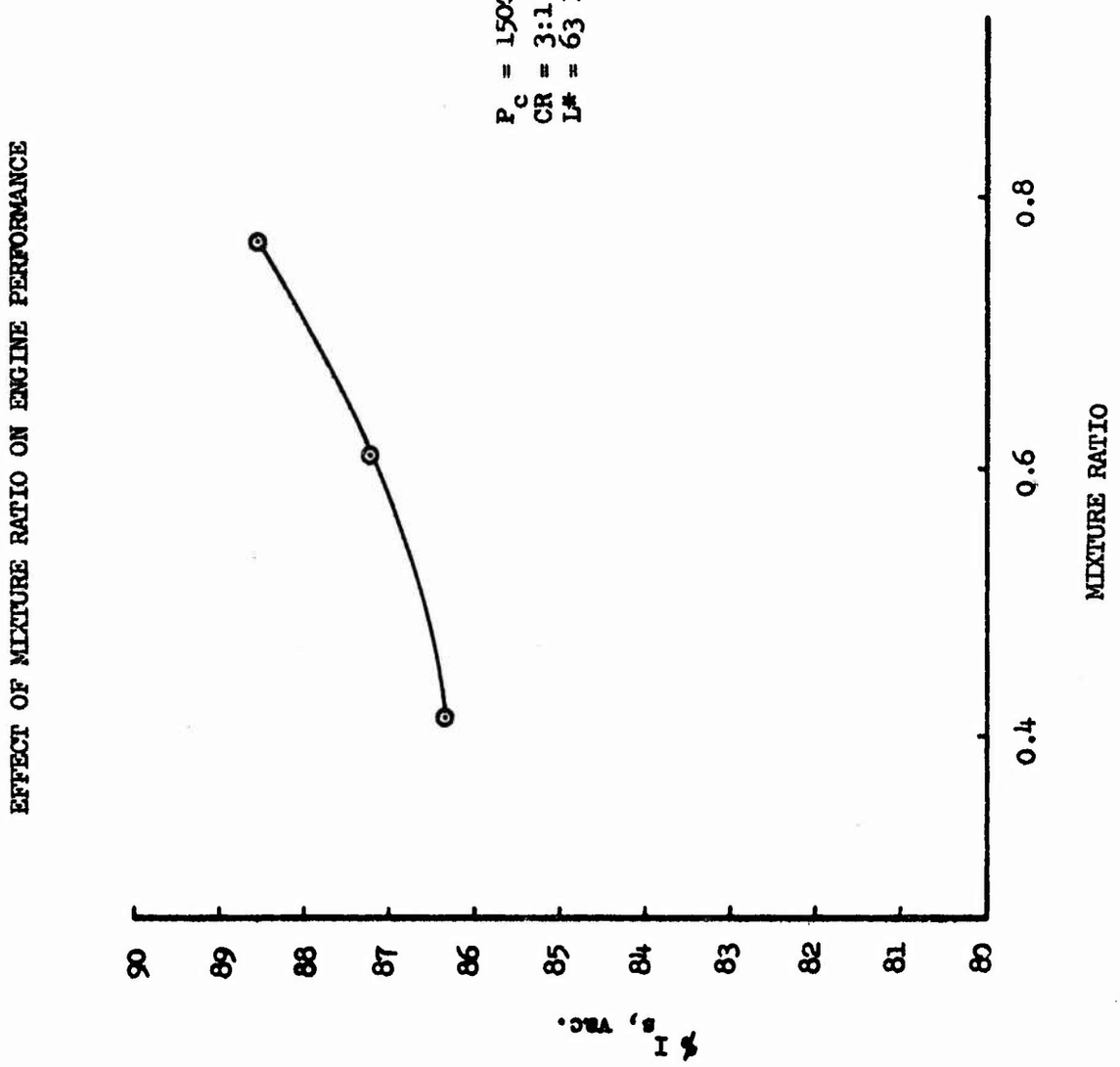
EFFECT OF MIXTURE RATIO ON ENGINE PERFORMANCE
P_c = 1500 psia
CR = 3:1
L* = 63 IN.
% I_s, vac.
90
89
88
87
86
85
84
83
82
81
80
0.4
0.6
0.8
MIXTURE RATIO

Figure 36

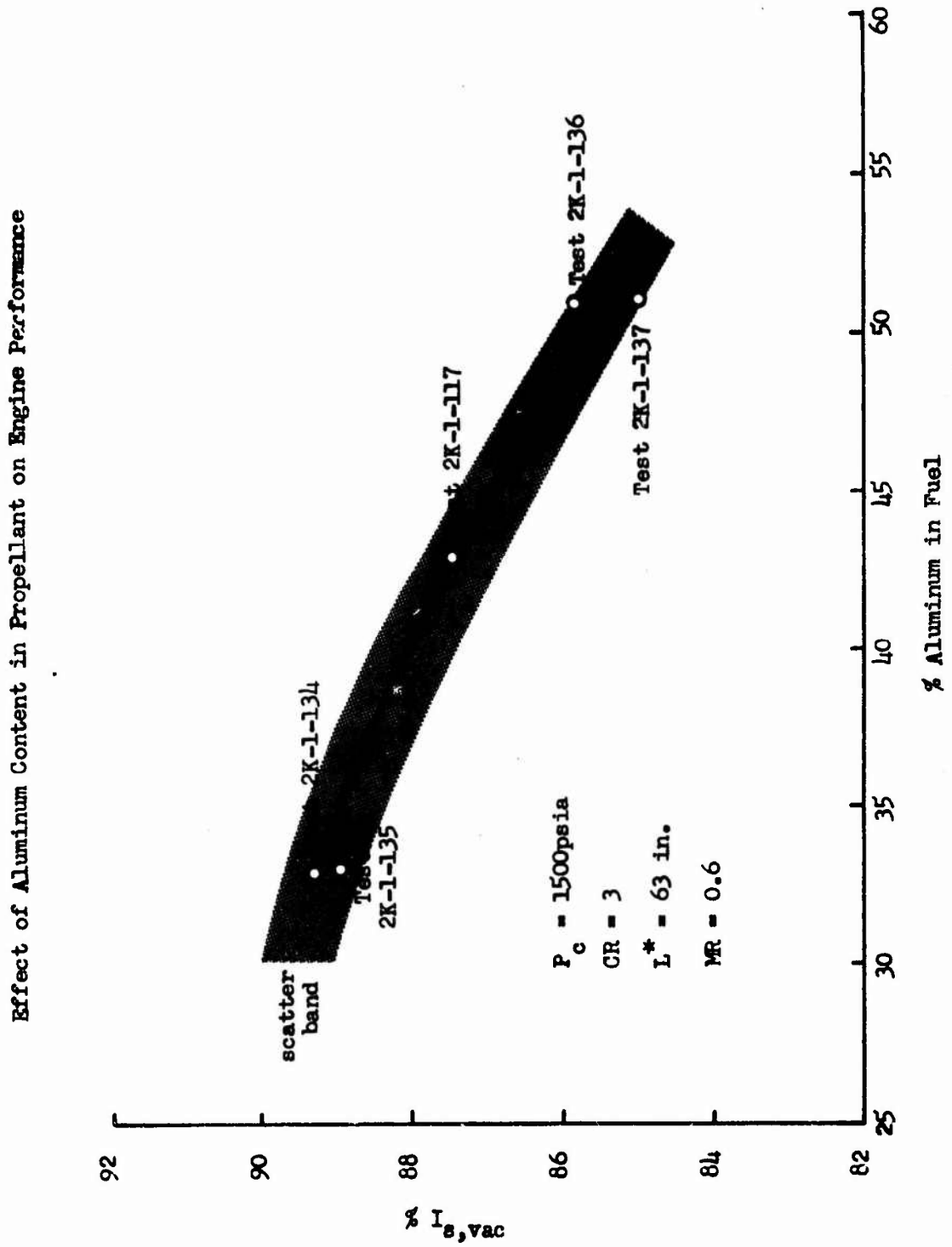
Effect of Aluminum Content in Propellant on Engine Performance
scatter band
2K-1-134
Test 2K-1-135
Test 2K-1-117
Test 2K-1-136
Test 2K-1-137
P_c = 1500psia
CR = 3
L^* = 63 in.
MR = 0.6
% $I_{s,vac}$
% Aluminum in Fuel
92
90
88
86
84
82
25
30
35
40
45
50
55
60

Figure 37

Figure 37, a curve of efficiency versus aluminum content in the fuel, is consistant with past investigations (Ref. 7) which observed macimum performance to be achieved with fuels containing 33% Aluminum powder. This figure also presents an estimate of the degree of experimental scatter present in the data. It may be seen that the variation in specific impulse between the two tests at each propellant extreme is approximately 0.5%.

SECTION IV

HARDWARE MAINTAINABILITY AND DURABILITY

The previous quarterly report (Reference 3) presented a table of 12 sea level 2K tests with reference made in each case to the durability exhibited by the hardware used. In addition, comments pertinent to hardware maintainability were made. Because all tests subsequent to those presented in the table utilized engine components of ATJ Graphite, and because the comments on handling of the hardware are still applicable, no additional information can be included in this report. Reference is made to the third report for information pertaining to engine hardware maintainability and durability.

SECTION V

CONCLUSIONS AND RECOMMENDATIONS

On the basis of the work accomplished as of this report period, the following conclusions and recommendations are made:

A. CONCLUSIONS

1. In most cases, the effect of deleting all particles less than 0.5 microns on the calculated particle mass median is insignificant. In those cases where inclusion of the particles appears desirable, an estimate of their number, rather than actual count, will suffice.

2. Significant errors in the calculated mass median are possible when the method of counting employed considers an actual count of small particles and only a small portion of the entire available sample. More consistent results are attained when a minimum count of 1000 particles 0.5 microns and larger is employed.

3. Variances do exist in the particle results obtained using an electron and an optical microscope. These variations are, in addition, a function of the particular operator performing the analysis.

4. The measured particle size and consequent two-phase flow performance losses appear to be mildly influenced by the chamber length and operating mixture ratio. No apparent influence on these parameters is exhibited by chamber pressure or aluminum content in the fuel.

5. The energy release efficiency of this particular injector/chamber configuration is strongly influenced by the absolute length of the chamber. Lesser influence is exhibited by chamber pressure and mixture ratio.

6. Overall engine efficiency is primarily a function of length, mixture ratio, and aluminum content in the fuel. No significant influence is attributed to chamber pressure.

B. RECOMMENDATIONS

Based on analysis of results obtained as of this report period, the following recommendations are made:

1. A re-analysis of the particle samples collected during the 13 sea level 2K tests must be done in compliance with new techniques and procedures. Future test samples should be analyzed using both the electron and the optical microscope to ensure that a full range of particle sizes is observed.

2. Tests included in the revised test plan should be continued to evaluate the altitude performance and establish the influence of design and operating parameters on performance losses at larger expansion ratios. The differences in two-phase performance losses between sea level and altitude nozzles must be ascertained before reliable extrapolation of existing data can be achieved.

SECTION VI

PLANNED FUTURE WORK

The following activities are planned during the fifth quarter of this program:

A. Shipment and installation of all components necessary to 2K and 15K simulated altitude testing at the Arnold Engineering Development Center (Tullahoma, Tennessee) will be completed.

B. Twelve simulated altitude tests at the 2,000 lb thrust level will be completed.

C. Simulated altitude testing at the 15,000 lb thrust level will be initiated.

D. Particle sample analysis and performance analysis to determine the effect of variable engine parameters on two-phase flow losses and overall performance will be continued.

E. Future work in the area of performance analysis will consist first of a re-evaluation of the particle sizes presented in a previous section. Once the correct particle size has been determined, the modified data will be used in the prediction of 2K and 15K simulated altitude performance. Once this prediction technique has been verified, the final data analysis will employ the results of both sets of data in the extrapolation to engines of 30K and 100K thrust levels.

REFERENCES

1. A Study of the Effects of Engine Parameters on Two-Phase Flow Performance Losses Using N_2O_4/Alumizine Propellants (U), Aerojet-General Report 11205 Q-1, December 1965.

2. A Study of the Effects of Engine Parameters on Two-Phase Flow Performance Losses Using N_2O_4/Alumizine Propellants, (U), Aerojet-General Report 11205 Q-2, (Technical Report AFRPL-TR-66-60), March 1966.

3. A Study of the Effects of Engine Parameters on Two-Phase Flow Performance Losses Using N_2O_4/Alumizine Propellants (U), Aerojet-General Report 11205 Q-3, (Technical Report AFRPL-TR-66-132), June 1966.

4. R. S. Valentine, L. E. Dean, J. L. Pieper, An Improved Method for Rocket Performance Prediction, Aerojet-General Corporation, PTDR 9642:034, 8 October 1965.

5. Study of High Effective Area Ratio Nozzles for Space Craft Engines, Final Report NAS 7-136-F, Vol. 2, June 1964, Aerojet-General Corporation.

6. Investigation of Non-Equilibrium Flow Effects in High Expansion Nozzles, UAC Final Report B910056-12, Contract NASW-366, September 20, 1963.

7. Improved Titan Predevelopment Program, Aerojet-General Reports 212/SA9-Q-4, 5, 6, Contract AF 04(694)-219, SA9, and SA15, July 1964 to February 1965.

8. Analytical Investigation of the Two-Phase Flow Low Frequency Combustion Instability Problem, Technical Report AMDR 9635-013, 13 April 1966.

9. C. E. Lapple, Fluid and Particle Mechanics, Edwards Brothers, Inc., Ann Arbor, Michigan, First Edition, 1956, pp. 314.

10. Dynamics of Two-Phase Flow in Rocket Nozzles, UTC 2102-FR, United Technology Center, September 1965.

11. Cheung, H., and N. S. Cohen, Performance of Solid Propellants Containing Metal Additives, AIAA J. 3: pg. 250-258, 1965.

12. Investigation of Particle Growth and Ballistic Effects on Solid Propellant Rockets, UTC 2128-FR, 1 Jan. 1965 - 31 December 1965, Contract NOw 65-0222-f.

UNCLASSIFIED

Security Classification

DOCUMENT CONTROL DATA · R&D

(Security classification of title, body of abstract and indexing annotation must be entered when the overall report is classified)

1 ORIGINATING ACTIVITY (Corporate author) Aerojet-General Corporation	2a REPORT SECURITY CLASSIFICATION Confidential 2b GROUP 4

3 REPORT TITLE

A Study of the Effects of Engine Parameters on Two-Phase Flow Performance Losses Using N_2O_4/Alumizine Propellant

4 DESCRIPTIVE NOTES (Type of report and inclusive dates)

Fourth Quarterly, 1 June 1966 through 31 August 1966

5 AUTHOR(S) (Last name, first name, initial)

Hartsell, James O.
Ditore, Michael J.

6 REPORT DATE 15 September 1966	7a TOTAL NO OF PAGES 102	7b NO OF REFS 12
8a CONTRACT OR GRANT NO AF 04(611)-11205 b PROJECT NO c AFSC Project 3058 d	9a ORIGINATOR'S REPORT NUMBER(S) AGC 11205-Q-4 9b OTHER REPORT NO(S) (Any other numbers that may be assigned this report) AFRPL-TR-66-231	

10 AVAILABILITY/LIMITATION NOTICES

CPIA Distribution

11 SUPPLEMENTARY NOTES	12 SPONSORING MILITARY ACTIVITY Rocket Propulsion Laboratory Air Force System Command Edwards, California

13 ABSTRACT Studies were conducted to quantitatively evaluate the effects of liquid-engine design and operating parameters on two-phase flow performance losses using an N_2O_4/Alumizine-gel propellant combination. The theoretical-experimental efforts, conducted concurrently, consist of performance evaluations covering a range of variables sufficiently wide to provide an adequate basis for specific impulse prediction for large-scale engines. The theoretical analysis was made of two-phase flow performance losses resulting from the existence of aluminum oxide in the nozzle exhaust. Particle samples, collected during each 2K engine test, are being analyzed to determine the representative particle size and distribution data for the analysis. A one-dimensional gas particle flow analysis is being used to determine the performance losses. Preliminary computations indicate that the use of the mass median for particle size classification yields performance losses comparable to those derived when the particle distribution is used in the analysis. Forty-two 2K engine tests were successfully conducted. Some of these tests were performed to resolve the feed system pressure-oscillation and hardware erosion problems encountered in early experimental testing. Observed specific impulse efficiency was nominally

(Continued)

DD FORM 1473

Security Classification

Security Classification

14 KEY WORDS	LINK A		LINK B		LINK C	
	ROLE	WT	ROLE	WT	ROLE	WT

INSTRUCTIONS

1. ORIGINATING ACTIVITY: Enter the name and address of the contractor, subcontractor, grantee, Department of Defense activity or other organization *(corporate author)* issuing the report.

2a. REPORT SECURITY CLASSIFICATION: Enter the overall security classification of the report. Indicate whether "Restricted Data" is included. Marking is to be in accordance with appropriate security regulations.

2b. GROUP: Automatic downgrading is specified in DoD Directive 5200.10 and Armed Forces Industrial Manual. Enter the group number. Also, when applicable, show that optional markings have been used for Group 3 and Group 4 as authorized.

3. REPORT TITLE: Enter the complete report title in all capital letters. Titles in all cases should be unclassified. If a meaningful title cannot be selected without classification, show title classification in all capitals in parenthesis immediately following the title.

4. DESCRIPTIVE NOTES: If appropriate, enter the type of report, e.g., interim, progress, summary, annual, or final. Give the inclusive dates when a specific reporting period is covered.

5. AUTHOR(S): Enter the name(s) of author(s) as shown on or in the report. Enter last name, first name, middle initial. If military, show rank and branch of service. The name of the principal author is an absolute minimum requirement.

6. REPORT DATE: Enter the date of the report as day, month, year, or month, year. If more than one date appears on the report, use date of publication.

7a. TOTAL NUMBER OF PAGES: The total page count should follow normal pagination procedures, i.e., enter the number of pages containing information.

7b. NUMBER OF REFERENCES: Enter the total number of references cited in the report.

8a. CONTRACT OR GRANT NUMBER: If appropriate, enter the applicable number of the contract or grant under which the report was written.

8b, 8c, & 8d. PROJECT NUMBER: Enter the appropriate military department identification, such as project number, subproject number, system numbers, task number, etc.

9a. ORIGINATOR'S REPORT NUMBER(S): Enter the official report number by which the document will be identified and controlled by the originating activity. This number must be unique to this report.

9b. OTHER REPORT NUMBER(S): If the report has been assigned any other report numbers *(either by the originator or by the sponsor)*, also enter this number(s).

10. AVAILABILITY/LIMITATION NOTICES: Enter any limitations on further dissemination of the report, other than those imposed by security classification, using standard statements such as:

(1) "Qualified requesters may obtain copies of this report from DDC."

(2) "Foreign announcement and dissemination of this report by DDC is not authorized."

(3) "U. S. Government agencies may obtain copies of this report directly from DDC. Other qualified DDC users shall request through

_____."

(4) "U. S. military agencies may obtain copies of this report directly from DDC. Other qualified users shall request through

_____."

(5) "All distribution of this report is controlled. Qualified DDC users shall request through

_____."

If the report has been furnished to the Office of Technical Services, Department of Commerce, for sale to the public, indicate this fact and enter the price, if known.

11. SUPPLEMENTARY NOTES: Use for additional explanatory notes.

12. SPONSORING MILITARY ACTIVITY: Enter the name of the departmental project office or laboratory sponsoring *(paying for)* the research and development. Include address.

13. ABSTRACT: Enter an abstract giving a brief and factual summary of the document indicative of the report, even though it may also appear elsewhere in the body of the technical report. If additional space is required, a continuation sheet shall be attached.

It is highly desirable that the abstract of classified reports be unclassified. Each paragraph of the abstract shall end with an indication of the military security classification of the information in the paragraph, represented as *(TS), (S), (C), or (U)*

There is no limitation on the length of the abstract. However, the suggested length is from 150 to 225 words.

14. KEY WORDS: Key words are technically meaningful terms or short phrases that characterize a report and may be used as index entries for cataloging the report. Key words must be selected so that no security classification is required. Identifiers, such as equipment model designation, trade name, military project code name, geographic location, may be used as key words but will be followed by an indication of technical context. The assignment of links, rules, and weights is optional.

Security Classification

87%. The range of efficiency variation, with one exception, was ±1% depending upon operating conditions. A minimum specific impulse efficiency was observed for a chamber pressure of 500 psia, an L^* of 33, and a chamber contraction ratio of 3. Two-phase flow performance losses were calculated to be nominally 2% of the theoretical specific impulse and further, the influence of design and operating variables on two-phase flow performance were found to be insignificant at the sea level expansion ratio. The single most significant loss was determined to be energy release loss; the absolute magnitude varying with engine design, but was found to be insensitive to mixture ratio or chamber pressure.